Alpe Adria
Medical Physics

Udine 2003
Opatija 2006
Graz 2008
Ljubljana 2010
Trieste 2012
Budapest 2014
Zagreb 2016
Novi Sad 2017
Graz 2019
Ljubljana 2022
June 1-3

Conference Proceedings

Proceedings
of the
10th Alpe-Adria Medical Physics Meeting

Ljubljana, Slovenia. June 1-3, 2022

- AAMPM 2022 -

Organised by:
Medical Physics Section of Slovenian Biophysical Society (DBS)
Slovenian Society of Radiographers (ZDRI)

In cooperation with:
Austrian Society for Medical Physics (ÖGMP)
Associazione Italiana di Fisica Medica (AIFM)
Croatian Society of Medical Physics (HDMF)
Hungarian Society of Medical Physics (MOFT)
Slovak Society of Medical Physics and Biophysics (SKBS)
Serbian Association of Medical Physicists (DMFS)
Association of Medical Physicists in Bosnia and Herzegovina (UMFUBIH)
Association for Medical Physics and Biomedical Engineering (ZMFBI)

Editors:
Božidar Casar
Ignasi Méndez Carot
Primož Peterlin
Attila Šarvari

Reviewers:
Mirjana Budanec, Božidar Casar, Dario Faj, Hrvoje Hršak, Marija Jeremić, Slaven Jurković, Renata Longo, Duško Lukarski, Renato Padovani, Primož Peterlin, Borislava Petrović, Mara Severgnini, Petra Tomše, Árpád Tóth, Uwe Wolff, Urban Zdešar, Brigitte Zurl

Published in electronic form by:
Društvo biofizikov Slovenije / Slovenian Biophysical Society, Jamova 39, Ljubljana

Year of publication:
2022

URL:
https://medifiz.org/aampm2022/

COBISS ID:
110551299

Zapis CIP:
Kataložni zapis o publikaciji (CIP) pripravili v Narodni in univerzitetni knjižnici v Ljubljani
COBISS.SI-ID 110551299
ISBN 978-961-90942-6-6 (PDF)

Contents

Preface	**5**
Scientific Programme	**7**
Contributions	**13**
Index of Authors	**144**
Acknowledgements	**147**

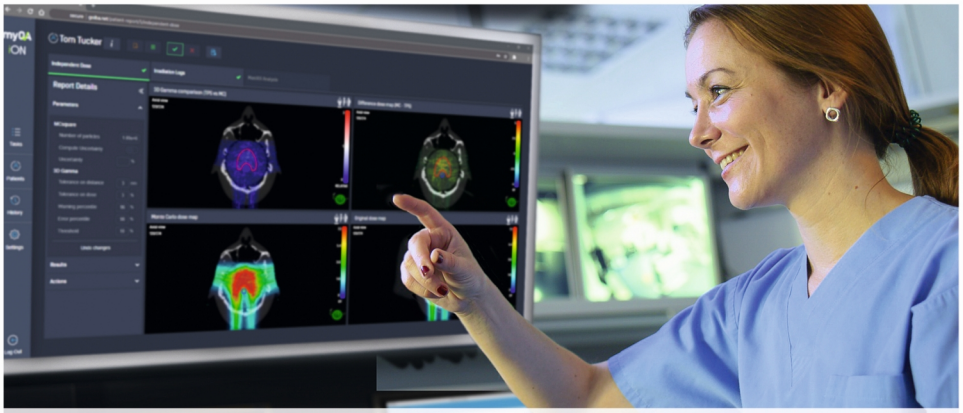

Discover IBA News 2022

Validate your beam model

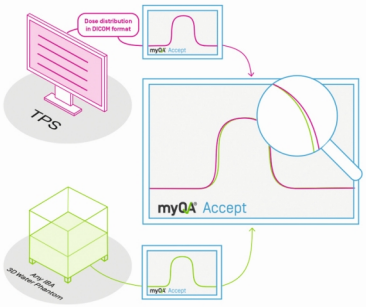

3D Dose Cube Import

Validate your beam model against your pre-commissioned or commissioned linac with myQA® Accept 9.0 – the only commissioning and annual QA software able to support this functionality. **Read more here:**

Shaping the future of Patient QA

Proven film-class efficiency for your Patient QA

Interested to hear about customer experience with myQA® SRS or MatriXX Resolution one year after release to the market? **Check out the ESTRO program.** Also, stay tuned to learn more about our latest enhancements and further compatibility with your linac range.

Shaping the future of Proton Therapy

ConformFLASH®

Maximizing the true benefit of proton FLASH

FLASH is a key research area that may dramatically improve the clinical relevance of proton therapy for patients around the world. IBA is very well positioned to drive the development of FLASH irradiation, the next major innovation expected in radiation therapy. **Discover more here:**

DynamicARC®

Faster, Simpler, Sharper

IBA is developing a new delivery technique called DynamicARC® proton therapy. It allows dynamic irradiation while the gantry is rotating, with the advantages of both Pencil Beam Scanning (PBS) and Bragg Peak but without the exit dose. **Discover more here:**

* ConformalFLASH® and DynamicARC® are registered brands of the IBA's Proton FLASH irradiation solution and the IBA's Proton Arc therapy solution currently under research and development phase. It will be available for sale when regulatory clearance is received.

AAMPM_2022_Facts_Br_E_ Rev1_0522 I © IBA 2022 I All rights reserved

Preface

Dear colleagues, dear friends,

It is our pleasure to welcome you at the 10th Alpe Adria Medical Physics Meeting in Ljubljana.

Since their beginning in 2004, the biennial Alpe-Adria Medical Physics meetings (initially called Austrian, Italian, Slovenian and Croatian Medical Physics Meeting) have been committed to the same goal: strengthening the cooperation and advancing the knowledge in the field of medical physics among the experts in the region. As such, these meetings are complementing rather than competing with the larger meetings like the also biennial EFOMP congresses.

The present meeting brings 8 invited lectures, 16 short oral presentations and 21 poster presentations from the areas of radiation therapy, radiation protection, medical imaging, and nuclear medicine. The topics covered span from long-ranging themes of MR imaging, artificial intelligence and particle therapy to clever practical solutions of the problems encountered in everyday life at a clinic. The meeting would have been near impossible without the vendors which complement the scientific programme with an exhibition of their latest technological solutions in the foyer.

We hope that the conference will succeed in its mission, facilitating making new acquaintances, sowing seeds for new collaborations, expanding knowledge, and sparkling new ideas.

Primož Peterlin
Attila Šarvari

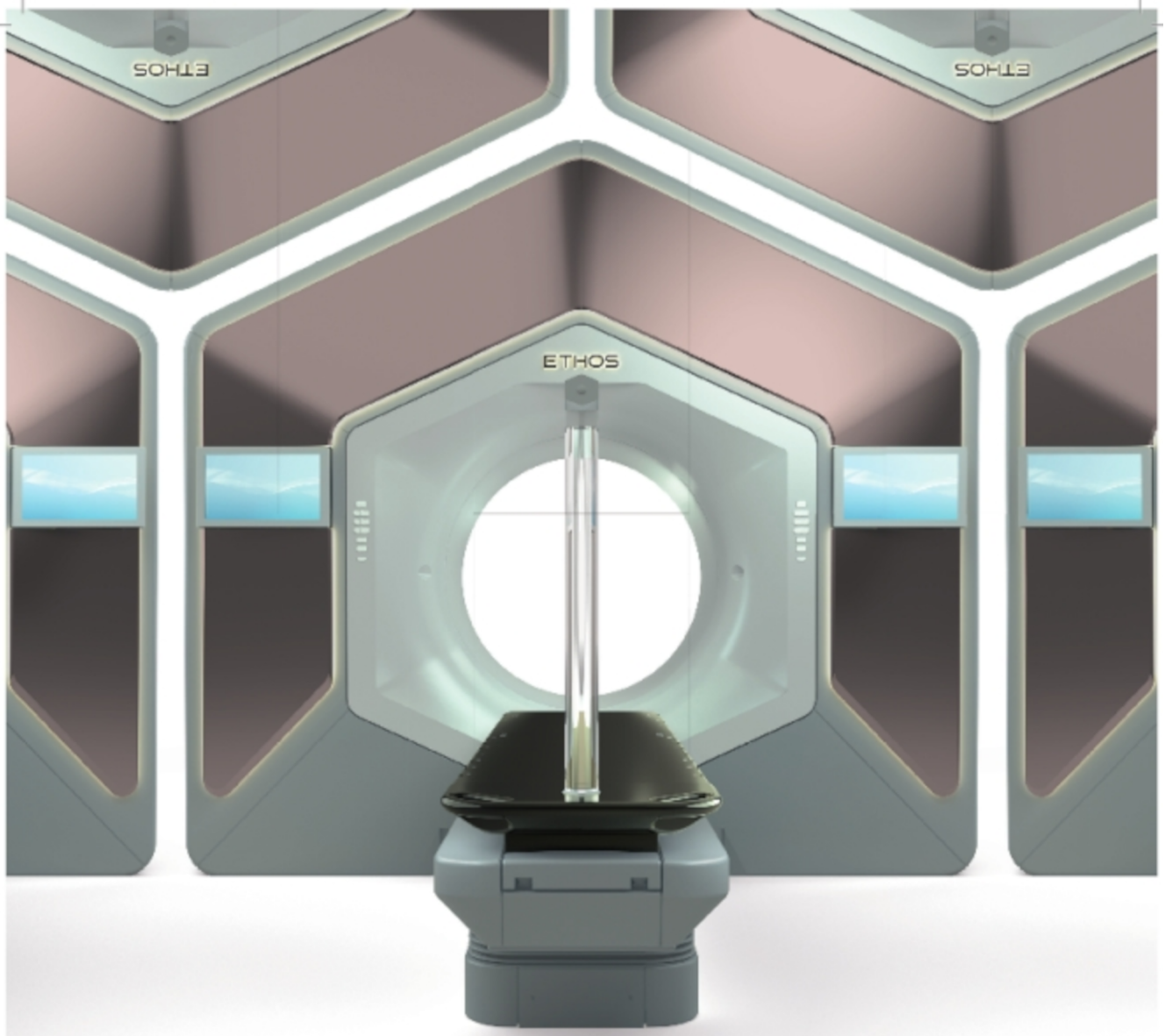

The more efficient, flexible, personal

& intelligent way to outsmart cancer.

With Ethos™ therapy, you can adapt treatment plans daily while transforming your cancer fight completely.

Ethos therapy is our AI-driven holistic solution that lets you choose the most appropriate treatment option based on daily changes in patient anatomy. It also delivers an entire adaptive treatment in a typical 15-minute timeslot, from setup through delivery. Redefine how you fight cancer—experience Ethos therapy at varian.com/ethos today.

Safety Information: Radiation may cause side effects and may not be appropriate for all cancers.

© 2020-2022 Varian Medical Systems, Inc. Varian is a registered trademark of Varian Medical Systems, Inc.

varian
A Siemens Healthineers Company

ETHOS™

Scientific Programme

Wednesday, June 1, 2022

19:00	Welcome reception

Thursday, June 2, 2022

8:00	Registration
9:00	Opening (Attila Šarvari, Primož Peterlin)
9:15-10:30	*Invited lectures: From past AAMP meetings to future radiotherapy* *Chairperson: Brigitte Zurl*
9:15	Božidar Casar (OI Ljubljana): An overview of AAMP meetings
9:30	Dietmar Georg (AKH Wien): MR in radiation technology -- a game changer?
10:30-11:00	Coffee break
11:00-12:45	*Invited lectures: Novel techniques* *Chairperson: Ignasi Méndez, Rihard Hudej*
11:00	Michele Avanzo (CRO Aviano): Artificial intelligence: Changing medical physics
11:45	Simon Mihály (Univ. Debrecen): On the use of AI-based autocontouring tools, a single institution experience
12:05	Josh Naylor (NHS Poole): Surface Guided Radiotherapy: the next leap in safety and quality after IGRT and IMRT
12:45-14:15	Lunch break / Poster Exhibition / Vendor Exhibition
14:15-15:15	*Short oral presentations: Nuclear medicine & Radiation protection* *Chairperson: Renata Longo, Marija Jeremić*
14:15	Dea Dundara Debeljuh (KBC Rijeka): Advance on image processing and optimization procedures in SPECT/CT imaging
14:30	Carlo Algranati (APSS Trento): Radiation protection classification of healthcare personnel at the Trento proton therapy center
14:45	Andraž Koritnik (ZVD Ljubljana): Assessment of the number and distribution of patients undergoing recurrent CT exams in Slovenia
15:00	Angelika Osanna-Elliott (AKH Wien): Communication process for QA enforcement in a large Central European hospital

15:15	Michele Signoriello (ASUGI Trieste): Basic safety assessment focused on effective dose to population, related to the management of solid and liquid wastes produced in clinical practices of Trieste (Italy) nuclear medicine department
15:30-16:00	Coffee break
16:00-17:15	*Short oral presentations: Radioherapy* *Chairperson: Peter Winkler, Primož Peterlin*
16:00	Alessio Boschini (AULSS2 Treviso): Dosimetrical evaluation effects of a simulated gravity induced shifting on linac mounted detector during patient pretreatment QA
16:15	Attila Šarvari (OI Ljubljana): Gantry angle verification using the CIRS ISO cube phantom on the Varian Halcyon linear accelerator
16:30	Ignasi Méndez (OI Ljubljana): Big data analysis on the calibration of radiochromic films
16:45	Eugenia Moretti (Udine Univ. Hospital): Commissioning and initial patient-specific verification experience with the first European installation of the GammaPod™ stereotactic breast radiosurgery system
17:00	Sašo Pulko (UKC Maribor): Automatic import and positioning of linac's couch top
19:00	Social event

Friday, June 3, 2022

8:00	Registration
8:30-10:45	*Invited lectures: Challenges in modern radiotherapy* *Chairperson: Uwe Wolff*
8:30	Markus Stock (MedAustron): Chances and challenges of a dual particle facility
9:15	Božidar Casar (OI Ljubljana): Characteristics of detectors for relative dosimetry in small fields
10:00	Slaven Jurković (KBC Rijeka): Verifying intensity modulated radiotherapy treatment dose delivery through a national audit
10:45-11:15	Coffee break
11:15-13:15	*Invited lecture (History of science) & Short oral presentations: Medical Imaging* *Chairperson: Tomislav Bokulić*
11:15	Werner Schmidt (ÖGMP): Gottfried Spiegler (1891-1970) & Medical Physics in Austria 1897-1938
11:45	Ana Božanić (KBC Rijeka): Digital breast tomosynthesis dose survey in Croatia
12:00	Ana Marija Kožuljević (Univ. Zagreb): Exploring the use of gamma-ray polarization in positron emission tomography
12:15	Manca Podvratnik (ZVD Ljubljana): Slovenian dose survey in pediatric radiology
12:30	Kristian Stojšić (KBC Rijeka): Role of medical physicist in magnetic resonance imaging at University hospital Rijeka
12:45	Stevan Vrbaski (Univ. Trieste): Application of Dukesim software in material decomposition studies

13:00 Urban Zdešar (ZVD Ljubljana): IAEA project on remote and automated quality control programme for radiography and mammography equipment

13:15 Closing ceremony

Saturday, June 4, 2022

10:00-13:00 Practical workshop (Institute of Oncology Ljubljana):
1) Output measurement on Varian Halcyon in a IBA Blue Phantom COMPACT
2) Patient QA measurement on Varian Halcyon with Scandidos Delta4
3) Measument on Varian TrueBeam STX with IBA myQA SRS detector

List of posters

P1 Paola Bregant (ASUGI Trieste): The Italian hospital network for the clinical training of the International Master in medical physics

P2 Hrvoje Brkić (Univ. Osijek): Development of a pregnant female phantom and calculation of fetal dose during a photon breast radiotherapy

P3 Anja Lazović (IORS Beograd): Assessment of the CT scan and CBCT doses for different imaging protocols used in radiotherapy

P4 Angelika Osanna-Elliott (AKH Wien): Implementation of a dose management system in a large Central European hospital

P5 Carlo Algranati (APSS Trento): Use of proton therapy in pediatric patients: breast-leukemia case

P7 Ozren Čudić (OI Vojvodina): Use of 3D printed bolus in brachytherapy

P8 Tadeja Forjanič (OI Ljubljana): The effect of longitudinal setup errors in craniospinal irradiation on the dose distribution at the field junction areas

P10 Tamara Jovanović (UKC Niš): Clinical involvement in the hybrid procedure for dosimetric verification of volumetric modulated arc therapy using Compass system

P11 Miloš Kopunović (UKC Niš): AAA and Acuros XB dose calculation algorithms comparison in treatement planning for lung cancer radiation therapy

P12 Vanda Leipold (Univ. Osijek): Effects of changes in surface-to-volume ratio of planning target volumes on dose distributions for stereotactic radiation therapy plans: a comparison between Varian Edge and Accuray Cyberknife

P13 Mirjana Papić (OI Vojvodina): Radiotherapy CT imaging of three antropomorphic phantoms -- dose to organs at risk in pediatric and adult imaging protocol

P14 Nina Pavlović (UKC Kragujevac): Irradiation of inoperable bilateral breast and regional lymphatic cancer with FiF technique

P15 Primož Peterlin (OI Ljubljana): Harnessing the wisdom of the crowd: risk estimate based on opinions of a team of dissenting experts

P16 Sašo Pulko (UKC Maribor): Connection between oncology information system and treatment planning system for optimazing the process of treatment planning

P17 Andrej Strojnik (OI Ljubljana): Clinical implementation of constant dose-rate VMAT in the Eclipse treatment planning system

P18 Manda Švabić Kolacio (KBC Rijeka): Validation of Monaco TPS Monte Carlo based calculation algorithm through Monte Carlo particle transport simulation

P19 Urša Beguš (Univ. Ljubljana): Urinary excretion rate of I-131 during treatment of benign thyroid diseases -- a pilot study

P20 Gašper Strnad (Univ. Ljubljana): Individual dosimetry of targeted radionuclide therapy for treatment of somatostatin receptor-positive GEP NET

P21 Urška Poje (Univ. Ljubljana): Daily quality control in digital mammography using quantitative image analysis

P22 Elena Hristovska (GOB Skopje): Comparing simultaneous integrated boost and sequential boost in laryngeal and parotid gland head and neck cancer patients

Members of the Alpe-Adria Medical Physics scientific committee:

Mirjana Budanec
Božidar Casar
Dario Faj
Stipe Galić
Hrvoje Hršak
Marija Jeremić
Slaven Jurković
Sona Kovacova
Gabriel Kralik
Renata Longo
Dushko Lukarski
Tibor Major
Pavol Matula
Ignasi Méndez
Ivana Mišković
Renato Padovani
Csilla Pesznyák
Primož Peterlin
Borislava Petrović
Mara Severgnini
József Varga
Uwe Wolff
Urban Zdešar
Brigitte Zurl

20 YEARS AGO, WE INVENTED SGRT

We're still the market leaders

There's a reason all 15 of the top 15 US News and World Report's 'Top Hospitals for Cancer' use Vision RT's AlignRT technology** to track patient position in real time.

It's the leading solution for accuracy and workflow efficiency — with more than 100 peer-reviewed publications, spanning a wide range of indications including DIBH, SRS, SBRT, extremities and more.

Find out more about our solutions for patient-centered treatment, featuring automatic beam-hold and accuracy down to the sub-half-millimeter.

visionrt.com/leaders

**Applications mentioned using Horizon camera are work in progress and will require additional purchase. Not currently cleared for sale in the US.*
***Based on US News & World Report's "2021-2022 Best Hospitals for Cancer".*

visionrt | Safety. Ingenuity. Community.

Contributions

AN OVERVIEW OF AAMP MEETINGS

Božidar Casar[1]

[1] *Institute of Oncology Ljubljana*

MR IN RADIATION TECHNOLOGY – A GAME CHANGER?

Dietmar Georg[1]

[1]*Medical University of Vienna, Department of Radiation Oncology*

ARTIFICIAL INTELLIGENCE: CHALLENGES FOR THE MEDICAL PHYSICISTS

Michele Avanzo[1]

[1]*Centro di Riferimento Oncologico di Aviano (CRO) IRCCS, Aviano(PN), 33081, Italy*

Purpose/Introduction

Artificial intelligence (AI) includes technologies aiming at giving machines or computers the ability to perform human-like cognitive functions such as learning, problem-solving and decision making. This presentation aims at describing the main AI applications in the medical physics field and the main challenges for the medical physicists.

Materials/Methods

AI systems based on machine learning or deep learning are currently used as a support for taking decisions in a clinical environment, and also support the specialist in the detection of abnormal tissues, in diagnosing diseases, in segmenting organs or lesions. Other applications include fast image acquisition, the improvement of image quality in diagnostic imaging, automated quality assurance of radiation devices, and automated planning of treatment in radiotherapy.

Results

The interest of the medical physicists' community in AI has increased dramatically in the last few years. Given their understainding of the physical processes at the basis of radiological sciences and their skills in data analysis, Medical Physicists can play a major role in the implementation of AI systems in clinical practice.

Discussion

In an environment where AI is used, the Medical Physicist's tasks include curation of input data, measuring how imaging acquisition parameters influence the response of AI systems, and designing quality assurance programs. Medical Physicists are also trained to prevent and analyze accidents by using risk assessment. Finally, as they will also contribute to the dissemination of this knowledge within their institutions by taking active role in education and training of other healthcare professionals. Efforts by medical physics organization are currently aimed at expanding their curriculum to include aspects of AI.

Conclusions

Medical Physicists are one of the key figures involved in safe implementation AI within a multidisciplinary team and, in exchange, AI will expand the MP's traditional tasks.

References

1. Zanca F, Hernandez-Giron I, Avanzo M, et al. Expanding the medical physicist curricular and professional programme to include Artificial Intelligence. Physica Medica 2021;83:174–83.
2. Avanzo M, Porzio M, Lorenzon L, et al. Artificial intelligence applications in medical imaging: A review of the medical physics research in Italy. Physica Medica Volume 83, March 2021, Pages 221-241.
3. Avanzo M, Wei L, Stancanello J, Vallieres M, Rao A, Morin O, et al. Machine and deep learning methods for radiomics. Med Phys 2020;47:e185–202. https://doi.org/10.1002/mp.13678

ON THE USE OF AI BASED AUTOCONTOURING TOOLS, A SINGLE INSTITUTION EXPERIENCE

Mihály Simon[1], Judit Papp[1], Emese Csiki[1], Árpád Kovács[1]

[1] *University of Debrecen Clinical Centre Clinic of Oncoradiology*

Purpose/Introduction

Manual segmentation of CT or MR images has been reported to most time-consuming process of radiation therapy and it can introduce inter- and intra-observer variability. Often some form of auto-segmentation is employed to mitigate these effects. Artificial intelligence (AI) has great potential to transform the clinical workflow of radiotherapy and has been implemented in image segmentation mainly in a supervised segmentation form. The aim of this presentation is to introduce a guideline-based image segmentation tool and share our experinece with it.

Materials/Methods

Convolutional neural network based auto segmentation models have been shown to increase consistency and efficiency in organ delineation. Supervised segmentation utilizes previous knowledge in form of training samples, using either public datasets or previously annotated user data. One of the pifalls of supervised segmentation could be an incorrectly trained model which results in consistently inccorrect contours. Another possible issue where these trained models could underperform is when a scan has artifacts either from an ICD, a dental implant or hip replacement. Furthermore due to surgery some patient has solitary parallel organs (kidneys, lungs, parotid glands). The University of Debrecen implemented the MVision AI tool in August 2020. MVision is a cloud based AI tool to annotate CT and MR images based on international guidelines eliminating these aforementioned pitfalls. Based on the gender and exam protocol MVision can automatically assign scans to appropriate model and auto-contour them. Scan are de-identified before send in accordance with GDPR regulations and contoured based on international contouring guidelines.

Results

Since August 2020 the Universitiy of Debrecen sent approximately 4600 scans to MVision. The detailed distribution of scans between models are shown in Figure 1.

Discussion

AI based segmentation can help to reduce the workload of clinical staff and brings consistency into organ delineation, however the quality assurance of such tools are not clearly established yet.

References

1. Y. Fu et al., "Artificial Intelligence in Radiation Therapy," in IEEE Transactions on Radiation and Plasma Medical Sciences, vol. 6, no. 2, pp. 158-181, Feb. 2022, doi: 10.1109/TRPMS.2021.3107454.
2. Liesbeth Vandewinckele et al., "Overview of artificial intelligence-based applications in radiotherapy: Recommendations for implementation and quality assurance" Radiotherapy and Oncology, Volume 153, 2020, Pages 55-66, ISSN 0167-8140, https://doi.org/10.1016/j.radonc.2020.09.008.

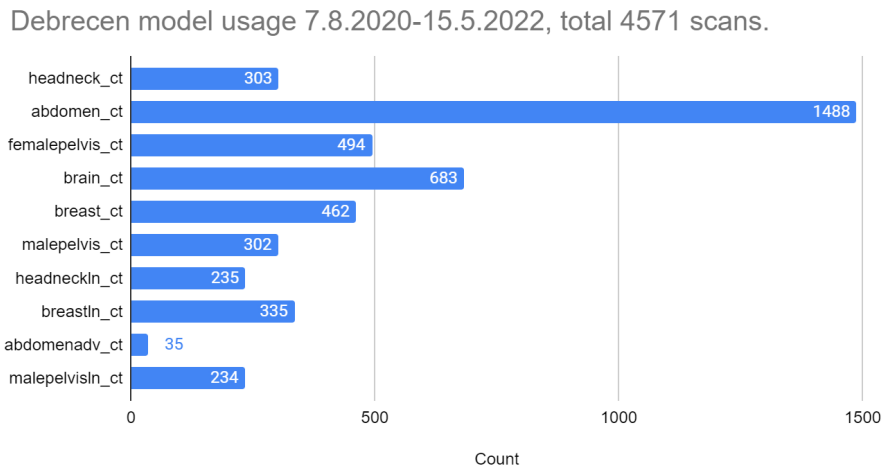

Fig.1: Total number of scans sent to MVision by the University of Debrecen by AI model.

SURFACE GUIDED RADIOTHERAPY: THE NEXT LEAP IN SAFETY AND QUALITY AFTER IGRT AND IMRT

Josh Naylor[1]

[1]*University Hospitals Dorset NHS Foundation Trust, United Kingdom*

Purpose/Introduction

Surface imaging has been rapidly adopted as a key tool for high quality image-guided radiotherapy - with benefits to both patient safety and quality of treatment. Between 2016 and December 2019 the number of Surface Guided Radiotherapy (SGRT) installations worldwide grew from 800 to 2000 [1].

A brief overview of how SGRT works will be given, as well as some of the benefits of its use such as: reduced set-up time; increased accuracy; error reduction; and real-time beam gating for both safety and enhanced functionality. Alternate applications of SGRT technology will be discussed, such as 4dCT scanning and verifying patient identity.

The various options for SGRT solutions from different manufacturers will be compared. The author's experience of commissioning multiple SGRT systems will be presented, as well as on-going quality assurance requirements. This will be placed in the context of the recent AAPM Task Group report 302 on SGRT [1] and can serve as a practical guide for physicists tasked with implementing SGRT in their centres.

The clinical experiences of the first year of using SGRT at the author's centre will be discussed, with data on how SGRT has impacted SABR lung treatments as well as case studies on a shell-free patient and the VisionRT postural video feature.

Advanced use of SGRT will then be covered, sharing plans for how the author's centre wish to use the technique in the future, as well as future developments of the SGRT market as a whole - including an exciting new technology that uses Cerenkov imaging to visualise surface radiation dose in real-time.

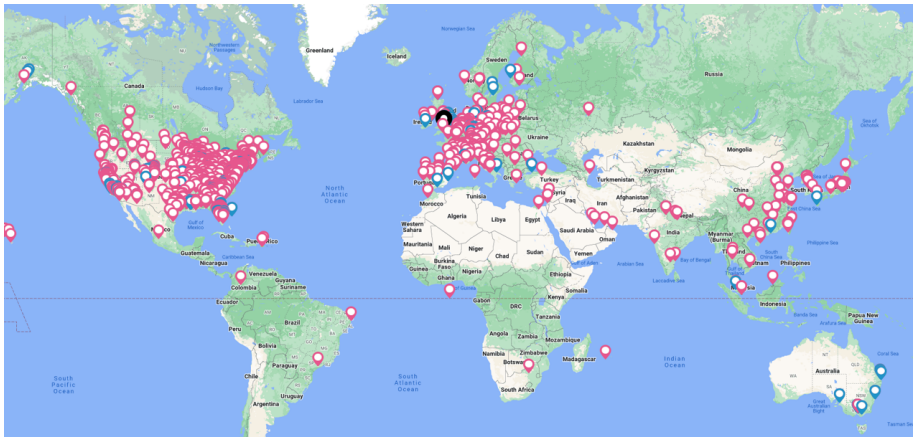

SGRT installations worldwide

The SGRT options available

References

1. Al-Hallaq HA, Cerviño L, Gutierrez AN, et al. AAPM task group report 302: Surface-guided radiotherapy. Med Phys. 2022;1-31. https://doi.org/10.1002/mp.15532

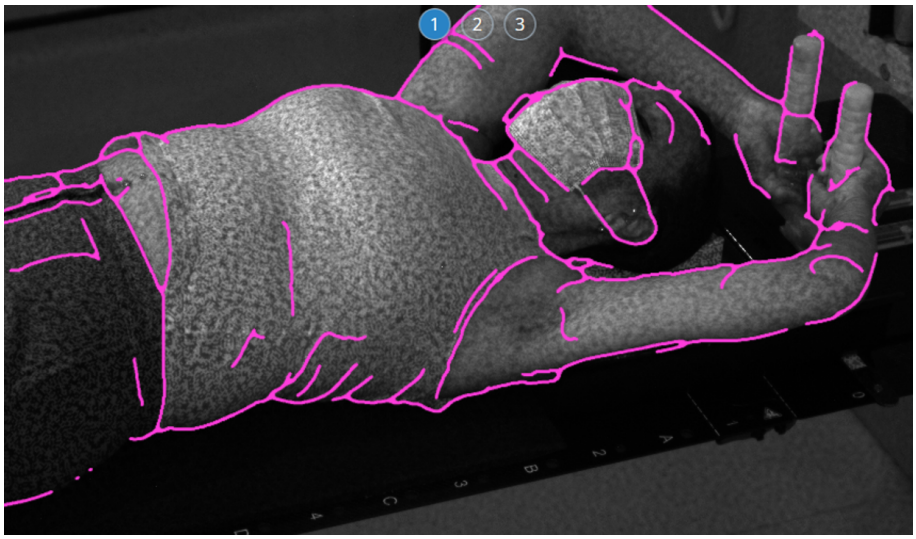

Postural video feature for patient set-up

CHANCES AND CHALLENGES OF A DUAL PARTICLE FACILITY

Markus Stock[1]

[1]*EBG MedAustron GmbH, Wiener Neustadt*

CHARACTERISTICS OF DETECTORS FOR RELATIVE DOSIMETRY IN SMALL FIELDS

Božidar Casar[1]

[1]*Institute of Oncology Ljubljana*

VERIFYING INTENSITY MODULATED RADIOTHERAPY TREATMENT DOSE DELIVERY THROUGH A NATIONAL AUDIT

Slaven Jurković[1], Đeni Smilović Radojčić[1], David Rajlić[2], Manda Švabić Kolacio[2], Nevena Obajdin[2]

[1]Medical Physics Department, University Hospital Rijeka, Rijeka, Croatia; Department of Medical Physics and Biophysics, Faculty of Medicine, University of Rijeka, Rijeka, Croatia
[2]Medical Physics Department, University Hospital Rijeka, Rijeka, Croatia

Purpose/Introduction

Various types of independent audits in radiation oncology may contribute to improvements of local quality assurance systems and clinical practice. Particularly, dosimetry audits may be a tool for verification of treatment planning system (TPS) modelling and treatment delivery. The audit methodology should be feasible to be performed at different sites, on different devices and equipment used. As such it should not be too complex and time consuming, but it should be as accurate as required by international recommendations. Therefore, such methodology should be carefully developed and verified in experimental conditions.

During the past 15 years, Medical Physics Department of University Hospital Rijeka has organized several national audits related to radiation oncology. Early ideas were actuated by the IAEA Quality Team in Radiation Oncology (QUATRO) which carried out an official IAEA audit at University Hospital Rijeka in 2007. Therefore, the survey related to quality control practice [1] and national audit dedicated to equipment quality control were organized and conducted [2]. A step forward was national dosimetry audit of treatment planning systems [3]. Results of both audits were related to the IAEA projects "CRO6008 Upgrading the Quality Assurance and Quality Control Programmes in Radiotherapy" and "CRO6010 Reinforcing and Further Developing a Quality Assurance/Quality Control Programme in Radiotherapy" which were performed as joint ventures of medical physics departments of UH Rijeka and UH Osijek. During 2014. audit related to administrative part of QA/QC system in radiation oncology was performed nationwide. The aim was to introduce updated QA/QC protocols released by the State office of Radiation and Nuclear Safety to build capacities of the national quality system. This was also one of activities of the IAEA project "CRO6012 Developing a Quality Assurance and Quality Control Programme for the Clinical Use of Advanced Radiotherapy Techniques".

Advanced radiotherapy techniques require rigorous absorbed dose delivery validation. The procedures should be developed, experimentally verified, and incorporated in a comprehensive quality assurance programme via commissioning and regular patient pre-treatment verification of the absorbed dose distributions. Methodology developed and results acquired within the scope of the recent IAEA project CRO6019 "Verifying Intensity Modulated Radiotherapy Treatment Dose Delivery - Method Development, Standardization and Implementation through a National Audit" will be presented.

Of the five radiation oncology centres in Croatia where intensity modulated radiotherapy (IMRT) and/or volumetric arc therapy (VMAT) are performing, four participated. These centres use different devices, systems, and methodologies for absorbed dose delivery and pre-treatment verification. At present, a discrepancy between the advantages that advanced techniques offer, and inter-institutional standardization required for achieving similar levels of radiation therapy delivery quality exists countrywide.

The aims of the audit were to analyse different types of absorbed dose distributions in terms of quality and deliverability, and to validate whether in-house pre-treatment verification results correlate to those of an external audit.

Materials/Methods

Carrying out a national audit can be divided in numerous parts: in-house development and verification of comprehensive methodology to be applied for on-site audit, assembling a questionnaire on application of advanced radiation oncology techniques, measurement and acquisition of data through on-site auditing, validation of data acquired during the audit and creation of guidelines and recommendations.

The in-house measurements were carried out using 6 MV X-ray beam with flattening filter. Dose calculations were performed using Monte Carlo (MC) based dose calculation algorithm built in the Elekta Monaco (ver. 5.11) treatment planning system. The algorithm provides two options of absorbed dose reporting referred to as dose to medium (in medium), and dose to water (in medium). All calculations for this research were performed as dose to medium [4-6]. Dose measuring systems used for methodology development were PTW Octavius 4D and IBA Matrixx. The Octavius (FigureÂ 1) consists of a cylindrical, rotational phantom along with a 2D array with 1405 detectors. An external inclinometer mounted on the gantry provides dose measurements as a function of gantry angle keeping the 2D array perpendicular to the beam axis. The central chamber of the array was cross calibrated with a PTW Semiflex ionization chamber.

The dose measuring system used for the audit was the IBA Matrixx 2D with 1020 ionization chambers (Figure 2) along with IBA MultiCube phantom. This system was chosen due to its feasibility for transportation between sites. Also, it is robust, straight forward, and easy to calibrate on-site. In house calibration of the 2D detector in absorbed dose was performed using measurements obtained by Farmer-type ionization chamber in water phantom.

As a part of commissioning of both dose measuring systems the output factors were measured for field sizes, from 1×1 cm^2 to 25×25 cm^2, and linearity was examined for MU settings ranging from 1 to 500 MU.

Central part of the methodology development was to correlate 3D and 2D verification approaches to be applied for the audit. Therefore, multiple comparisons between dose measuring systems were performed. That includes square fields, multiple pyramid shape fields and dose distributions of ten IMRT patient plans for three anatomical sites: head and neck, central nervous system, and prostate.

The measured dose distributions were obtained in stationary (beams at zero gantry angle - perpendicular composite) and rotational (each delivered beam with different gantry angle is perpendicular to the detector array - true composite) modes using the Octavius phantom. The Octavius reconstructed and Monaco calculated dose matrices were compared using 2D and 3D gamma analysis with 2%/2mm, 3%/2mm and 3%/3mm tolerance criteria and 10% dose threshold. For the IBA Matrixx system only 2D gamma analysis was used with the same tolerance criteria, measured and calculation dose distributions were obtained with fixed gantry angle.

Additionally, point dose measurements at isocenter in Octavius phantom were performed using the Pinpoint ionization chamber. Measured values were compared with absorbed dose calculated using the MC based calculation algorithm in Monaco TPS as well as with measured values acquired using the Octavius system.

The main drawback of 2D array systems is relatively low resolution, especially when measuring highly modulated absorbed dose distributions. In contrast, radiochromic film has superior spatial resolution while retaining absorbed dose measurement accuracy. In order to exploit this advantage, radiochromic film dosimetry methodology [7] was also implemented during the audit. EBT3 film was used as a reference 2D dosimeter to assess the accuracy by which the 2D array performs the dose plane reconstructed in the phantom. The film was placed on top of the Octavius/Matrixx detectors inside the respective phantom.

Results

Figure 3 shows the difference of 2D arrays and Semiflex ionization chamber measurements assessing the detector linearity. The absolute dose measurements as a function of MU agree within 0.07% above 5 MU, and the differences not exceed 1.4% for more than 1 MU. The regression coefficient between ionization chamber measured values and Octavius/Matrixx measured values was R^2=0.999998 and R^2=0.999999 respectively.

The comparison of measured and calculated output factors are shown at a lower part of Figure 3. The measured output factors were found to be within a range of 2% when compared to the ionization chamber measurements and Monaco calculations for field sizes larger than 2×2 cm^2. The largest discrepancies were observed for field size 1×1 cm^2, especially for the Matrixx measurement.

In this study, comparison of gamma analysis results and dose reconstruction algorithms of Octavius Verisoft and IBA Matrix OmniPro was performed using a series of test procedures. The comparison between calculated and reconstructed dose measurement with Octavius and Matrixx system of a "pyramid"-like delivery (composed of 5 field-in-field shapes) is shown in Figure 4.

The both dose profiles show very good agreement with a 2D gamma passing rate higher than 99% for both 2D arrays, using 2%/2mm tolerance criteria .

Gamma analysis for IMRT dose distributions for three anatomical sites H&N, CNS and prostate are shown in Figure 5.

Discussion

The global gamma analysis was employed with three different tolerance criteria (3%/3mm, 3%/2mm, 2%/2mm) and 10% threshold. The gamma index was calculated for the Matrixx planar (2D) gamma (perpendicular composite), both Octavius cases (perpendicular composite and true composite), Octavius volumetric (3D gamma and true composite) and 2D film (perpendicular composite) dose distributions. The ANOVA test showed a statistically significant difference of gamma index values only for 2%/2mm tolerance criteria. 2D gamma index for perpendicular composite delivery for Octavius is significantly different with p=0.003216, p=0.003973, p=0.003702 and p=0.000118 when compared to 2D matrixx, 2D and 3D volumetric Octavius true composite and 2D gamma index for film, respectevily.

The comparison of the results of PinPoint dose measurements with measured values acquired using the Octavius system shows agreement within 2% (1.33±0.62%). The comparison between MC Monaco absolute dose calculations and measurements obtained with the Octavius 2D array system show the similar agreements, within 3% (1.43±0.89%). The inferior agreement was found when compared measurement with Matrixx and calculated values, up to 6% (3.88±2.11%). Agreement of film measurement and calculated values was within 3% (1.57±0.56%).

Conclusions

Experimental comparison of detectors revealed that 2D ionization chambers array system can provide sufficient accuracy of dose delivery and it is therefore suitable for audit measurements. To acquire data with better resolution, radiographic film is introduced as additional detector.

References

1. Švabić M, Jurković S, Faj D, Kasabašić M, Smilović Radojčić Đ, Ivković A (2008). Practices of radiotherapy equipment quality control in radiotherapy centres in Croatia. Collegium Antropologicum 32(S2):217-219.

Figure 1: Verification System OCTAVIUS 4D: OCTAVIUS detector 1500, motorized cylindrical phantom and VeriSoft patient plan verification software.

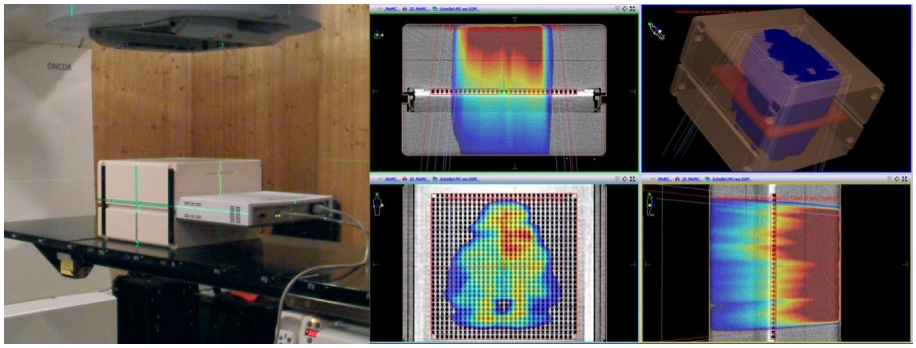

Figure 2: Verification system IBA Matrixx, MultiCube phantom and IBA OmniPro I'mRT+ verification software.

2. Jurković S, Diklić A, Kasabašić M, Radojčić Đ, Švabić M, Ivković A, Faj D (2011). Survey of equipment quality control in radiotherapy centres in Croatia: First results. Archives of Industrial Hygiene and Toxicology, 62(3):255-260.
3. Jurković S, Švabić M, Diklić A, Smilović Radojčić Đ, Dundara D, Kasabašić M, Ivković A, Faj D (2013). Reinforcing of QA/QC programs in radiotherapy departments in Croatia: Results of treatment planning system verification. Medical Dosimetry 38(1):100-104.
4. Radojčić Đ, Kolacio M, Radojčić M, Rajlić D, Casar B, Faj D, Jurković S (2018). Comparison of calculated dose distributions reported as dose-to-water and dose-to-medium for intensity-modulated radiotherapy of nasopharyngeal cancer patients. Medical Dosimetry 43(4):363-369.
5. Radojčić Đ, Casar B, Rajlić D, Kolacio M, Méndez I, Obajdin N, Debeljuh D, Jurković S (2020). Experimental validation of Monte Carlo based treatment planning system in bone density equivalent media. Radiology and Oncology 54(4):495-504.
6. Kolacio M, Brkić H, Faj D, Radojčić Đ, Rajlić D, Obajdin N, Jurković S (2021). Validation of two calculation options built in Elekta Monaco Monte Carlo based algorithm using MCNP code. Radiation Physics and Chemistry 179:109237.
7. Méndez I, Rovira-Escutia J, Casar B (2021). A protocol for accurate radiochromic film dosimetry using Radiochromic.com. Radiology and Oncology 55(3):369-378.

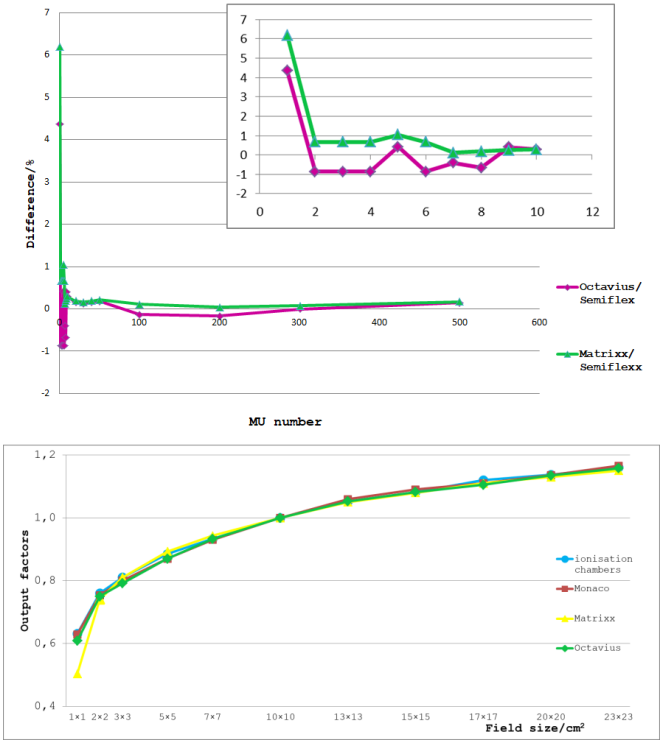

Figure 3: Basic characteristics of the Matrixx and Octavius 2D array measurements in respective phantoms, showing comparison of 2D array and ionization chamber measurements assessing the detector linearity (upper), the field size dependence, showing the output factors measured with ionization chambers (PinPoint and Semiflex), OCTAVIUS, Matrixx and calculated with Monaco MC TPS (lower).

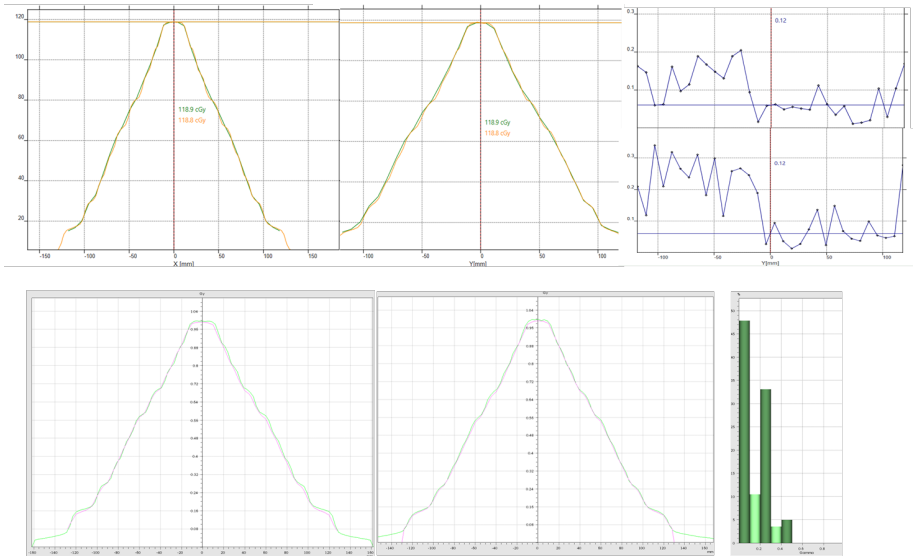

Figure 4. Dose profile comparison between Monaco calculated dose and reconstructed dose measurements with IBA Matrixx (upper) and PTW Octavius (lower) for static pyramid test.

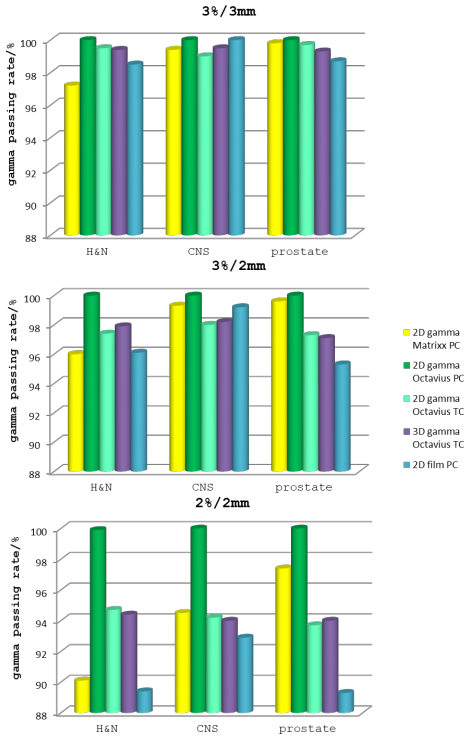

Figure 5. Results of the gamma analysis for three IMRT dose distributions (H&N, CNS and prostate). The gamma index was calculated as planar (2D) gamma for Matrixx (perpendicular composite), both optons for Octavius (perpendicular composite and true composite), volumetric (3D gamma) for Octavius (true composite) and 2D gamma for film (perpendicular composite) dose distributions.

GOTTFRIED SPIEGLER (1891-1970) & MEDICAL PHYSICS IN AUSTRIA 1897-1938

Werner F. O. Schmidt[1]

[1]*Austrian Society for Medical Physics (ÖGMP), Vienna, austria*

Purpose/Introduction

In this work I take a look back in history - medical physics 100 years ago /1/. After discovery of X-rays and radioactivity in the fall of the 19th century regulations on their use in medicine were completely missing, demonstrated by many accidents - hundreds to thousands of them even lethal. Reasons were not only radiation, but also mishandling of high voltages, exploding tubes, poisonous chemistry etc.

The medical profession "roentgenologist" was not established before the 1920's, so every doctor could "play" with units often without understanding them physically and technically, trying to make good images and/or therapies. X-ray units were often produced by small factories, specialised only on parts (e.g., tubes) of the complete system. Knowledge on radiation protection had to be developed in many steps often driven by "experiences on patients and personal". Also missing: international agreements on activity- and dose-units of radiation. From today's point of view it was an "anarchic period of learning".

At the university of Vienna physicians were studying these innovations also. One of them was Guido Holzknecht (1872-1931). He built up a new department, was active in research and education and tried to set up the profession "roentgenologist". He was open to technical advancements, developed a "chromoradiometer", based on color changes of different salts as "radiation measurement device", and introduced a dose unit "H" to quantify radiation dose. In different papers in the 1920s he also complained on missing technical and physics experience in roentgenology /2/.

So, following a paper of Isaak Hirsch in 1927 /3/ he formulated criteria for correct technical use of X-rays including radiation protection. It became clear that these topics exceeded knowledge and qualifications of medical doctors. So he set an important step for future medical physics!

Materials/Methods

From the times bevor World War I a law in Austria existed concerning to issue certificates by legally accepted, non-governmental institutions ("Versuchsanstalten"), esp. in technical matters. So in 1927 the "Röntgentechnische Versuchsanstalt" was established "to review and certify Roentgen units (incl. tubes), measurement devices as well as films and its chemistry including contrast agents" in a "strong scientific examination" /4/. First head of the institute was Gottfried Spiegler. But who was Gottfried Spiegler?

Gottfried Spiegler (1891-1970), born in Berlin, grew up in Vienna. His father was medical doctor, his mother "member of the cultural Viennise society". He studied physics in Vienna, interrupted by World War I when he was "wireless radio operator" in the Austrian army. During a sudden army retraction he lost papers of his thesis and had to reconstruct it "from memory". He received his doctorate in 1919, in 1922, 100 years ago, he joined Holzknechts institute as a scientific staff member, in 1927 he became head of the new "Röntgentechnische Versuchsanstalt". In this year Holzknecht described his work as: "Since 30 years industry and medicine have to work together but often this leads to unsatisfactory results. They are too different and need an `interpreter', equipped with a `Janus-Head' able to look in both directions".

The role of this "interpreter" was dedicated to Gottfried Spiegler /4/.

Results

Specialists for X-rays as well as for radioactivity (handling and "radium-treament") were rare, regulations not available, but Spiegler started his work - in quite miserable conditions, eg missing rooms, measurement devices and money. Nevertheless in the next decade he built up an active working group (1938 10 staff members). Additional challenges came from a second cancer center in Vienna ("Wien-Lainz") dealing esp. with radium-treatments requiring knowledge of radiochemistry. His work and contributions in this time are documented in more than 30 papers dealing with roentgenology as well as radiation technics and physics. He was a specialist in handling and extracting informations from films (see also his late work /5/), he developed Radium standard-sources to check chambers and introduced chamber measurements with hearable "clicks" after a certain dose interval to check not only dose but also dose-rate. These developments were published in an anniversary documentation in 1938 /6/. One of these instruments, a "Film-Sharpness Meter", developed by two members of his staff (Juris & Rudinger) is shown in the Virtual Museum of Medical Physics from the AAPM (https://museum.aapm.org/).

Discussion

But in March 1938 Austria was occupied by Hitler, Spiegler lost his job and had to emigrate to the UK in 1939. He was supported there by the SPSL ("Society for Protection of Science and Learning", see, e.g., https://en.wikipedia.org/wiki/Council_for_At-Risk_Academics). Letters, requests, job applications etc. of Spiegler are stored there and still available. 3 troublesome and frustrating years without possibilities to work in radiology are documented. Fortunately in 1942 he was recruited by the Royal Marsden Cancer Hospital in London and worked there until 1956 esp. in radiology but also with new developments like high-energy units. Additionally to many publications he published his book "Physikalische Grundlagen der Röntgendiagnostik" in 1957 /5/. 1943 he was also cofounder of the HPA (Health Physics Association; today IPEM /7/).

Conclusions

Spiegler did not return to Vienna after war but his work was recognized esp. by Roentgen societies in Austria and Germany. In 1966 he was honoured on his 75 birthday /8/, in 1967 he received the Roentgen-medal in Remscheid/Ger. After his death in 1970 W. V. Mayneord published an impressive obituary /9/ on him.

In a lecture Spieglers life esp. from 1922-1938 and his contributions to roentgenology and radiation physics will be presented as well as a short look on his coworkers and their ways before and after 1938.

References

1. Schmidt W (2021). Gottfried Spiegler. Strahlenschutz Aktuell 55(2):21-55.
2. Angetter DC (2012). Guido Holzknecht: Pionier der Röntgenologie. Strahlenschutz Aktuell 46(2):26-34.
3. Hirsch IS (1927). Physikalisch-technische Grundlagen der Röntgentherapie. Verlag Julius Springer.
4. Holzknecht G (1928). Die Röntgentechnische Versuchsanstalt des Vereins Elektrotechnische G. Spiegler Versuchsanstalten in Wien. Fort Röntgenstr 37:866-872.
5. Spiegler G (1957). Physikalische Grundlagen der Röntgendiagnostik. Stuttgart: Georg Thieme Verlag.
6. Kienböck et al (1938). Das 10-jährige Bestehen der Röntgentechnischen Versuchsanstalt Wien. Sonderdruck Fort Röntgenstr 57(1):1-23.
7. Haggith JW (1983). History of the Hospital Physicists' Association. Northumberland Press.

8. Walther KM (1966). Lebensbild Gottfried Spiegler 75 Jahre. Münch Med Woschr 24:1307.
9. Mayneord WV (1970). Obituary Dr. G. Spiegler. Br J Radiol 43:503.

Gottfried Spiegler (1938).

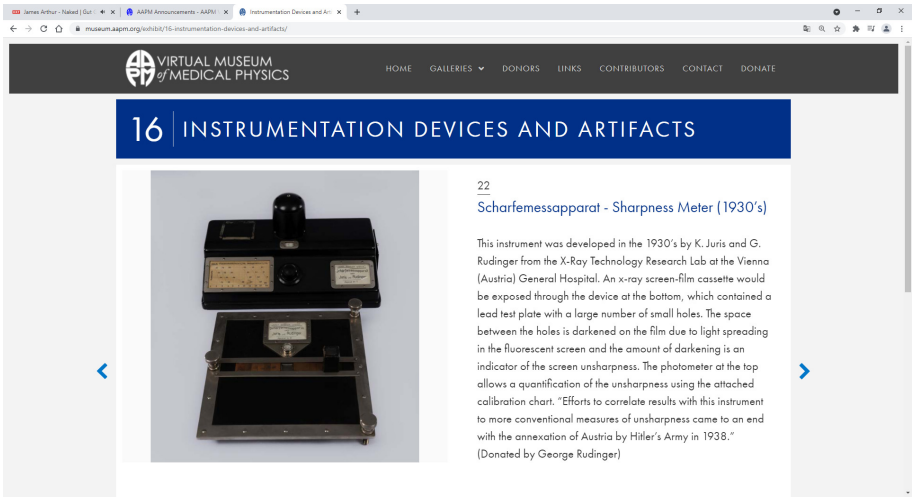

"Film-Sharpness Meter", developed by two members of Spiegler's staff (Juris & Rudinger) is shown in the Virtual Museum of Medical Physics from the AAPM.

Gottfried Spiegler (1966).

ADVANCE ON IMAGE PROCESSING AND OPTIMIZATION PROCEDURES IN SPECT/CT IMAGING

Dea Dundara Debeljuh[1], Ivan Pribanić[2], Slaven Jurković[2]

[1]Medical Physics Department, University Hospital Rijeka, Rijeka, Croatia Radiology Department, General Hospital Pula, Pula, Croatia Department for Medical Physics and Biophysics, Faculty of Medicine, University of Rijeka, Rijeka, Croatia
[2]Medical Physics Department, University Hospital Rijeka, Rijeka, Croatia Department for Medical Physics and Biophysics, Faculty of Medicine, University of Rijeka, Rijeka, Croatia

Purpose/Introduction

Hybrid SPECT/CT imaging systems used in nuclear medicine necessitate imaging data assessment and optimization of imaging procedures. Development of advanced independent image processing, post-processing and analysis procedures can considerably contribute to the efficiency and comprehensiveness of the quality programme. Once system performances are quantitatively validated and relevant physical parameters are calculated, methodology related to the optimization of respective medical procedures could be performed to enhance quality of imaging data. Medical Physics Department of the University Hospital Rijeka has long history of dealing with quality system related to application of ionizing radiation in medicine. An advanced parts of the system are developed with International Atomic Energy Agency (IAEA) support under projects of technical cooperation. Therefore, abovementioned activities are planned to be performed under the IAEA project CRO6021: The Implementation of advanced quality assurance and quality control (QA/QC) programme in nuclear medicine. The project is led by the Medical Physics Department of the University Hospital Rijeka and will be conducted during the 2022-2023. Associate institution is General Hospital Pula, Croatia. Initial results can be divided in two parts: one concerning advanced image processing algorithms dedicated to the evaluation of essential physical parameters, as intrinsic uniformity, modulation transfer function (MTF), spatial resolution, and acquisition time optimization. Development of independent algorithms require understanding of respective physical principals and mathematical models which enable control of calculation process. The second part is dedicated to the optimization of the Myocardial Perfusion Imaging (MPI) in two collaborating hospitals. Assessment of different imaging device-reconstruction algorithm-correction combinations using an anthropomorphic phantom was performed through evaluation of spatial resolution and contrast-to-noise ratio.

Materials/Methods

Algorithms for image processing, post-processing and analysis were developed using various open-source Python libraries. Herein, Numpy was used for image manipulation and pixel related calculations like filtering both in spatial domain and in Fourier space. Matplotlib was used to visualize the image matrix, and Scipy was used for curve fit in modelling of intrinsic image of point source field. Pydicom was used for DICOM image modifications, particularly for access and manipulation of DICOM header elements. Furthermore, Scikit-image was used mostly for development of image reconstruction algorithm, as it supports Radon and inverse Radon image transformations and several image filters. Finally, a general image processing and analysis toolkit, the SimpleITK, was used for image processing operations. Jaszczak phantom (Data Spectrum Corporation) images, multiple head registration/centre of rotation (MHR/COR) phantom images with five point-sources and single point-source images were used for development and validation of own algorithms. For experimental part of the investigation related to the optimization of the MPI procedure an anthropomorphic torso

phantom with myocardium, lungs, liver and the spinal cord (Data Spectrum Corporation) was used. Imaging was performed by one conventional Symbia T2 (Siemens Healthineers) with low energy high resolution collimator, and one advanced Symbia Intevo Excel (Siemens Healthineers) with IQ SPECT and SmartZoom collimator. Biodistribution of 99mTc-tetrofosmin in the body was simulated (1): 0.083 MBq/mL in left ventricular (LV) wall, 0.004 MBq/mL in the inner chamber, 0.050 MBq/mL in the liver and 0.004 MBq/mL in the chest. Acquisition protocols defined during preparation of the system for clinical use were used (table in Fig. 1). Images acquired by conventional device were reconstructed using standard FBP algorithm and, additionally, using the IR algorithm with/without scatter correction. IQ SPECT acquisitions involved both the SPECT and CT acquisitions. In the later, imaging data were reconstructed using advanced IR algorithm either with both SC and AC or correction free. Reconstruction parameters are shown in table in Fig. 1. Overall, five MPI systems were considered: conventional SPECT device with FBP (Symbia-FBP), conventional SPECT device with IR (Symbia-IR), conventional SPECT device with IR and SC (Symbia-IR-SC), IQ SPECT device with AIR, SC and AC (IQ-AIR-SC-AC) and correction free IQ SPECT device with AIR (IQ-AIR). Transaxial slices were realigned according to cardiac orientation to obtain short-axis slices. Short-axis image evaluation was performed through physical image quality descriptors (1, 2): LV wall thickness, sharpness index and contrast between the LV wall and the inner chamber. According to phantom specification, the wall thickness is 1 cm. The assumed sharpness index and contrast of an ideal detector are 1 and 100%, respectively.

Results

An independent algorithm for integral intrinsic uniformity calculation of the point source close to detector (less than 2 FOV) was developed. The algorithm follows National Electrical Manufacturers Association (NEMA) standards with addition of curvature correction procedure (Fig.2). Intrinsic uniformity results calculated by the SPECT system software were found to be, on average, 2% lower than the ones calculated with developed algorithm. An algorithm to calculate MTF for SPECT system using point source images was also developed. It extracts experimentally determined point-spread function from point source image and calculates its representation in a Fourier domain. Moreover, a spatial resolution analysis of MHR/COR phantom images is enabled using additional algorithm which locates point sources placed in the phantom. It fits the Gaussian function in x and y directions and calculates the full width at half maximum (FWHM) values as a measure of tomographic spatial resolution. Furthermore, a FBP reconstruction algorithm for SPECT imaging was developed. Current version of the algorithm supports Ramp, Shepp-Logan, Cosine, Hamming and Hann image filters (3). Complementary to a FBP reconstruction algorithm, an algorithm supporting iterative reconstruction of tomographic images was implemented using open-source program TomoLab (Fig. 3). Nuclear medicine imaging procedures are characterized by long acquisition times required to attain appropriate count statistics and consequently better reconstructed image quality (4). Hence, the possibility of acquisition time optimization is also investigated and a noise invariant algorithm to simulate reduced time acquisition was developed. The algorithm uses a Bernoulli trial method on a pixel-wise level to ascertain which pixel values to hold in an output image thus creating a simulated reduced time image from full-time images with preserved noise statistics (5, 6). The simulated images were validated against reduced time planar images of 57Co uniform flood source. If image quality of a reduced acquisition time images is found to be diagnostically acceptable, the acquisition time can be modified. An evaluation of MPI systems was performed analysing different image quality descriptors. Results for LV wall thickness, sharpness index and contrast between the left ventricular (LV) wall and the inner chamber are shown in the table in Fig. 4. Differences between types of MPI systems in terms of wall thickness and contrast between the left ventricular (LV) wall and the inner chamber could be also visually evaluated (Fig. 5).

Discussion

Objective verification of various QC parameters necessitates an independent evaluation. Therefore, an in-house system tailored to specific requirements is developed. The discrepancy between results obtained by own algorithm and system intrinsic uniformity results seems systemic and is attributed to different weighting factors used by the manufacturer in the NEMA filtering step or due to use of the near-field model for intrinsic uniformity image, enabling better fit and consequently curvature corrections. Intrinsic uniformity verification algorithm is already implemented in regular QC procedures and reference values are established. Independent reconstruction algorithms enable objective validation of SPECT system reconstruction performance. Moreover, they enable reconstruction of images independent of the SPECT system used for imaging or developed (simulated) virtually. Furthermore, using independent software for reconstruction enables an inter-system reproducible SPECT quantification of the activity (4). An in-house noise invariant algorithm to simulate reduced time acquisition was developed to investigate image quality acquisition time dependency. Its application will be subject of further investigation. MPI system characterization shown superiority of hybrid IQ-AIR-SC-AC in terms of image analysis of spatial resolution and contrast-to-noise ratio. A deterioration of image quality was observed if corrections free IQ SPECT is used, resulting in performances comparable to those of conventional systems. Image quality of conventional systems increases when passing from standard FBP to IR, and from IR to IR with scatter correction. Further investigation will be dedicated to simulations of pathological heart with perfusion defect.

Conclusions

Development of independent image processing algorithms may enable validation of respective quality control parameters, increase the quality of reconstructed imaging data and, therefore, enable additional relevant information. Additionally, a characterization of imaging systems through an evaluation of imaging data is a prerequisite for successful optimization process.

	Symbia T2			Symbia Intevo Excel	
Collimator	LEHR			SmartZoom	
Matrix size	64×64			128×128	
Zoom	1.45			1	
Pixel size	6.6			4.8	
Detectors	Both detectors			Both detectors	
Number of projections	64			34	
Starting angle	45			59	
Degrees of rotation	90			104	
Detector configuration	90			76	
Orbit	Non Circular Orbit			Cardio-Centric	
Energy window	Single energy window: photopeak Dual energy window: photopeak and lower scatter			Dual energy window: photopeak and lower scatter	
Computed tomography	-			130 kV, reference 55 mAs (Care Dose 4D), collimation 2×4 mm, pitch 1.0, slice 5 mm	
Reconstruction algorithm/correction	FBP	IR	IR-SC	AIR-SC-AC	AIR
Reconstruction parameters	Butterworth filter: cut-off 0.4, order 5	15 iterations, 8 subsets, 13.2 mm Gaussian post-filter		10 iterations, 3 subsets, 10 mm Gaussian post-filter	

Figure 1: Acquisition and reconstruction parameters used in MPI for conventional and advanced systems.

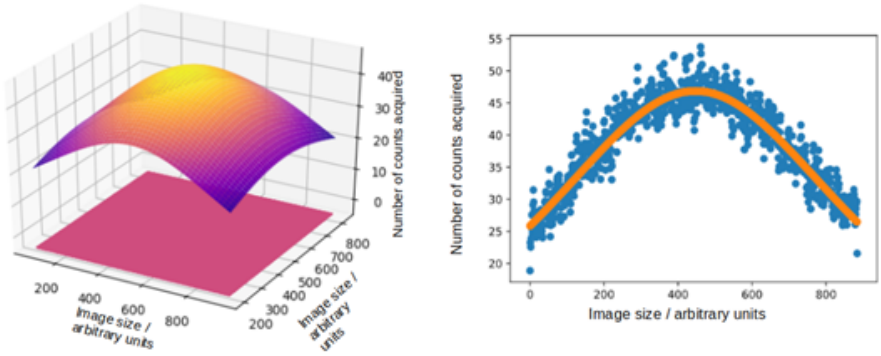

Figure 2: Model of near field (left) imaged using 99mTc point-source and detector without collimators and a fit of the model to the measurements (right).

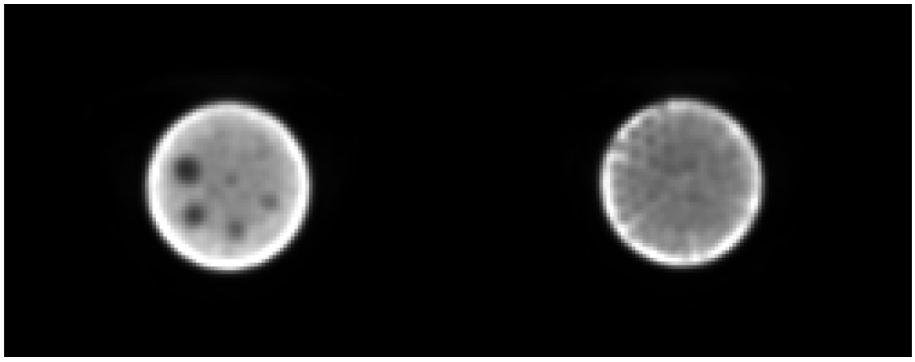

Figure 3: Iterative reconstruction achieved using independent open-source TomoLab code. Images show axial plane section of Jaszczak phantom showing “cold” spheres and “cold” rods section.

References

1. Zoccarato O, Scabbio C, De Ponti E, Matheoud R, Leva L, Morzenti S, Menzaghi M, Campini R, Claudio Marcassa, Del Sole A, Garancini S, Crivellaro C, Brambilla M, Lecchi M. Comparative analysis of iterative reconstruction algorithms with resolution recovery for cardiac SPECT studies. A multi-center phantom study. J Nucl Cardiol 2014;21(1):135-48. https://doi.org/10.1007/s12350-013-9821-0. Epub 2013 Nov 23.
2. Imbert L, Poussier S, Franken PR, Songy B, Verger A, Morel O, Wolf D, Noel A, Karcher G, Marie P-Y. Compared Performance of High-Sensitivity Cameras Dedicated to Myocardial Perfusion SPECT: A Comprehensive Analysis of Phantom and Human Images. J Nucl Med 2012; 53(12):1897-1903. https://doi.org/10.2967/jnumed.112
3. Gonzalez R, Woods R. Digital image processing. Pearson, 2018.
4. Peters S, van der Werf N, Segbers M, van Velden F, Wierts R, Blokland K, Konijnenberg M, Lazarenko S, Visser E, Gotthard M. Towards standardization of absolute SPECT/CT quantification: a multi-center and multi-vendor phantom study. EJNMMI Phys 6, 29 (2019). 10.1186/s40658-019-0268-5
5. De Nijs R. Comment on: ‘A Poisson resampling method for simulating reduced counts in nuclear medicine images’. Phys Med Biol 60, 5711–5715 (2015). 10.1088/0031-9155/60/14/5711
6. White D, Lawson R S. A Poisson resampling method for simulating reduced counts in nuclear medicine images. Phys Med Biol 60, N167–N176 (2015). 10.1088/0031-9155/60/9/N167

MPI system	Wall thickness (cm)	Sharpness index (cm^{-1})	Contrast between LV wall and inner chamber (%)
Symbia-FBP	2.52±0.03	0.48 ±0.01	47.00±1.09
Symbia-IR	2.31±0.06	0.51±0.01	57.44±1.41
Symbia-IR-SC	2.14±0.05	0.56±0.01	63.76±1.41
IQ-AIR-SC-AC	1.97±0.04	0.64±0.01	70.34±1.22
IQ-AIR	2.44±0.04	0.51±0.01	54.28±1.15

Figure 4: Results for LV wall thickness, sharpness index and contrast between the LV wall and the inner chamber for different MPI systems.

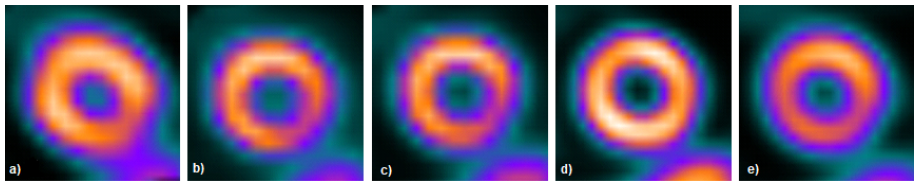

Figure 5: Short-axis images obtained by different MPI systems: Symbia-FBP (a), Symbia-IR (b), Symbia-IR-SC (c), IQ-AIR-SC-AC (d) and IQ-AIR (e).

RADIATION PROTECTION CLASSIFICATION OF HEALTHCARE PERSONNEL AT THE TRENTO PROTON THERAPY CENTER

Carlo Algranati[1], Stefano Lorentini[1], Ilenia Giovannini[1], Trianni Annalisa[2]

[1]*U.O. Protonterapia, APSS-Trento*
[2]*U.O. Fisica Sanitaria, APSS-Trento*

Purpose/Introduction

At the Trento Proton Therapy Center, proton beams in pencil beam scanning mode with a maximum energy of 230 MeV are accelerated, used for clinical applications and related quality controls. The system consists of a cyclotron room (not accessible to healthcare personnel), an experimental room (with occasional access), and two treatment rooms called Gantry 1 and Gantry 2, each with a control room called T.C. Room 1,2 (Fig. 1). The Gantry rooms are used to deliver radiant treatments with protons. Quality controls, which consist of quality checks of the equipment and checks to verify the treatment plans delivered to patients, are also performed. This work aims to present the radioprotection classification of the personnel performed on the group of operators of the Center consisting of physicians, medical physicists, technicians (a clinical group and a physics group) and nurses.

Materials/Methods

A workload of 500 treatments per year is estimated, with up to 50 patients per day (25 per gantry). Patient-specific quality controls are carried out for each treatment plan (about 700 plans/year considering boost treatments). In addition quality controls of the equipment are required by current Italian legislation and are performed by medical physicists and technicians the physics group. The radiation sources considered are the following: treatment nozzle (range shifter), patient, patient QA phantoms, water-phantom, Argon cloud in the gantry rooms. A uniform distribution of the personnel in the various tasks can be assumed based on the declared workload. The contributions of the various sources are described in Tab. 1 and are based on measurements or calculations.

Conclusions

Based on the evaluations, physicians, medical physicists and nurses receive above 0.5 mSv/year whereas technicians receive about 2 mSv/year (Tab. 2). Therefore all personnel involved in managing patients inside the gantry are classified B according to Italian Law (1).

References

1. DECRETO LEGISLATIVO 31 luglio 2020, n. 101

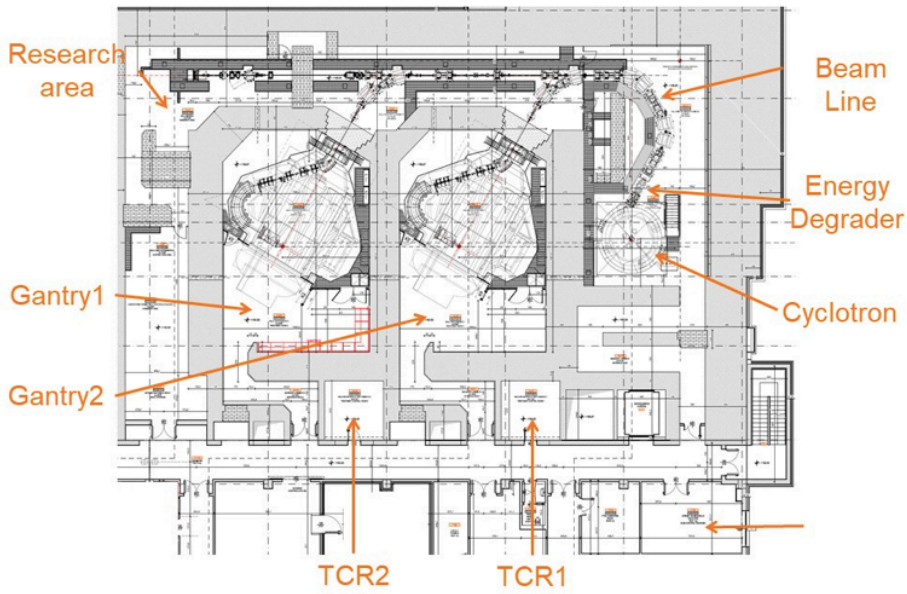

Fig.1: map of the Proton Therapy Center of Trento in the area that is dedicated to treatments. There are two gantry rooms and two control rooms called TCR and an experimental line. Adjacent to Gantry 1 is the area of the cyclotron, which continues with the beam transport line.

Contributions	µSv/h	Time (h/week)				
		Physicians	Technicians	Physicists	Technicians MP Group	Nurses
Treatment nozzle	2.3	-	8.5	1	1	3
Patient	2.3	3.5	4.0	-	-	3
Patient QA Phantom	12.7	-	-	1	1	-
Water-phantom	2.3	-	-	0.1	0.1	-
Gantry room cloud	0.005	3.5	18	4.5	4.5	12
Gantry room (neutrons)	0.0125	3.5	18	4.5	4.5	12
TCR (photons)	0.0075	0.5	11	4.5	4.5	4
TCR (neutrons)	0.0125	0.5	11	4.5	4.5	4

Tab. 1: dose rates from the different contributions and operators' workload.

Operators	E (mSv)
Physicians	0.4
Technicians	1.4
Physicists	0.7
Technicians MP Group	0.7
Nurses	0.7

Tab. 2: equivalent dose for different operators' categories.

ASSESSMENT OF THE NUMBER AND DISTRIBUTION OF PATIENTS UNDERGOING RECURRENT CT EXAMS IN SLOVENIA

Andraž Koritnik[1], Damijan Škrk[2]

[1]*Institute od Occupational Safety (Ljubljana, Slovenia)*
[2]*Slovenian Radiation Protection Administration (Ljubljana, Slovenia)*

Purpose/Introduction

Medical diagnostic imaging using ionizing radiation represents one of the largest contributors to ionizing radiation exposure of population [1]. Despite a higher frequency of conventional radiography procedures, CT examinations represent the major contributor to radiation exposure [2]. The aim of this study was to assess number of patients undergoing multiple CT exams leading to cumulative effective dose (CED) higher than 100 mSv and determine their age and gender distribution.

Materials/Methods

Data was retrieved retrospectively from established radiation dose monitoring systems covering approximately 50% CT scanners installed in Slovenia and more than 75% perfromed CT exams. The threshold value of 100 mSv was set. The number of patients with CED ≥ 100 mSv only from recurrent CT exams during a feasible time period between 1 and 2.5 years was identified. Age and gender distribution of these patients were assessed to identify the magnitude of patients.

Results

Of the nearly one hundred thousand (95,863) patients who underwent 129,799 CT exams during the period of between 1 and 2.5 years, a total of 246 (1.2%) patients received a CED of ≥ 100 mSv with an overall median CED of 3.5 mSv and maximum of 327 mSv. More than 80% of patients are older than 50 years and more than 70% are male patients.

Conclusions

The yardstick of 100 mSv is usually set as threshold of the dose at which some organs may have increased probability of certain cancers like of bone marrow, thyroid, bladder, breast, colon and lung may occur [3]. Compared to the other worldwide studies finding the percentage around 1% patients who has received a CED ≥ 100 mSv [4-6], similar results were found in Slovenia.

References

1. NCRP Report No. 160: Ionizing Radiation Exposure of the Population of the United States National Council on Radiation Protection and Measurements, Bethesda, MD (2009)
2. Mettler Jr. FA, Mahesh M, Bhargavan-Chatfield M, Chambers CE, Elee JG, Frush DP, et al. Patient exposure from radiologic and nuclear medicine procedures in the United States: procedure volume and effective dose for the period 2006–2016. Radiology 2020;17:192256

3. Rehani MM, Hauptmann M. Estimates of the number of patients with high cumulative doses through recurrent CT exams in 35 OECD countries. Phys Med. 2020 Aug;76:173-176.
4. Brambilla, M., Vassileva, J., Kuchcinska, A. et al. Multinational data on cumulative radiation exposure of patients from recurrent radiological procedures: call for action. Eur Radiol 30, 2493–2501 (2020)
5. Rehani, M.M., Yang, K., Melick, E.R. et al. Patients undergoing recurrent CT scans: assessing the magnitude. Eur Radiol 30, 1828–1836 (2020)
6. Probability of receiving a high cumulative radiation dose and primary clinical indication of CT examinations: a 5-year observational cohort study BMJ Open 2021;11:e041883

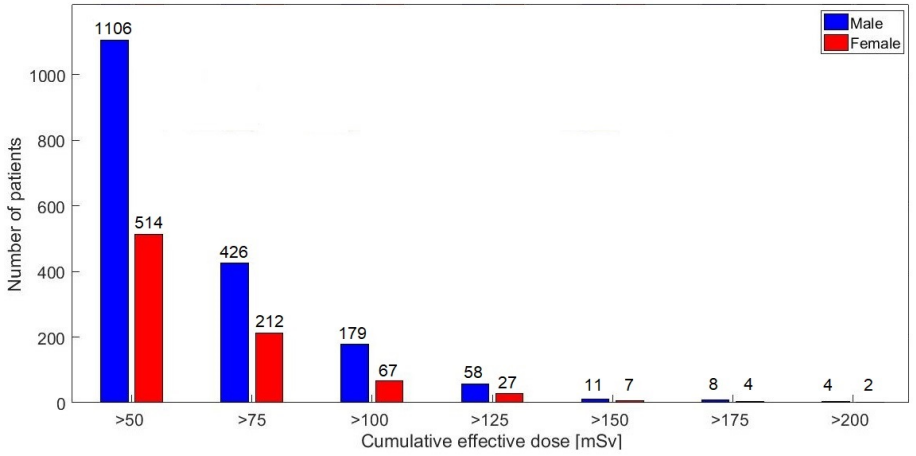

Distribution of patients by the received CED (≥ 50 mSv).

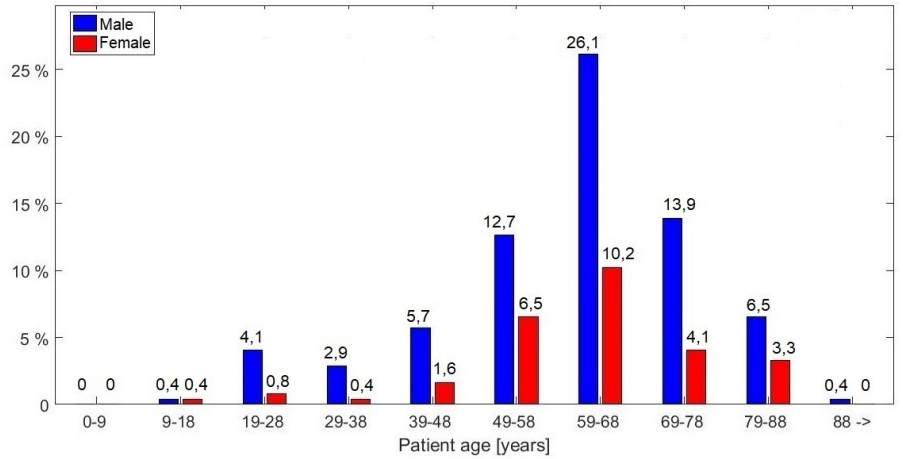

Age distribution of male and female patients who received CED ≥ 100 mSv.

	Mean	Median	Percentile		Maximum
			75^{th}	95^{th}	
Male patients	18	11	24	61	294
Female patients	14	9	19	47	327
Male patients (< 18 years old)	10	4	12	33	120
Female patients (< 18 years old)	8	3	10	21	109

CED [mSv] characterisation (statistics) of multiple exposed patients.

IMPLEMENTATION OF A DOSE MANAGEMENT SYSTEM IN A LARGE CENTRAL EUROPEAN HOSPITAL

Angelika Osanna-Elliott[1], Natasa Brasik[1], Angelica de Leon[1], Alexander Gruber[1]

[1] *Universitätsklinikum AKH Wien, Austria*

Purpose/Introduction

Our hospital is associated with a medical university and has 120 x-ray devices for diagnostic and interventional radiology. For dose management, the Qaelum tqm|DOSE dose management system was purchased and is being implemented. In this presentation, we would like to report on the ongoing project. The medical physics team of the radiology clinic is coordinating the project of implementing the system, leading the efforts to clean the data and start the work of dose teams. Here, we are showing first results.

Materials/Methods

Dose teams were defined according to organisational units in the hospital. For the first phase, six dose teams for the x-ray equipment in the General and Childrens Radiology department have been formed. Each dose team consists of one medical physicist, one radiographer and one radiologist. For the first 6 months, weekly meetings are scheduled; the plan is for monthly meetings for the following 6 months and ad-hoc meetings thereafter. Also, the communication process with IT and Qaelum local support was formalized.

Results

93 % of the x-ray equipment have successfully been implemented in tqm|DOSE. Dose reference values are being defined and linked and automated warning messages (alerts) are being triggered by tqm|DOSE. The alerts are supposed to be discussed in the weekly dose team meetings.

Discussion

Efficiency of dose teams very much depends on the amount of commitment, time and sxpertise of the dose team members.

Conclusions

Implementing a dose management system for a large general hospital is a complex task and needs a very structured approach. Clear lines of communication need to be implemented before the project start. Personnel turnover makes it difficult to streamline such a project.

References

1. https://qaelum.com/

BASIC SAFETY ASSESSMENT FOCUSED ON EFFECTIVE DOSE TO POPULATION, RELATED TO THE MANAGEMENT OF SOLID AND LIQUID WASTES PRODUCED IN CLINICAL PRACTICES OF TRIESTE (ITALY) NUCLEAR MEDICINE DEPARTMENT

Michele Signoriello[1], Maria Rosa Fornasier[1], Benedetta Santoro[2], Fulvia Arfelli[3], Mara Severgnini[1]

[1]ASUGI - Azienda Sanitaria Universitaria Giuliano Isontina (Trieste)
[2]Department of Physics, University of Trieste (Italy)
[3]Department of Physics, University of Trieste (Italy) Division of Trieste, Istituto Nazionale di Fisica Nucleare (INFN), Trieste (Italy)

Purpose/Introduction

Patient administration procedures in a Nuclear Medicine (NM) Department result in an amount of radioactive wastes (mostly solid and liquid) produced during everyday clinical practices. In our study the compliance with Directive 2013/59/EURATOM [1] by assessing the total effective annual dose due to the radionuclides activities released into the environment by NM Department of Cattinara Hospital (Trieste), for diagnostic and therapeutic administered radiopharmaceuticals procedures, was investigated. The European directive was transposed by the Italian Government into the Italian Radiation Protection Legislative Decree 101/2020 [2]. Both norms establish that the total annual effective dose expected to be incurred by a representative person of the general public, due to an authorized practice, is acceptable when it does not exceed 10 μSv/y.

Materials/Methods

Two release pathways of discharged radioactivity into environment by Trieste Nuclear Medicine Department were considered: liquid wastes due to the excreta of both inpatients and outpatients, that are inserted in the city pipe system and processed in the sewage treatment plant before being released into Trieste Gulf; and airborne releases during incineration of solid waste materials. Advanced environmental screening models to assess the impact of discharged radionuclides in coastal waters and in atmosphere are provided by NCRP [3] and IAEA [4] international guidelines. A coastal water screening model was adopted to evaluate the release of liquid waste discharged in Trieste gulf by Servola treatment plant [5] (see image_1). The atmospheric dispersion of airborne releases by Ecoeridania incinerator plant based in Forlì [6], Italy, was estimated by applying a Gaussian plume approach (see image_2). Finally, a possible accidental fire scenario, involving unsealed radioactive materials and occurring in Nuclear Medicine Department hot laboratories was investigated by using HotSpot Health Physics Codes [7]. The Hotspot software provides a useful tool to assess the atmospheric release of radioactive materials through an advanced three dimensional Gaussian model [8]. The simulation was performed considering two existing local atmospheric conditions, one with mild wind and the other with strong wind called Bora.

Results

The total annual effective dose to the reference person of the population was estimated to be 5.3·10^-3 μSv/y for discharged liquid waste into coastal waters of Trieste gulf, and 1.4·10^-4 μSv/y for the atmospheric airborne releases in the surrounding area of incinerator plant (see image_3). The workers involved in the maintenance of the sewage treatment plant receive a total annual effective dose of 4.3 μSv/y, instead for the incinerator operators the total imparted dose is 5.9·10^-8 μSv/y (see image_4). Regarding the accidental fire event scenario the maximum dose delivered to a possible receptor at a certain distance from the source term is 3.3·10^-8 Sv with mild wind (see image_5), and 7.5·10^-8 Sv with strong Bora wind (see image_6).

Discussion

First of all, the potential radiological consequences of radionuclides discharge into the environment, resulting from the management of liquid and solid wastes produced by Trieste NM Department authorized clinical procedures have been investigated through different advanced screening models. The models' mathematical formalism provides an accurate analysis description, based on realistic assumptions, resulting in detailed total annual effective dose estimations for reference person and workers that could be affected by discharged radioactive wastes [9]. Even though the analysed models give reliable results, an in-depth study to evaluate the accuracy of annual dose exposure calculations is necessary, carrying out a dedicated and exhaustive mathematical analysis to quantify data uncertainties. In addition a comparison with experimental measurements is suggested, this kind of comparative study could be performed, in Italy, by the support of regional environmental protection agencies. The second section of our work is dedicated to the development of a fast and simple approach to estimate the impact of a radionuclides mixture and its distribution in the environment, due to a general fire accident in hot-laboratories of a Nuclear Medicine Department. During an accidental fire scenario decision-makers need to implement countermeasures as soon as possible to minimise the radiation-induced risks for the population, so they need quick and reliable information about the spread of the radioactive source term and the spatial local contamination distribution of the dispersed radioactivity into the environment. In this accident situation the Gaussian plume 3D model provided by HotSpot software has the advantage of offering a good compromise between the quality of information obtained and its computational effort, once the exposure pathway, the type of radionuclides involved and the physical mechanisms underlying the radionuclides dispersion have been outlined [10-11]. In general the 3D Gaussian model has been widely used and verified by the scientific community to assess atmospheric dispersion calculations, so it generally produces results that agree well with experimental data in simple meteorological and terrain conditions [8].

Conclusions

The situations expected to be the most probable exposition circumstances, in terms of internal and external contaminations, were analysed: workers involved in the management of the sewage sludge in the Servola sewage treatment system and of incinerated solid wastes in Forlì incinerator treatment plant; then a representative member of the public set along the coastal waters, in an area close to the incinerator and at a certain distance from possible hazardous fire event involving airborne radioactivity releases. The total annual effective dose estimated, due to both NM authorized practice and accidental fire event, resulting in the release of radionuclides into the environment, are lower than the established limit of 10 μSv/y [1-2]. Hence, the results obtained in this work are in compliance with the basic safety standards issued both by the European 2013/59/EURATOM directive and by the Italian Radiation Protection Legislative Decree 101/2020. Therefore the calculations performed will be part

of an update authorization report to be submitted to national Regulation Authorities, as they are in total agreement with the regulatory stipulations.

(a)

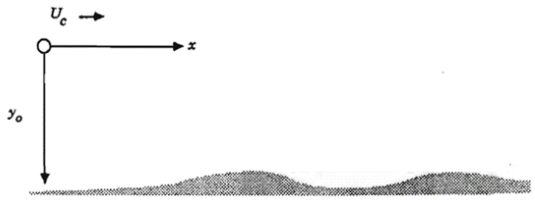

(b)

$$C^{shoreline}(x) = \frac{962\, W_0 U_c^{0.17}}{D x^{1.17}} \times \exp\left(-\frac{7.28 \cdot 10^5\, U_c^{2.34} y_0^2}{x^{2.34}}\right) \times \exp\left(-\frac{\lambda_i x}{U_c}\right)$$

$C^{shoreline}(x)$ is the concentration along shoreline at receptor position of the radionuclide in consideration (Bq/m³);
W_0 is the annual radionuclide release rate at the discharge point (Bq/s);
U_c is the velocity of the coastal current (m/s);
D is the water depth of the radionuclide effluent outfall at the discharge point (m);
x position of a possible general public receptor along the shoreline (m);
y_0 is a constant release point is located at a distance from the shoreline (m);
λ_i is the radioactive decay constant of the specific radionuclide (s^{-1}).

Advanced coastal water screening model description: (a) View from the top of the sewage treatment plant discharge pipe system extending into the Trieste gulf, Italy [5]; (b) Panoramic view of coastal region with diffusion parameters indicated and final equation to calculate the radionuclide concentration along the shoreline at the receptor position [3-4].

References

1. Council Directive 2013/59/Euratom of 05/12/2013 laying down basic safety standards for protection against the dangers arising from exposure to ionising radiation, and repealing Directives 89/618/Euratom, 90/641/Euratom, 96/29/Euratom, 97/43/Euratom and 2003/122/Euratom. Official Journal of the European Union 17/01/2014: No. L 13.
2. Decreto Legislativo 31/07/2020 No. 101. Attuazione della direttiva 2013/59/Euratom, che stabilisce norme fondamentali di sicurezza relative alla protezione contro i pericoli derivanti dall'esposizione alle radiazioni ionizzanti, e che abroga le direttive 89/618/Euratom, 90/641/Euratom, 96/29/Euratom, 97/43/Euratom e 2003/122/Euratom e riordino della normativa di settore in attuazione dell'articolo 20, comma 1, lettera a), della legge 4 ottobre 2019, n. 117. Gazzetta Ufficiale della Repubblica Italiana 12/08/2020: No. 201; N. 29/L. Last amendment in Gazzetta Ufficiale della Repubblica Italiana 01/06/2021: No. 130.
3. National Council on Radiation Protection and Measurements. Screening Models for Releases of Radionuclides to the Atmosphere, Surface Water, and Ground. Report No. 123. Bethesda, MD: NCRP; 1996
4. International Atomic Energy Agency. Generic Models for Use in Assessing the Impact of Discharges of Radioactive Substances to the environment. Safety Reports Series No. 19. Vienna: IAEA; 2001.

(a)

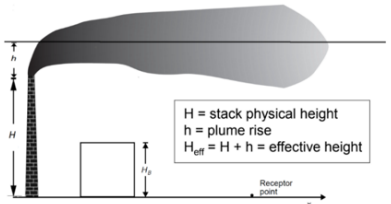

(b)

$$C = \frac{f \times Q \times P}{u} \quad ; \quad P = \frac{12}{\sqrt{2\pi^3}} \times \frac{\exp\left[-\left(\frac{H^2}{2\sigma_z^2}\right)\right]}{x\sigma_z}$$

C is the average atmospheric concentration at the receptor position (Bq/m^3);

f is the fraction of the time the wind blows toward the receptor of interest (default value 0.25);

Q is the annual average discharge rate for the specific radionuclide (Bq/s);

u is the mean wind speed at the height of the release point (m/s);

P is the Gaussian diffusion factor appropriate for the height of release and downwind distance considered (m^{-2});

H is the height of the stack where the release point is set (m);

x is the downwind distance for a general public receptor (m);

σ_z is the vertical diffusion parameter (m).

Advanced atmospheric dispersion screening model description: (a) View from the top of the Ecoeridania incinerator based in Forlì, Italy [6]; (b) Air flow plume distribution in undisturbed dispersion condition, without building wake effect (H > 2.5 HB) and final equation to calculate the radionuclide average atmospheric concentration at the receptor position [3-4].

5. AcegasApsAmga SpA. – Hera Group. https://www.acegasapsamga.it (accessed July 20, 2021).
6. Gruppo EcoEridania – Essere SpA. https://gruppoecoeridania.com/le-aziende/essere/ (accessed July 20, 2021).
7. HotSpot Health Physics codes (Version 3.1.2 - February 11, 2020). https://narac.llnl.gov/hotspot (accessed December 7, 2020).
8. Homann SG, Aluzzi F. HotSpot Health Physics Codes Version 3.0 User's Guide. National Atmospheric Release Advisory Center at Lawrence Livermore National Laboratory. Livermore, CA: LLNL; 2014.
9. Xu S, Söderman AL. SSM Report 2009. Screening calculations for radioactive waste releases from nonnuclear facilities, 2. Stockholm: Swedish Radiation Safety Authority; 2009.
10. Urso L, Kaiser J C, Woda C, Helebrant J, Hulka J, Kuca P, Prouza Z. A fast and simple approach for the estimation of a radiological source from localised measurements after the explosion of a radiological dispersal device. Radiat Prot Dosimetry 2014;158:453-60. https://doi:10.1093/rpd/nct263.
11. Musolino S V, Harper F T, Buddemeier B, Brown M, Schlueck R. Updated Emergency Response Guidance for the First 48 h after the Outdoor Detonation of an Explosive Radiological Dispersal Device. Health Phys 2013;105:65-73. https://10.1097/HP.0b013e31828a8fb1.

	Coastal waters	Atmospheric dispersion
Radionuclides	Total Annual Effective Dose [μSv/y]	
Diagnostic practices		
F-18	$1.5 \cdot 10^{-5}$	$2.6 \cdot 10^{-120}$
Tc-99m	$2.1 \cdot 10^{-5}$	$3.6 \cdot 10^{-37}$
In-111	$1.6 \cdot 10^{-4}$	$1.9 \cdot 10^{-8}$
I-123	$1.1 \cdot 10^{-5}$	$5.1 \cdot 10^{-20}$
Therapeutic practices		
I-131	$5 \cdot 10^{-3}$	$1.4 \cdot 10^{-4}$

Total annual effective dose estimations to representative person of the population evaluated through advanced screening models assessment, due to the radionuclides discharged into coastal surface water and airborne atmospheric releases by the Trieste NM Department in diagnostic and therapeutic clinical practices.

Workers	Sewage system	Incinerator plant
External exposure [μSv/y]	4.3	$1.4 \cdot 10^{-9}$
Internal exposure [μSv/y]	$8.9 \cdot 10^{-5}$	$5.8 \cdot 10^{-8}$

Total annual effective dose estimations for sewage and incinerator plant workers according to two different possible exposition conditions (external and internal contamination), for radionuclides employed in diagnostic and therapeutic procedures (18-F, 99m-Tc, 111-In, 123-I and 131-I) in the Trieste NM Department.

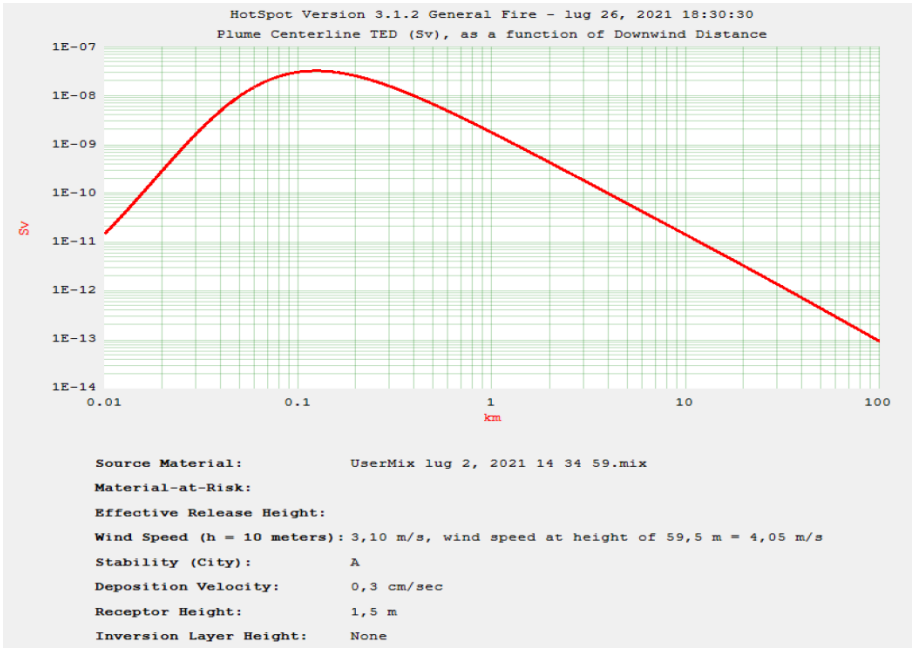

HotSpot software simulation plots performed for the scenario with a mild wind from the West: (a) TEDE (Total Effective Dose Equivalent - Sv) as a function of downwind receptor position (x). The maximum TEDE value lies at 3.3·10^-8 Sv, and it is reached at distance of 0.1 km from the source term origin.

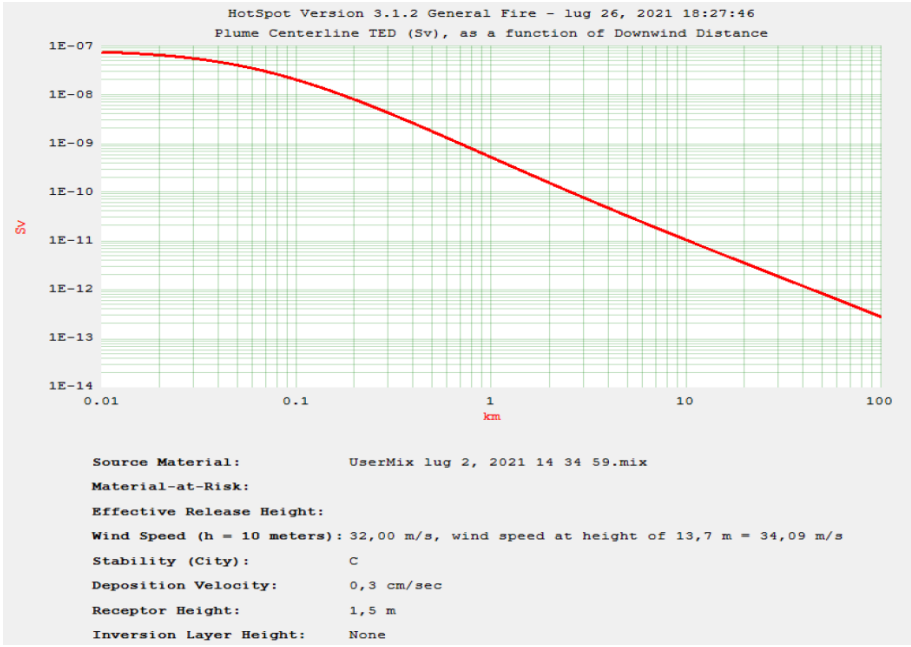

HotSpot software simulation plots performed for the scenario with a strong Bora wind from the ENE: (a) TEDE (Total Effective Dose Equivalent - Sv) as a function of downwind receptor position (x). The maximum TEDE value lies at 7.5·10^-8 Sv, and it is reached at distance of 0.01 km from the source term origin.

DOSIMETRICAL EVALUATION EFFECTS OF A SIMULATED GRAVITY INDUCED SHIFTING ON LINAC MOUNTED DETECTOR DURING PATIENT PRETREATMENT QA

Alessio Boschini[1], Giuseppe Rinaldin[1], Sara Barbiero[1], Davide Canonico[1], Davide Maestri[1], Luca Bindoni[1]

[1]*AULSS2 - Marca Trevigiana Treviso, Italy*

Purpose/Introduction

The purpose of this study is to investigate the effects on dosimetric evalutation in patient pretreatment QA of mounting displacement of a transmission detector (Dolphin, IBA Dosimetry) on linac head (Elekta Versa HD).

Materials/Methods

Named dosimeter ought to be mounted on the applicator hooks on the gantry head. Once plan fluence is measured during delivery, plan dose is recalculated via a proprietary TPS (Compass, IBA dosimetry) on simulation CT. The detector setup routine includes geometric calibration, in order to correct for displacements between detector and field center occurring during the mounting phase. Nonetheless, this fails to capture possible displacements occurring during plan delivery, should the hooks not firmly hold the detector. In this scenario, as the gantry rotates the detector shifts along the hooks' mounting direction because of gravity. We untightened the clamps in order to cause a 1.5mm shifting, measured by the geometry calibration software module itself. This ultimately causes signature shapes in dose difference between recalculated and original dose on simulation CT to appear. The effect would be particularly noticeable when considering stereotactic-like plans. We explored this effect magnitude considering a set of 3D static arc plans made with Monaco and calculated in a water cylinder, varying collimator aperture, length and direction of gantry rotation and initial geometry calibration. Five gantry rotation patterns were investigated: 180-to-180cw (A), 180-to-0cw (B), 270-to-90cw (C), 180-to-0ccw (D) and 90-to-270ccw (E). Used collimator apertures are 15mm, 30mm and 50mm along the shifting direction and 50mm in the perpendicular one, to keep the central simulation CT slice used for evaluation free from edge effects. Initial geometry calibration is called L or R whether it is performed with gantry angle 270° or 90°.

Results

The effect is most relevant with patterns D and E and calibration L with respectively 13.8% and 13.2% max dose differences between original and recalculated. The shape of this effect is distinctively that of a mirrored clove shaped hot area and cold area in respect to the center, at the edge of the central ring whose diameter is the collimator aperture. The magnitude of the effect decreases with increasing collimator aperture, reaching 6% for pattern D and calibration L. The effect shape in patterns B, C, D and E calibration L mirrors respectively D, E, B and C with calibration R. Within pattern A, the effect is still noticeable with both calibrations, although smoothed, reaching 4.9% max dose difference with 15mm diameter.

Discussion

This effect might be subtle to detect because of the number of factors contributing to its arise. Of striking importance is of course the initial correction due to geometric calibration which combined with the proper gantry rotation might hinder or maximize the dose difference. When evaluation is done via 3D gamma analysis, the effect will lower the passing rate, resulting in suboptimal action level definition.

Conclusions

Mounting displacement during gantry rotation might lead to noticeable dosimetric inadequacies when considering PTV coverage and nearby OAR avoidance during pretreatment evaluation. We propose QA strategies to detect and avoid this effect. Similar issues may potentially arise in every gantry corotating detector-based (i.e.:EPID) pretreatment QA.

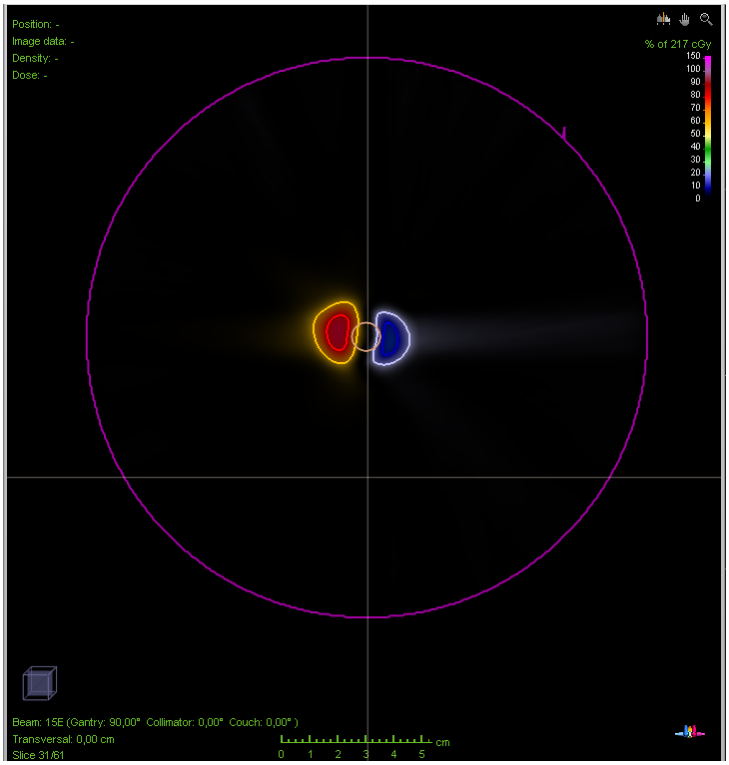

Fig.1 : Dose difference clover-like pattern arising in configuration E with 15mm collimator aperture and L calibration as viewed on Compass (IBA Dosimetry) software. A 15mm diameter structure was made in the center of the water cylinder in order to evaluate the effect.

GANTRY ANGLE VERIFICATION USING THE CIRS ISO CUBE PHANTOM ON THE VARIAN HALCYON LINEAR ACCELERATOR

Denis Brojan[1], Attila Šarvari[1]

[1]*Institute of Oncology Ljubljana*

Purpose/Introduction

With the introduction of the Halcyon (Varian Medical Systems) linear accelerator the gantry angle verification test has been put on trial. On regular C-arm linear accelerators cardinal gantry angles can be checked with the spirit level that one attaches to the collimator. Halcyon has a spirit level integrated on the gantry head, but it is very inconvenient to verify the gantry angle in such a way. It also has a closed housing that renders such a measurement impossible without removing the covers. For this reason, we searched for an alternative way to verify cardinal gantry angles. An appropriate solution was found, that involves the analysis of a single portal image of the CIRS ISO Cube Phantom.

Materials/Methods

The CIRS ISO Cube phantom (REF #1) contains a unique center point fiducial and the exterior is machined with concentric circle rings to allow the user to assess all setup errors, including rotations. One concentric ring is on the top of the phantom while the other is on the bottom. In the middle of the phantom a center point fiducial is built in and it represents the isocenter when the lasers are aligned to the engraved markings on the phantoms exterior. On the portal image taken at gantry angle 0 the two circle rings are visible, one inside the other, with a fiducial at the center (figure 1). The rings are visible on the x-ray image, because the thickness of the phantom in the region of the rings is lesser than elsewhere. Using the Eclipse scripting API v15.6 we created a C# script (REF #2), that can be run in Eclipse treatment planning system, with which one can analyze the portal image of the phantom. The script reads the image opened in the context window and displays it for analysis. The user aligns a set of overlaid circles (red and blue) with the rings on the image (figure 2). Zooming, panning and changing the Window/Level are available in order to help with the optimal adjustment of the circle positions. The distance between circle centers is automatically calculated and converted into gantry angle deviation with the formula: delta phi = arcsin(delta x/2a), where delta x is the distance between circle centers, and 2a is the distance between the rings in the cube.

In the planning system, we created a plan with 6 different fields with gantry angles from 0 to 5 with 1 increment. At the treatment unit, we placed the ISO CUBE on the table top and aligned it with spirit level as well as with the lasers (figure 3). For the correct setup verification, a CBCT scan was performed and the necessary shifts were applied. A total of six portal images with 1 gantry angle difference were acquired.

Results

Images were analyzed with the script in the Eclipse treatment planning system. The overlaid circles were manually moved and aligned with the rings on the image. Circles can be moved with the cursor with a step of 0.1 mm in all directions. A deviation that is a difference between the planned gantry angle and the angle calculated by HGA script was calculated. The maximum deviation of 0.08 was detected at gantry angle 3.0 (table 1).

Discussion

With the help of the script we tested only the deviation of the gantry angle with the MV portal imager. The same script can be used for testing the correctness of the angle of the kV imager. This can be done simultaneously with the gantry angle test as the kV imager is perpendicular to the MV imager and the ISO cube phantom has similar rings on lateral sides.

Conclusions

We have succeeded in finding an alternative way for gantry angle verification. This method has proved to be appropriate also for use on conventional linear accelerators. Disadvantage of the test is that it is more time consuming, however, that is not so if one also performs others tests at the same time like laser alignment check, isocenter coincidence check, radiation field/light field alignment checks etc. Even though that the Eclipse script needs a human interaction and the results are then subjective, the results are still precise. This method in not appropriate if you require high precision, where the high precision spirit levels with the accuracy of 0.02 mm/m are superior to the image analysis method.

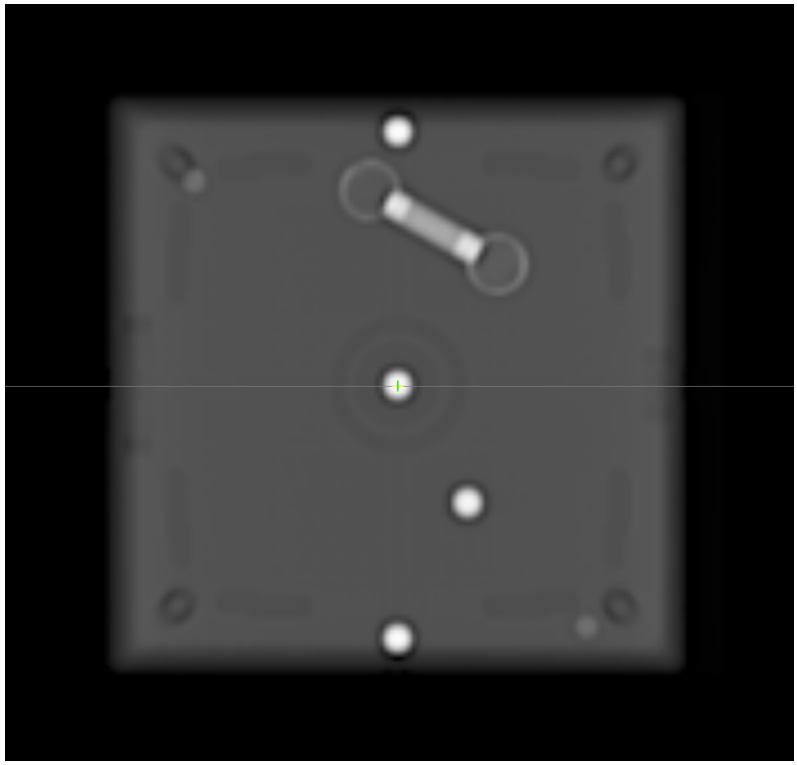

Fig. 1:A X-ray image of an ISO CUBE phantom

References

1. https://www.cirsinc.com/products/radiation-therapy/daily-iso-phantom/

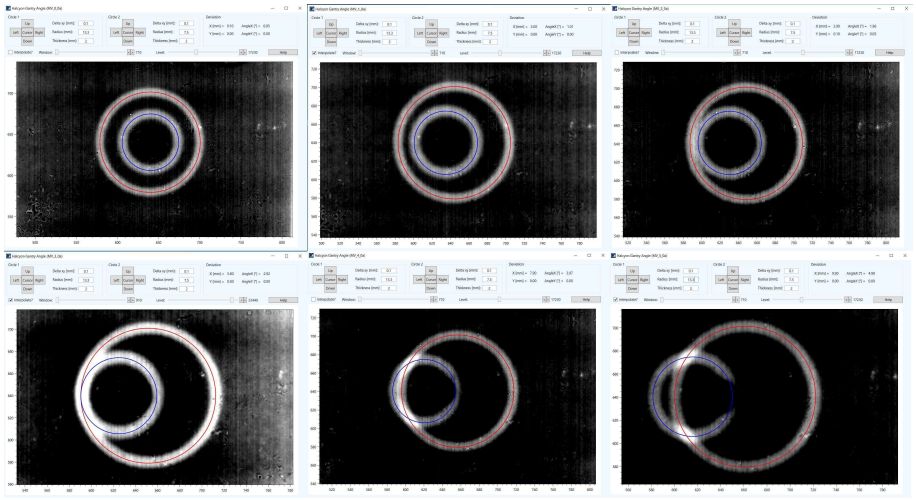

Fig. 2: MV images of the ring at 6 different gantry angles

2. https://github.com/brjdenis/VarianESAPI-HalcyonGantryAngle
3. EJ. Pyyry, W. Keranen; Varian APIs: A handbook for programming in the Varian oncology software ecosystem (https://varianapis.github.io/VarianApiBook.pdf)
4. Eclipse Scripting API Reference Guide; Varian Medical Systems

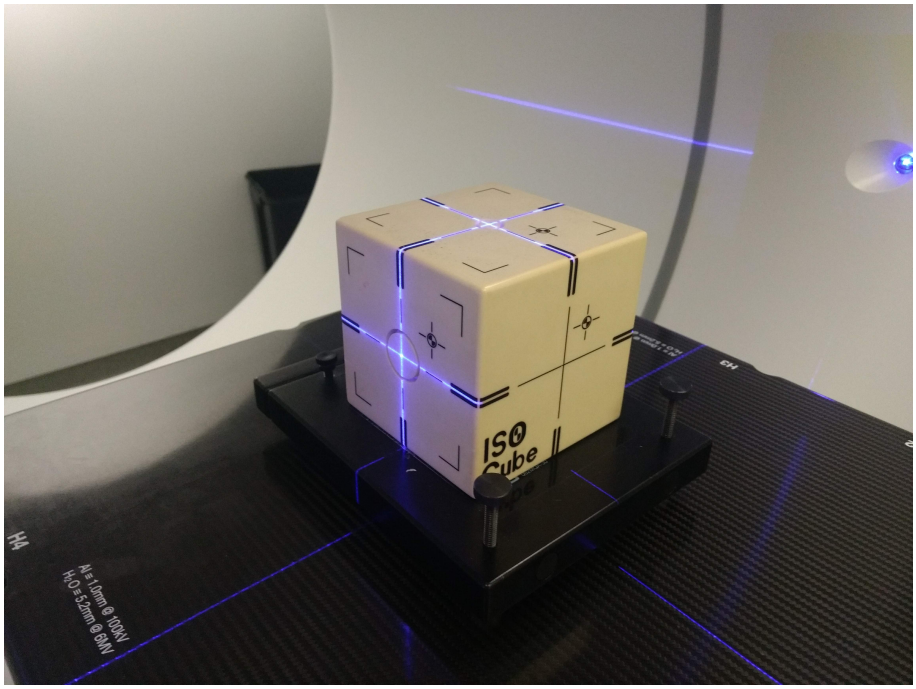

Fig. 3: Set-up of the ISO CUBE phantom at the Halcyon treatment unit

	gantry angle [°]		
field	linac	measured	deviaton [°]
MV_0	0.0	0.05	0.05
MV_1	1.0	1.01	0.01
MV_2	2.0	1.96	-0.04
MV_3	3.0	2.92	-0.08
MV_4	4.0	3.97	-0.03
MV_5	5.0	4.98	-0.02

Table 1: Results of the calculate angle deviation for 6 different angles

COMMISSIONING AND INITIAL PATIENT-SPECIFIC VERIFICATION EXPERIENCE WITH THE FIRST EUROPEAN INSTALLATION OF THE GAMMAPOD STEREOTACTIC BREAST RADIOSURGERY SYSTEM

Eugenia Moretti[1], Giorgia Condarelli[2], Vito Gagliardi[1], Marika Guernieri[1], Daniela Marfisi[1], Chiara Reverberi[3], Marco Trovo'[3], Paolo Scalchi[1]

[1]Medical Physics Unit, Udine University Hospital, Italy
[2]Medical Physics Spec. School, Catania University, Italy
[3]Radiation Oncology Unit, Udine University Hospital, Italy

Purpose/Introduction

In December 2021, the Radiotherapy centre of the University Hospital of Udine became the first site in Europe (the third in the world beyond two USA centres) to go live with the GammaPodTM System (Xcision Medical Systems, Columbia, MD), a novel Radiotherapy technology specifically designed for the stereotactic partial breast irradiations (S-PBI). The device is based on the combination of a radiation focal spot with sharp dose fall-off at the isocenter created by 25 non-overlapping rotating cobalt-60 sources and a continuous translation in three axes of the patient in prone position. Stereotactic localization of the breast is achieved by a vacuum-assisted breast immobilization cup with built-in stereotactic frame. The first 4 patients underwent 4-fraction adjuvant PBI for a total dose of 28 Gy, while the subsequent treatments concerned till today (late march 2022) 20 patients who received two different single-fraction radiation schemes: a preoperative fraction of 30 Gy and a postoperative fraction of 18.4 Gy. In this work we present the mechanical and dosimetric tests designed to characterize the GammaPodTM System for the clinical use and the preliminary results of the patient-specific quality checks (PSQC) of the first S-PBI treatments.

Materials/Methods

The system is based on a double-shelled bowl collimator in which the sources are located in the outer shell (the source carrier) and the collimator constitutes the inner shell (the collimator carrier). The inner collimator has 2 sets of predrilled holes with projected nominal 15 and 25 mm diameters at the radiological isocenter. Both carriers rotate together during treatment to spread out the dose to normal tissue by collimator switching. The reference output relative to the largest collimator was measured at the isocenter with a dedicated PMMA breast cup following a method suggested by Yi and Becker (Phys. Med., 2021) based on IAEA TRS 483 and the Exradin A1SL ion chamber. The output was independently verified by both OSL (optically stimulated luminescence) dosimeters provided by Imaging and Radiation Oncology Core (IROC) and EBT3 Gafchromic® films (ISP, Wayne, NJ). The 15-mm collimator output factor (OF) was obtained using different compact ion chambers (Exradin A1SL, PTW31021, IBA CC01, IBA Razor chamber and Razor Nano chamber), a PTW microdiamond detector as well as OSL dosimeters and EBT3 films, and compared to Monte Carlo calculation by Xcision. Concerning patient-specific quality assurance (PSQA), our strategy combine absolute and relative dose measurements: the first one were performed positioning small-cavity ion chambers in low dose gradient single points in a water-filled breast cup matching the patient, while relative dose distributions are obtained by using the 2D Detector SRSMapcheckTM (SNC) in the PMMA breast phantom. The approach of the water cup was chosen to verify the effective clinical plan as we utilized

the specific cup used to immobilize and treat the patient and we placed the chamber in positions representative of the clinical target. The 2D maps measured by SRSMapcheckTM were validated against the relative dose distributions measured by previously calibrated radiochromic films (EBT3/EBT-XD type depending on the dose level).

Results

The deviation between OSL and Exradin A1SL dosimetry range from -7.1% and 5.3%, while is 2.6% on the average (4% 2SD) for EBT3 films, thus implying mutual validation within their own uncertainties. OF measurements differ from the Monte Carlo value of 0.0% to a maximum of 1.0%. The performance in terms of PSQC was good. To date, all the ion chamber measurements performed in water cup matched the Xcision TPS with average (max) difference of -1.8% (8.5%). The maximum discrepancy was observed in points located in the most posterior regions of the target. Relative dose distributions measured by SRSMapcheckTM showed an average gamma passing rate of 94.9%±5.8% when applying a 3%/1 mm gamma criteria.

Conclusions

With this study, the GammaPodTM System installed at our institution has been successfully commissioned for clinical use. The preliminary results of our PSQA program show that the GammaPodTM can be used to deliver accurately S-PBI treatments.

References

1. Yu CX, Shao X, Zhang J, et al. GammaPod-a new device dedicated for stereotactic radiotherapy of breast cancer. Med Phys. 2013;40(5): 051703.
2. Yi B, Becker SJ., Simplified method for determining dose to a non-water phantom through the use of N D,w and IAEA TRS 483 for the GammaPod, Phys Med. 2021 Aug;88:138-141.

BIG DATA ANALYSIS ON THE CALIBRATION OF RADIOCHROMIC FILMS

Ignasi Méndez[1], Juan J. Rovira-Escutia[2], Božidar Casar[1]

[1]*Institute of Oncology Ljubljana, Slovenia*
[2]*Centro Nacional de Dosimetría, Spain*

Purpose/Introduction

Radiochromic.com is a SaaS application for radiochromic film dosimetry. SaaS applications enable Big data analysis of their databases. The aim of this study was to use the large database of Radiochromic.com film dosimetry studies as a research tool on calibration and recalibration of radiochromic films.

Materials/Methods

A sample of 1046 anonymized gamma index analyses comparing film and TPS (treatment planning system) doses were extracted from Radiochromic.com [1]. Each analysis was associated with its film calibration and, if applied, film inter-scan and lateral correction. The relationship between film pixel values and TPS doses in each gamma index analysis defined the film sensitometric curve, while the film calibration was designated as lot sensitometric curve. Recalibration of the lot sensitometric curve was simulated by using points from the film sensitometric curve.

The accuracy of film sensitometric curves, lot sensitometric curves, and three different recalibration methods to reproduce the relationship between film pixel values and TPS doses was evaluated by examining the difference between real values - either TPS doses or film pixel values - and fitted values - derived from the sensitometric curves.

Results

The lowest values of median absolute percentage errors (MdAPE) when comparing real and fitted values were obtained with film sensitometric curves, and the largest with lot sensitometric curves. The shape of the median (when summarizing all gamma index analyses) MdAPE as a function of dose is similar to the curve of uncertainty as a function of dose obtained by Vera et al.[2]. In figure 1 median MdAPE values as a function of dose are show for film sensitometric curves, lot sensitometric curves, and beta (i.e., dose rescaling) recalibration.

Conclusions

Radiochromic.com's database can be used as a research tool. The impact of calibration and recalibration methods on film uncertainties was shown. The dependence of film uncertainties with the dose confirms with a large sample the results of Vera et al.[2]. Dose rescaling is a recalibration method that can be used on gamma index analyses with relative doses.

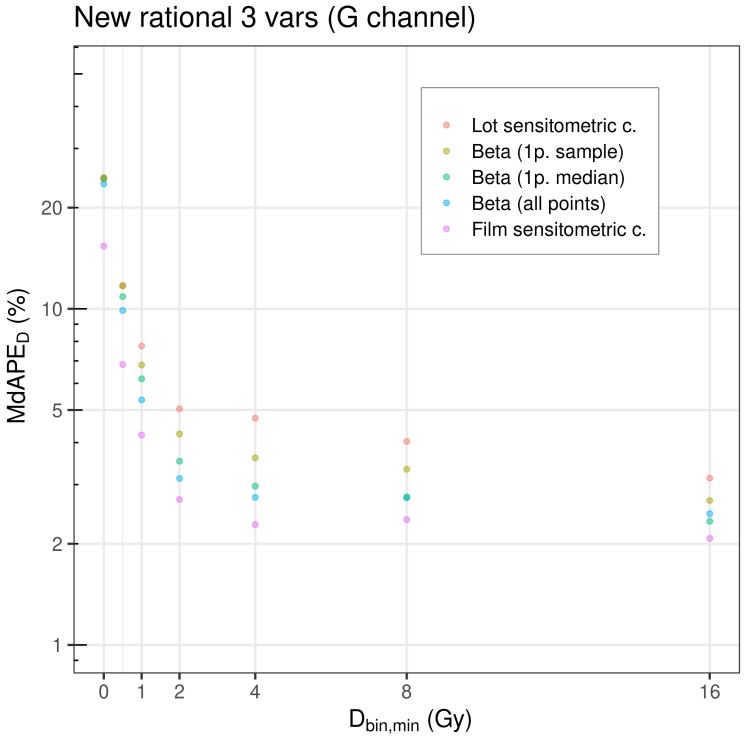

Median MdAPE values as a function of dose with different sensitometric curves.

References

1. [1] I Méndez I, JJ Rovira-Escutia, B Casar. "A protocol for accurate radiochromic film dosimetry using Radiochromic.com." Radiology and Oncology (2021) 55(3): 369-378.
2. [2] JA Vera-Sanchez et al. "Monte Carlo uncertainty analysis of dose estimates in radiochromic film dosimetry with single-channel and multichannel algorithms." Physica Medica 47 (2018): 23-33.

CONNECTION BETWEEN ONCOLOGY INFORMATION SYSTEM AND TREATMENT PLANNING SYSTEM FOR OPTIMAZING THE PROCESS OF TREATMENT PLANNING.

Sašo Pulko[1]

[1]*University Medical Centre Maribor, Slovenia*

Purpose/Introduction

The aim of this project was to establish a connection between our oncology information system (OIS) and treatment planning system (TPS) to transfer all important information for creating a plan from OIS and importing it to TPS. The result is an automatically created treatment plan on the basis of all the imported information.

Materials/Methods

Our clinical path for patients was designed as a completely paperless workflow. Because of that we needed to keep all information about patients in the OIS. Important part of this information is the number of fractions, total dose, preferred technique for irradiation and dose restrictions. Physicians put this information under separate prescriptions for every planning target volume (PTV). In our institution physicians create prescription in Mosaiq (it is called RadRx) for every PTV and they insert necessary information (name of the target, number of fractions, total dose, preferred technique). Our TPS has an option to create a script in python language and run this script inside TPS. We created a script which connects to OIS database and look for information about the patient which is open in TPS. If existing PTV in structure set match RadRx, information is transferred into TPS and plan is automatically created, Fig. 1. Name and number of a plan is automatically adjusted according to technique (Plan1 – 3D, IMRT – IMRT1 or VMAT1 for VMAT) and numbers of plans patient had in the past.

We created different classes of solutions that are selected on the basis of desired technique. If selected technique is 3D-CRT, BeamSet is automatically created for every PTV and templates for beams and OAR dose restriction are imported. MLCs and jaws are conformed to PTV and dose is calculated and rescaled to prescription. For palliative spine cases, bladder and rectum plan is almost finished (Fig. 2), on the other hand for breast and other palliative case additional beams and edit of the segment is needed.

If selected technique is VMAT/IMRT, single isocenter is created for all PTVs and based on localisation and dose prescription optimisation functions and clinical goals are imported. At the end script also automatically runs the optimisation. Optimisation is divided in three parts. In each part we have 5 cycles of 30 iteration. After every cycle the value of optimization function are adjusted.

In first part the dose to organ at risk is iteratively reduce. In second part dose conformation around PTV is increased. In the last part homogeneity to PTV is increased. Result of script for optimisation are showed in Fig. 3.

When plan is approved script for automatic plan transfer is lunched. Script send an RTP plan and DRR or CT images, depend on image protocol. Script get this information from the Mosaiq, where physician prescribed it.

Results

We ran the script on over 600 patients. At the moment we are able to import all information needed for creating a plan from OIS to TPS. For VMAT/IMRT cases we are able to create a clinically acceptable plan in the first attempt. For other cases we create a plan which needs some adjustment before it is clinically acceptable. Time reduction in plan preparation is between 15% for breast cases to 30 % for prostate cases, Fig. 4. Reduction of planners administrative error (beam name, plan name, diode, name, name of epi fields, ...) also decrees significantly from 3.5% to 1%.

Conclusions

At the moment we are able to import all information needed for creating a plan from OIS to TPS. For VMAT/IMRT cases we are able to create a clinically acceptable plan, for other cases we are able to create a plan which needs some adjustment before clinical acceptance. Time reduction in plan preparation is between 15 % for breast to 30 % for prostate cases. Reduction of planner's administrative errors also decrees significantly.

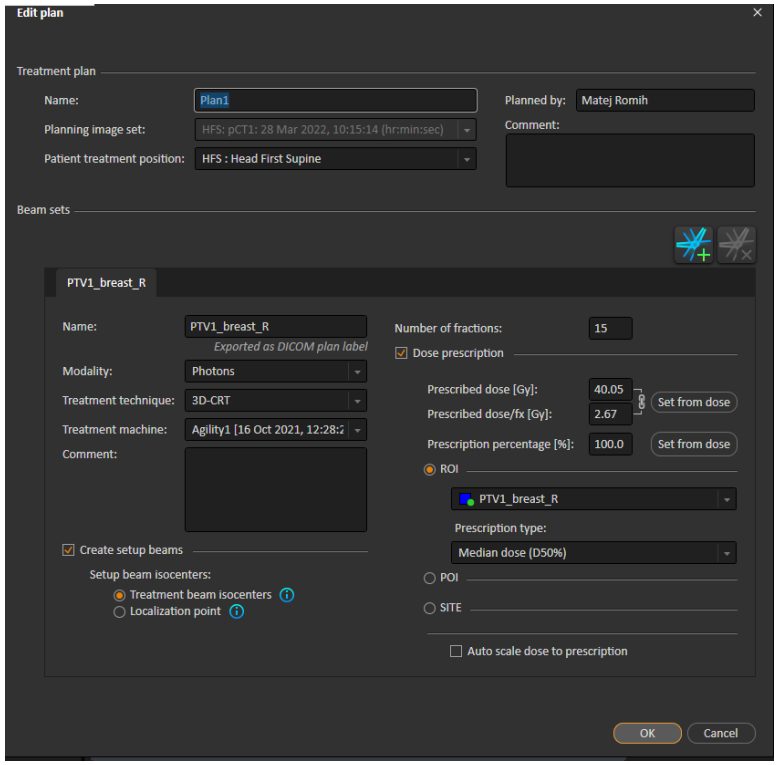

Fig. 1: All fields for creating plan were filled automatically with informations from Mosaiq, CT – DICOM header and planner (user who was logged-in).

Fig. 2: Example of script's final result for spinal metastasis 3D-CRT case.

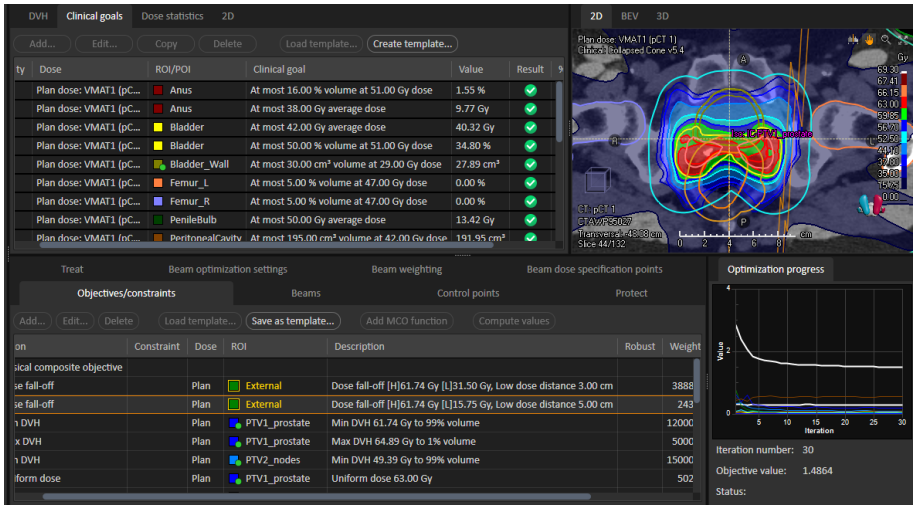

Fig. 3: Example of automatic VMAT planning for prostate cancer case.

Table 1:

Avreage days to completed the task - Planning				
Year	Prostate	Vulva/Uterus	Breast	Paliative cases
2020	7,8	5,1	5,7	2,1
2021	6,3	5,2	4,9	1,5
2022	5,3	3,2	3,3	1,1

Table 1: The presented results are average number of days between the day that physician finished with target delineation and the day that treatment plan was finished. Non-working days are also included. RayStation TPS was introduced in March 2021, the script that connected TPS and OIS was introduced in November 2021.

DIGITAL BREAST TOMOSYNTHESIS DOSE SURVEY IN CROATIA

Ana Božanić[1], Doris Šegota[2], Petra Valković Zujić[3], Maja Karić[4], Emina Grgurević Dujmić[5], Slaven Jurković[1]

[1]Medical Physics and Radiation Protection Department, Clinical Hospital Centre Rijeka, Kresimirova 42, Rijeka, Croatia Medical Physics and Biophysics Department, Medical Faculty, University of Rijeka, Brace Branchetta 20, Rijeka, Croatia
[2]Medical Physics and Radiation Protection Department, Clinical Hospital Centre Rijeka, Kresimirova 42, Rijeka, Croatia
[3]Radiology Department, University Hospital Rijeka, Kresimirova 42, Rijeka, Croatia Radiology Department, Medical Faculty, University of Rijeka, Brace Branchetta 20, Rijeka, Croatia
[4]Radiology Department, University Hospital Rijeka, Kresimirova 42, Rijeka, Croatia Radiological Technology Department, Faculty of Health Studies, Viktora Cara Emina 5, Rijeka, Croatia
[5]Radiology Department, Public Health Centre of Primorsko-Goranska County, Kresimirova 52A, Rijeka, Croatia

Purpose/Introduction

Mammography is a standard method of breast imaging using low energy X-ray beams. During past decade a new technique has been introduced in clinical practice worldwide - digital breast tomosynthesis (DBT). It is a 3D technique that can reduce or eliminate the tissue overlap effect. DBT systems also enable the reconstruction from 3D data into 2D synthesized mammography and, DBT in combination with synthesized mammography can provide better detection of breast cancer compared to standard mammography. Nevertheless, the increase in quality could lead to simultaneous increase of average glandular dose, therefore optimization is due. A valuable optimization tool is the use of diagnostic reference levels (DRLs). The aim of this work is to report on average glandular doses from DBT in Croatia and to propose the national DRL.

Materials/Methods

This study was carried out using data based on seven tomosynthesis units in health institutions in Croatia. It is a quantitative retrospective research study and involves the data of 1400 DBT images of 350 patients. Only craniocaudal (CC) and mediolateral oblique (MLO) views of female breasts were considered. Male patients, patients with implants and non-standard views were excluded. Average glandular dose (AGD), patient age, tube voltage (kVp), tube current and time product (mAs), target-filter combination and compressed breast thickness (CBT) were recorded. These parameters were obtained from the X-ray device data storage. The built-in dosimeter was previously calibrated and verified by independent measurements. DRL quantities were obtained according to data collection guidelines given by ICRP 135 [1]. The AGD values were recorded for both the CC and the MLO views for each breast separately. For each device, summary statistics were calculated for kVp, mAs and CBT. Median AGD was used as representative value for each institution. Third quartile of the median AGD values was proposed as the national diagnostic reference level for breasts of 50±5 mm thickness. National median value, also known as the achievable level, was also calculated. Additionally, median and third quartile of AGDs were calculated for six CBT rang es: 30–39 mm, 40-49 mm, 50–59 mm, 60–69 mm, 70-79 mm and 80-89 mm. If the number of images within a specific CBT range was less than ten per tomosy nthesis unit, the AGD value was excluded from the analysis to minimise sampling error.

Results

The mean and range values for kVp, mAs and CBT are shown in Table 1. Proposed national DRLs for tomosynthesis are 1.7 mGy, 1.7 mGy and 1.7 mGy for CC, MLO, and all projections, respectively. Achievable, values are 1.7 mGy, 1.7 mGy and 1.7 mGy for CC, MLO, and all projections, respectively. National DRLs are proposed also for for different breast thicknesses: 1.3 mGy for CBT range 30-39 mm, 1.5 mGy for CBT range 40-49 mm, 1.9 mGy for CBT range 50-59 mm, 2.4 mGy for CBT range 60-69 mm, 3.1 mGy for CBT range 70-79 mm, and 3.7 mGy for CBT range 80-89 mm. (Table 2.)

Discussion

Mean CBTs were similar across all institutions. Also, this study noted a similar mean tube voltage and mAs for 6 out of seven institutions. Slightly lower values were identified at institution 5 as compared to others. This could be because this device belongs to older generation of DBT systems and is of different manufacturer compared to all other included in the study. However, image quality comparison between devices was not performed as this is planned for the next phase of the research. Proposed national DRL values are comparable but slightly lower than values reported in other publications [2,3] and imply overall good practice. There are no notable differences between median and 3rd quartile values because the majority of DBT devices are of the same manufacturer and of the same manufacturing date. Numerous studies have been performed to determine the AGD in standard 2D mammography. Up to this date there are no established national DRLs for breast tomosynthesis in Croatia, only DRLs for 2D mammography were set. Since AGD is strongly correlated to CBT, analysis of data stratified by different breast thicknesses was also performed. This could be useful for optimization of the imaging practice even furthermore in detail.

Conclusions

DRLs are a valuable optimization tool of medical imaging procedures based on the use of ionizing radiation. To our knowledge, this is the first report of AGD values in breast tomosynthesis in Croatia. Overall, the results show acceptable and harmonized practice among institutions.

References

1. Vano E, Miller DL, Martin CJ, Rehani MM, Kang K, Rosenstein M, Ortiz-Lopez P, Mattsson S, Padovani R, Rogers A; Authors on behalf of ICRP. ICRP Publication 135: Diagnostic Reference Levels in Medical Imaging. Ann ICRP. 2017 Oct;46(1):1-144. doi: 10.1177/0146645317717209. PMID: 29065694.
2. Bouwman RW, van Engen RE, Young KC, den Heeten GJ, Broeders MJ, Schopphoven S, Jeukens CR, Veldkamp WJ, Dance DR. Average glandular dose in digital mammography and digital breast tomosynthesis: comparison of phantom and patient data. Phys Med Biol. 2015 Oct 21;60(20):7893-907. doi: 10.1088/0031-9155/60/20/7893. Epub 2015 Sep 25. PMID: 26407015.
3. McCullagh J, Phelan N. Digital Breast Tomosynthesis (DBT) Dose Survey and the establishment of a DRL for a National Breast Screening Service. Phys Med. 2017; 42: 361

Institution	Mean kVp ± SD	kVp Range	Mean mAs ± SD	mAs Range	Mean CBT ± SD (mm)	CBT range (mm)
1	32.4 ± 2.4	27 - 38	70.1 ± 12.4	33 - 94	58.4 ± 12.3	25 - 84
2	31.9 ± 2.7	26 - 40	64.4 ± 10.2	40 - 88	55.4 ± 13.6	21 - 85
3	30.8 ± 1.4	26 - 35	58.9 ± 13.1	38 - 146	51.0 ± 7.4	31 - 70
4	31.8 ± 2.5	26 - 38	68.8 ± 11.4	44 - 92	55.7 ± 13.4	21 - 81
5	29.3 ± 3.2	26 - 59	55.5 ± 16.1	27 - 99	51.4 ± 12.9	21 - 74
6	32.8 ± 2.8	27 - 43	65.3 ± 10.7	43 - 100	60.7 ± 12.6	27 - 99
7	32.5 ± 3.2	27 - 44	63.3 ± 11.1	35 - 86	58.0 ± 14.3	29 - 103

Table 1. Summary statistics for kVp, mAs and CBT for each institution

	AGD / mGy	
CBT / mm	median	3rd quartile
30 - 39 mm	1.3	1.3
40 - 49 mm	1.5	1.5
50 - 59 mm	1.9	1.9
60 - 69 mm	2.3	2.4
70 - 79 mm	3.1	3.1
80 - 89 mm	3.7	3.7

Table 2. Proposed national DRLs for CBT ranges for AGD in tomosynthesis

EXPLORING THE USE OF GAMMA-RAY POLARIZATION IN POSITRON EMISSION TOMOGRAPHY

Ana Marija Kožuljević[1], Tomislav Bokulić[1], Damir Bosnar[1], Mihael Makek[1], Siddharth Parashari[1], Luka Pavelić[2], Petar Žugec[1]

[1]*Department of Physics, Faculty of Science, University of Zagreb, Bijenička c. 32, 10000 Zagreb, Croatia*
[2]*Institute for Medical Research and Occupational Health, Ksaverska cesta 2, 10000 Zagreb, Croatia*

Purpose/Introduction

Measurement of gamma-ray polarization, which is important in many areas of fundamental and applied physics, may also be of great interest in biomedical imaging with Positron Emission Tomography (PET). Two gamma photons originating from positron annihilation are coincidently emitted back-to-back with exactly 511 keV energy and this distinctive features enable PET devices to identify them and distinguish them from the background events. However scatter and random coincidences still pose a challenge for imaging with PET, especially with the sources of very high activity. A feature of the annihilation gammas that has not been exploited in PET is their polarization. Namely, the two gamma quanta from positronium annihilation are generated with orthogonal polarizations and this correlation may be used as an additional information to classify true and false coincidences in PET. Simulation studies have shown that exploiting the polarization correlation of the annihilation quanta has a potential to improve the image quality, especially with sources of high emission rates where a probability to have a false positive coincidence is significant [1-3].

Gamma-ray polarization can be deduced in the process of Compton scattering, since the azimuthal scattering angle is preferentially perpendicular to the inital polarization vector. In events where both annihilation quanta undergo Compton scattering in their respective detectors, the initial orthogonality of the polarizations translates to the strong correlation of their azimuthal scattering angles. Clearly, background events will lack such correlation and hence this forms an additional handle to distinguish the true and the background coincidences. Typical instruments for measuring gamma polarization across different areas of physics, involve two detector layers: the scatterer to detect the recoil electron and the absorber to detect the scattered photon, both desirably with a good position resolution. The question arrises of how to cost-efficiently implement this in PET. Existing PET detectors encompass one highly segmented detector layer and adding another layer to enable the polarization measurement would dramatically increase the complexity and the cost of the system.

In this work we will present an alternative approach, where the polarization correlations are measured with detectors encompassing a single segmented layer, such that enable scaling-up the system efficiently. We have proved this concept experimentally [4] and we have been optimizing the detector configuration which will be used to construct a PET demonstrator able to exploit the gamma-ray polarization. We will give an overview of the activities undertaken at the University of Zagreb and partner intitutions within the "Single Layer Gamma-Ray Polarimeter for Medical Imaging Applications and Fundamental Physics Research (SiLGaP)" project.

Materials/Methods

We measure the polarization correlation of annihilation quanta using a system of two modules based on scintillator detectors read out by silicon photomultipliers (SiPM) (see Fig. 1). Each module has 64 scintillator crystals in 8x8 configuration optically coupled the the matching SiPM array. We have

assembled and tested modules of either LYSO:Ce (Eres@511 keV 13.7% ± 0.9%) or GAGG:Ce (Eres@511 keV 8.1% ± 0.5%) crystals with their sizes varying from 1.9 mm x 1.9 mm x 20.0 mm to 3.0 mm x 3.0 mm x 20.0 mm in order to compare the polarimetric performance depending on detector material and geometry. The signals are read out and processed by the TOFPET2 system [5]. During laboratory measurements two identical detector modules were placed 5 cm appart with a Na-22 source (1 uCi) in the middle. The setup was enclosed in a light-tight box with the temperature controlled at 18 ± 1 deg.

In the data analysis procedure, we select events in which both gamma photons undergo Compton scattering. This is achieved by requiring exactly two fired pixels per module (the scatterer and the absorber) and by selecting the energy window corresponding to Compton events. The Compton scattering angles θ and ϕ are reconstructed using the kinematic relations and the detector geometry, respectively. Finally, the distribution of the azimuthal angle difference ϕ_1 - ϕ_2 is obtained and its amplitude modulation is determined (see Fig. 2).

Results

We have extracted the polarimetric modulations depending on the kinematic event selection criteria and explored its dependence on detector geometry and material, resulting in modulation factors ranging from (0.26 ± 0.1)% to (0.34 ± 0.2)%. Generally higher modulation are obtained for those events with the more angular selection criteria are applied (see Table 1).

Discussion

We have demonstrated that the measurement of the polarization of the annihilation quanta is feasible with single-layer polarimeters in all assembled detector configurations. More precise energy and angular selection criteria lead to higher modulation factors. This points to the fact that finely segmented scintillators (cross section 2 mm x 2 mm) are the best choice to distinguish between the true coincidence events where the modulation is prononuced and the false coincidences where it is lacking.

The next step in our project is to assemble a PET demonstrator. It will contain four super-modules of the segmeneted scintillators, with 16 x 16 pixels in each module. The modules will be placed on the mechanical construction with aproximatelly 70 cm diameter (Fig. 4). The ring will have to possibility of precise rotation around the scanner axis in order to cover the full angular range needed for quality image reconstruction. Once assebmled and comissioned, the demonstrator will be tested at the University Hospital Centre Zagreb's nuclear medicine department using the appropriate phantoms. We expect these tests to quantify the feasibility of using the polarization of gamma radiation as an additional handle to select true events in PET imaging.

Conclusions

The polarization correlation of annihilation quanta can be successfully measured via Compton scattering in single-layer segmented scintillation detectors. The amplitude of the polarimetric modulation, and thus the ability to use this feature for signal/background discrimination in PET, is generally higher for more finely pixelated detectors. This confirmation is important since, the measurement of Compton events using the single-layer concept may be implemented in PET systems without significantly adding to their complexity. Further investigation involving an extended demonstrator system are underway to better assess the benefit of measuring the polarizations of annihilation quanta in PET.

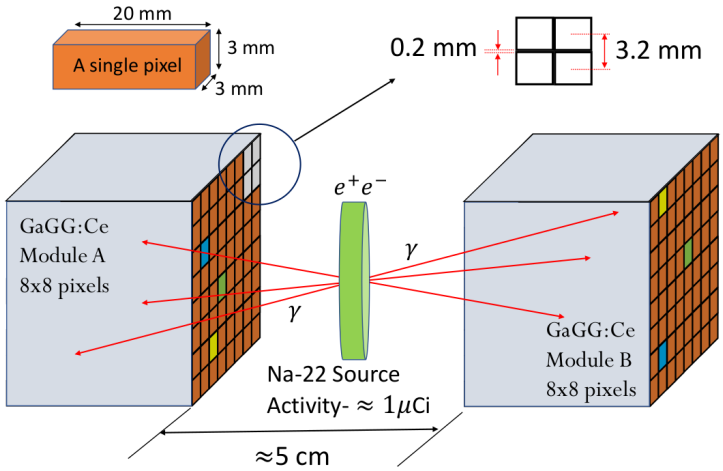

Fig. 1: A schematic drawing of the laboratory testing setup.

References

1. McNamara A et al. (2014), Towards optimal imaging with PET: An in silico feasibility study. Phys. Med. Biol., 59: 7587.
2. Toghyani M et al. (2016), Polarisation-based coincidence event discrimination: An in silico study towards a feasible scheme for Compton-PET. Phys. Med. Biol., 61: 5803.
3. Watts DP et al. (2021), Photon quantum entanglement in the MeV regime and its application in PET imaging. Nat. Commun., 12: 2646.
4. Makek M et al. (2020), Single-layer Compton detectors for measurement of polarization correlations of annihilation quanta. Nucl. Instrum. Methods Phys. Res. A, 958: 162835.
5. Francesco AD et al. (2016), TOFPET2: A high-performance ASIC for time and amplitude measurements of SiPM signals in time-of-flight applications. J. Instr., 11: C03042.

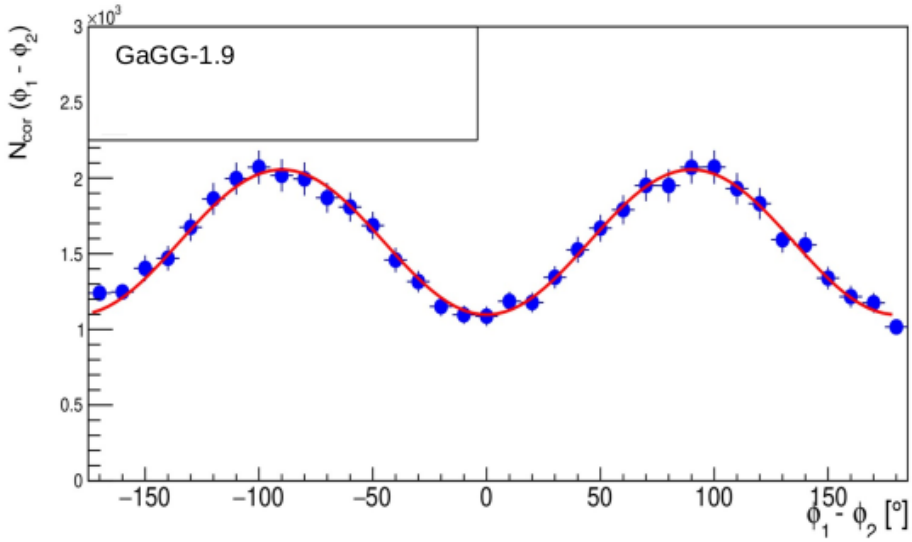

Fig. 2: An example of the obtained modulated azimuthal angle difference due to the polarization correlations.

Setup	$80° < \theta_{1,2} < 84°$		$77° < \theta_{1,2} < 87°$		$72° < \theta_{1,2} < 90°$	
	$\langle\Delta\phi\rangle$	μ	$\langle\Delta\phi\rangle$	μ	$\langle\Delta\phi\rangle$	μ
GaGG-1.9	15.3°	0.34 ± 0.02	15.3°	0.34 ± 0.01	15.3°	0.30 ± 0.01
GaGG-2.9	18.3°	0.29 ± 0.02	18.2°	0.29 ± 0.01	18.2°	0.26 ± 0.01
GaGG-3.0	18.9°	0.29 ± 0.02	18.9°	0.29 ± 0.01	18.8°	0.28 ± 0.01
LYSO-1.9	15.8°	0.33 ± 0.01	15.8°	0.32 ± 0.01	15.8°	0.31 ± 0.01
LYSO-2.0	16.9°	0.34 ± 0.02	16.9°	0.33 ± 0.01	16.7°	0.31 ± 0.01

Table 1: The summary of the extracted polarimetric modulation factor μ for different configurations and angular selection criteria.

Fig. 4: The mechanical construction for the PET demonstrator.

SLOVENIAN DOSE SURVEY IN PEDIATRIC RADIOLOGY

Manca Podvratnik[1], Urban Zdešar[1]

[1]*Institute of Occupational Safety, Ljubljana, Slovenia*

Purpose/Introduction

It has long since been established that children are more sensitive to ionizing radiation than adults. They also have a longer life span ahead of them in which they may develop radiation induced effects. This is why special attention is paid to radiation protection of our youngest patients. For this reason and because children have fewer natural diseases than adults, they are less often referred to radiological procedures by clinicians. And so, even though special attention should be paid to radiation protection of children, a statistically significant amount of data on radiation exposure of pediatric patients is not always easily available. Especially in smaller institutions, where pediatric patients are fewer, adult patient doses are evaluated and compared to national diagnostic reference levels (DRLs) on a regular basis, whereas imaging protocols for pediatric patients are not reviewed. A comprehensive Slovenian pediatric dose survey was carried out and results are presented in these short proceedings.

Materials/Methods

With the development of the DICOM standard, patient dose information is now being recorded for every medical exposure and saved in the metadata connected to the resulting medical image. The DICOM standard also introduced the radiation dose structured report (RDSR) for the specific purpose of patient dose recording (1). This made the development of patient dose tracking software possible. An in-house dose tracking system Orqa was used to collect data on pediatric radiation exposure in 15 Slovenian hospitals, this represents the majority of Slovenia's general hospitals. We focused on the available data, not all modalities and all the imaging units could be included in the survey. Due to the still limited accessibility of dosimetric data in older x-ray machines and CT scanners, this survey could not include all pediatric departments and all x-ray units, basically due to the fact that older equipment that does not have DAP meters needed to monitor patient exposure. Even though the data set used in the survey does not represent all imaged pediatric patients in a selected 3-year time period between 1st November 2018 and 2021, it nevertheless represents its large part. With respect to the availability of data, we focused separately on general radiography and computed tomography, leaving interventional procedures for future studies when more data is available.

Results

Patient dose levels vary considerably with patient age, size and weight. The methodology for age-grouping described in European PiDRL guidelines was used (2). For general radiography over 46.000 patients under the age of 18 were included in the survey, this represents 12,6% percent of the Slovenian pediatric population. Over 81.000 general radiography studies were carried out and 120.000 images and doses recorded. The largest number of procedures were carried out on patients at the age of 12, slightly more patients were male than female (57% to 43% respectively). For infants and toddlers, the most common radiography procedure is of the chest followed by the head. For older age groups the prevailing procedure is of the extremities (ankle, knee, hand, elbow, finger, foot etc.) due to injury and taken in emergency departments. We observed a generally good practice for pediatric imaging when comparing patient radiation exposures (or median dose area products DAP to be exact) to European pediatric DRLs.

The radiation doses in computed tomography are significantly higher than in general radiography and so the studies even fewer in number. In the three-year time period, we followed 19 CT scanners in 12 general hospitals, some of them were not yet working or being tracked during the entire 3 years. The data set includes slightly over 2.000 patients that underwent 2.500 computed tomography procedures. This represents 0,5% of children under the age of 18 in Slovenia, showing that CT examinations in children are fairly rare. The most common for all age groups is the CT examination of the head without the use of contrast agents. For patient radiation exposure estimation, two operational quantities are used: dose length product DLP and the CTDI dose index, both are estimations calculated based on scanner exposure parameters and standard phantoms. There are several limitations to this method for patient dose estimation, especially for smaller pediatric patients where doses are being underestimated (3). Nevertheless, the median DLPs were compared to European pediatric DRLs. Especially for smaller children, when patient head size differs considerably from adult sizes, we observed the use of dedicated pediatric imaging protocols. For older patients the median DLPs on some units on the other hand exceeded the European pediatric DRLs.

Conclusions

A comprehensive dose survey of the Slovenian pediatric population was carried out. Due to a limited availability of patient exposure data not all modalities and departments could be included. The focus of the survey was on data that was available. National diagnostic reference levels for pediatrics have not been established in Slovenia yet, the number of data collected is still not adequate and more importantly, several dedicated units for pediatric imaging are not included because of their age and non-compatibility with dose tracking software. Even though most data were collected on non-dedicated units, we found that most departments and imaging procedures have estimated median patient exposures below the European diagnostic reference levels. Nonetheless, the system for dose tracking is set up and in place for future surveys, when new machines replace old non-compatible units, more departments can be included and more information collected. With more information and experience more guidance on pediatric imaging protocol optimization may be given.

References

1. DICOM Digital Imaging and Communications in Medicine (DICOM). Supplement 94: Diagnostic X-Ray radiation Dose Reporting (Dose SR) (2005).
2. European Commission, Radiation Protection No. 185, PiDRL – European Diagnostic Reference Levels for Paediatric Imaging (2018).
3. American Association of Physicists in Medicine. Size-Specific Dose Estimates (SSDE) in Paediatric and Adult Body CT Examinations, AAPM Report No. 204 (American Association of Physicists in Medicine, College Park, MD) (2011).

ROLE OF MEDICAL PHYSICIST IN MAGNETIC RESONANCE IMAGING AT UNIVERSITY HOSPITAL RIJEKA

Kristian Stojšić[1], Slaven Jurković[2]

[1]*Medical Physics Department, University Hospital Rijeka, Rijeka, Croatia*
[2]*Medical Physics Department, University Hospital Rijeka, Rijeka, Croatia. Department of Medical Physics and Biophysics, Faculty of Medicine, University of Rijeka, Croatia*

Purpose/Introduction

This work depicts the role and challenges of medical physicist in clinical and research environment of magnetic resonance imaging in University Hospital Rijeka. This is also the first instance of such cooperation in the country. The aim was to establish a robust magnetic resonance imaging quality control system and to start the optimization process of clinical imaging. Cooperation in research studies that involve magnetic resonance imaging was also started with the project "The epidemiology of Parkinson's disease in Croatia and the influence of genetic factors and microbiota on the progression and treatment outcomes of the disease" (acronym GiOPARK).

Materials/Methods

Quality control system for magnetic resonance imaging was established using American College of Radiology and National Electronics Manufacturers Association (NEMA) standards. ACR protocol was chosen for assessment of general image quality parameters such as signal to noise ratio (SNR), slice position and thickness accuracy, uniformity and high contrast resolution. The assessment was performed using dedicated ACR compatible phantom. NEMA standards were chosen for quality control of each specific radiofrequency coil and its elements using uniform phantoms. Imaging data acquisitions are performed by Siemens Magnetom Aera 1,5 T device. Due to large number of data obtained during each quality control session and numerous calculations required, two computer algorithms were developed in MATLAB programming environment to automate the process.

Furthermore, several MRI clinical protocols were chosen for sequence optimization. The aim of sequence optimizations was to acquire the highest achievable image quality while keeping sequence time as short as possible. This was accomplished by varying several imaging parameters, e.g., diffusion mode and directions, b-values and averages, acquisition matrix and phase encoding direction. Resulting images were compared with the images acquired prior to sequence optimization.

As part of the GiOPARK project, the role of medical physicist is in calculating changes in free water within the substantia nigra of Parkinson's disease patients. This includes free water (FW) maps, FW-corrected diffusion tensor imaging (DTI), and conventional DTI measures of fractional anisotropy, mean diffusivity, axial diffusivity, and radial diffusivity. Calculations are made using bi-tensor model and variational framework. The algorithm dedicated to the determination of data of interest is under development. FMRIB Software Library (FSL) is used for all image corrections and conventional DTI measurements.

Results

MATLAB program results of slice thickness accuracy test and geometric accuracy test are shown in Figure 1. Region of interest (ROI) placement for SNR calculation and grey level image for a body

array coil element is shown in Figure 2. Table in Figure 3 shows results of SNR and non-uniformity calculations for complete body array coil.

An example of a diffusion imaging sequence for pelvis before and after the optimization is shown in Figure 4. There is a significant increase in resolution and overall image quality when optimization is performed.

Discussion

MRI quality control has become routine at our hospital. ACR protocol is conducted monthly, and radiofrequency coil quality control quarterly. The implementation of quality control showed poor performance of three radiofrequency coils, which were changed accordingly. This illustrates the necessity of comprehensive quality control of MRI system.

Sequences that were improved during optimization are included in routine MRI clinical protocols. Due to better resolution and discernibility of features, radiologists find it better to obtain required diagnostic information.

Conclusions

Work of medical physicist has been successfully integrated in clinical and research environment of magnetic resonance imaging at UH Rijeka. MRI quality control has become routine and, along with sequence optimization, already showed appropriate results. Knowledge of medical physics appears to be a great asset for the aforementioned part of the GiOPARK project. Future for scientific cooperation is promising since there are already two research projects in early stages. The projects are planned to focus on semi-automatic segmentation and classification of different tumors.

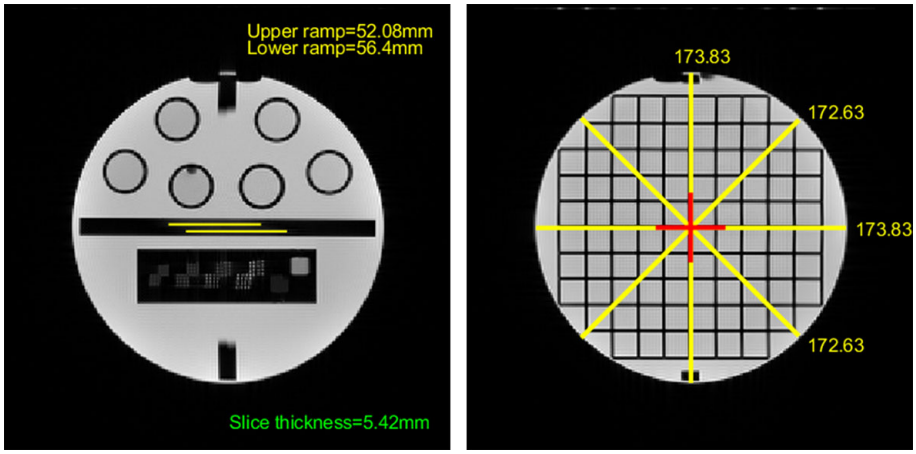

Figure 1: Example of MATLAB program results for ACR protocol. Left image shows result of slice thickness accuracy test. Right image shows result of geometric accuracy test.

References

1. Price R, Allison J, Clarke G, Dennis M, Hendrick RE, Keener C, et al. 2015 ACR Magnetic Resonance Imaging Quality Control Manual. 2015. American College of Radiology.

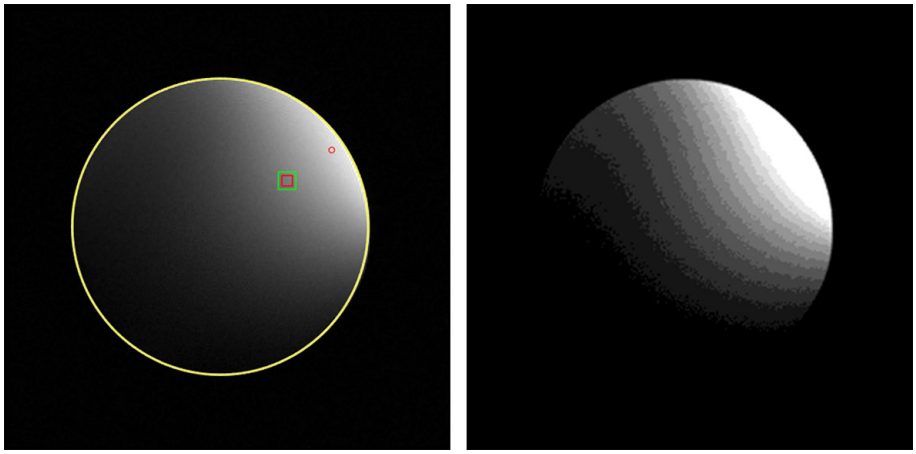

Figure 2: Example of MATLAB program results for body array coil quality control of a single coil element. Left image shows ROI placement for SNR calculation. Right image shows distribution of gray levels.

2. Guttuso T Jr, Bergsland N, Hagemeier J, Lichter DG, Pasternak O, Zivadinov XR (2017). Substantia Nigra Free Water Increases Longitudinally in Parkinson Disease. AJNR Am J Neuroradiol 39:479–84
3. Pasternak O, Sochen N, Gur Y, Intrator N, Assaf Y (2009). Free Water Elimination and Mapping from Diffusion MRI. Magnetic Resonance in Medicine 62:717–730

BODY ARRAY FLASH

Coil	N	Signal	Noise	SNR
BO1	43.93	401	3.8	105.51
BO2	43.65	404	4.13	97.71
BO3	43.34	392	3.73	105.06

Coil	Signal	Noise	SNR
B11	278.72	3.42	81.48
B12	265.86	3.47	76.58
B13	281.22	4.54	61.89
B14	255.17	4.05	63
B15	292	3.88	75.23
B16	276.11	3.5	78.98
B21	272.06	3.5	77.77
B22	277.92	4.32	64.28
B23	274.72	4.73	58.08
B24	255.89	4.59	55.77
B25	286.44	3.55	80.66
B26	276.39	2.92	94.54
B31	247.42	2.99	82.81
B32	274.58	3.51	78.32
B33	264.11	3.84	68.72
B34	271.78	3.91	69.45
B35	268.69	3.89	69.12
B36	277.25	3.29	84.24

BODY ARRAY SPIN ECHO

Coil	N	Signal	Noise	SNR
BO1	44.33	768	2.12	362.24
BO2	46.44	773	2.26	342.19
BO3	44.14	750	2.08	360.26

Coil	Signal	Noise	SNR
B11	525.83	2.77	189.61
B12	488.03	3.07	159.11
B13	510.42	3.22	158.65
B14	482.25	3.51	137.47
B15	546.61	3.25	168.13
B16	518.89	2.66	194.79
B21	504.89	3.13	161.44
B22	523.17	3.37	155.19
B23	540.5	3.43	157.79
B24	508.14	3.55	142.95
B25	538.42	2.61	205.91
B26	497.39	2.9	171.43
B31	479.36	2.42	198.27
B32	515.28	2.66	193.99
B33	500.11	3.12	160.16
B34	522.17	2.91	179.21
B35	510.94	2.75	185.48
B36	518.64	2.09	247.97

Figure 3: Table with results of SNR and non-uniformity (N) calculations for body array coil. BO1 to BO3 are labels for coil clusters, while B11 to B36 are labels for individual coil elements.

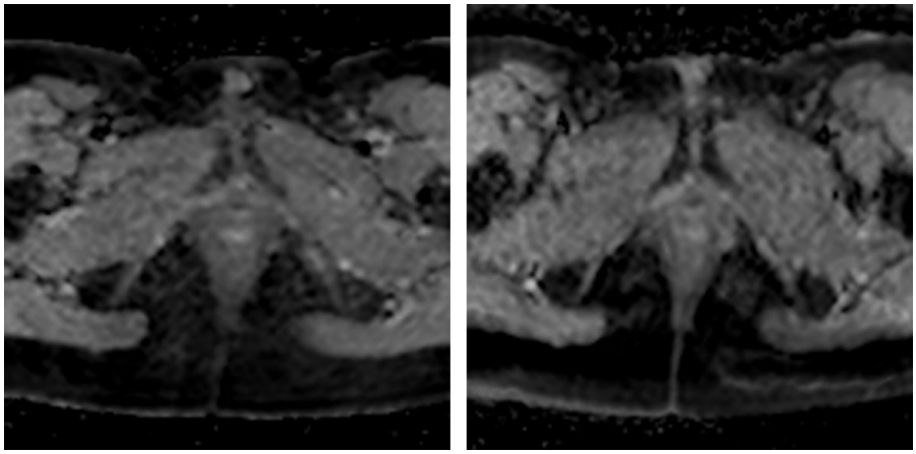

Figure 4: ADC maps for single layer image of pelvis. Left image was acquired before optimization process, while right image was acquired after optimization process.

APPLICATION OF DUKESIM SOFTWARE IN MATERIAL DECOMPOSITION STUDIES

Stevan Vrbaski[1], Ehsan Abadi[2], Adriano Contillo[3], Renata Longo[1], Paul Segars[2], Ehsan Samei[2]

[1]*University of Trieste, Italy*
[2]*Duke University, USA*
[3]*Elettra Sincrotrone Trieste, Italy*

Purpose/Introduction

In clinical imaging, new technologies are being constantly developed. Testing of critical scanning parameters and performance under specific clinical tasks on humans is not feasible due to ethical reasons. Physical phantoms as an alternative solution can be put under numerous imaging conditions but are limited in their complexity, and it becomes expensive to produce more detailed and diverse human anatomy. Ideally one would need an approach that 1) is able to represent a vast diversity of anatomical features, 2) does not expose humans to increased doses of radiation, 3) enables task-specific optimization, and 4) is efficient. In a virtual imaging setup, the full process of image acquisition is done in-silico by modeling all the necessary components [1] – source (beam propagation and scatter), radiation detector, and patients (Figure 1). Virtually created human anatomy (virtual patients) can be produced in large quantities and diversity; different pathologic features can be added, and scanning can be done multiple times. Finally, the exact anatomy of the virtual patient and all scanner-related parameters are known, thus providing a “gold standard” or “ground truth”. This is particularly interesting for the development and evaluation of new algorithms for improved clinical information, such as material decomposition, iodine quantification, radiomics, lesion detection, and image harmonization using the most advanced analytical and machine learning approaches. The Clinical Virtual Imaging Trials (CVIT) group at Duke University has developed DukeSim, an open-source software capable of simulating clinical CT image acquisition [2]. In this communication it will be presented and an example of application will be discussed.

Materials/Methods

In DukeSim software a photon-counting (PC) detector model has been implemented, available in state-of-the-art PC-CT scanners (Figure 2). Among other benefits, PC detectors are particularly interesting because of their intrinsic photon-thresholding feature suitable for spectral imaging applications. DukeSim software was used to obtain spectral images of detailed lung anthropomorphic phantom (XCAT in Figure 3). Obtained data were then analyzed with a newly developed algorithm for material decomposition, decomposing the images in arbitrary pairs of basis materials. The algorithm uses a singular-value-decomposition (SVD) approach to extract the most dominant physical contributions to image formation. An analytical method was applied to relate extracted principal components to basis material maps [3]. From material maps, quantitative information such as material density and effective atomic number (Zeff) were computed. Optimal threshold values were investigate for this specific application.

Results

Using the PCD model and XCAT lung phantom, the specific implementation of the material decomposition algorithm to the spectral data was applied. The density and Zeff maps obtained from spectral

data are obtained. We demonstrate that an optimal threshold value gives the same quality of decomposition as implementing several thresholds to the same detector.

Discussion

Using DukeSim, parameters such as radiation dose, threshold position, material composition, etc. have been altered to test the robustness of our algorithm and to find optimal conditions leading to the most accurate decomposition. This type of analysis wouldn't be feasible with clinical scanners.

Conclusions

DukeSim is a powerful and flexible simulation tool for clinical CT imaging. The application of the material decomposition algorithm in the DukeSim environment demonstrates promising contribution in tumor diagnosis and quantitative tissue inspection in the lung region.

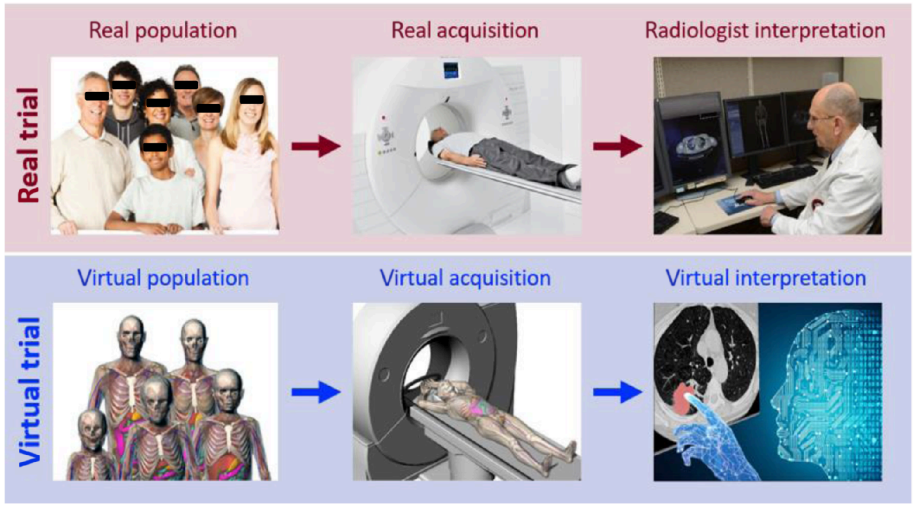

Workflow of virtual imaging trial vs traditional (real) trial

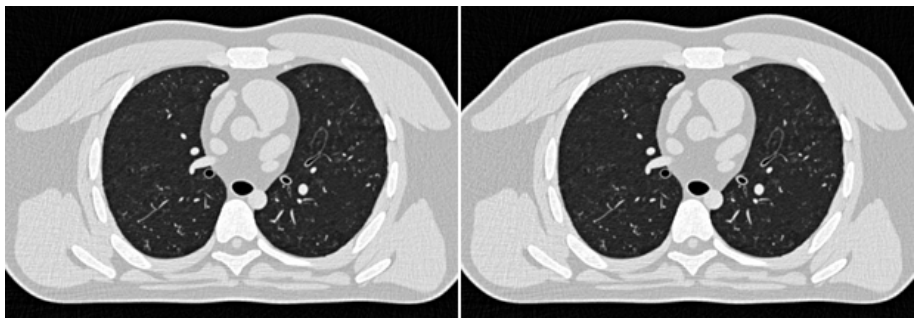

Reconstructed CT images at low (left) and high (right) energy threshold using the photon-counting detector model inside DukeSim

Example of XCAT phantom

References

1. Abadi E, Segars WP, Tsui BMW, Kinahan PE, Bottenus N, Frangi AF, et al. Virtual clinical trials in medical imaging: a review. J Med Imaging (Bellingham). 2020 Jul;7(4):042805.
2. Abadi E, Harrawood B, Sharma S, Kapadia A, Segars WP, Samei E. DukeSim: A realistic, rapid, and scanner-specific simulation framework in computed tomography. IEEE Trans Med Imaging. 2019 Jun;38(6):1457–65.
3. Stevan Vrbaski, Renata Longo, and Adriano Contillo "From spectral decomposition through SVD to quantitative description of monochromatic CT images: a phantom study", Proc. SPIE 12031, Medical Imaging 2022: Physics of Medical Imaging, (21 February 2022); https://doi.org/10.1117/12.2613130

IAEA PROJECT ON REMOTE AND AUTOMATED QUALITY CONTROL PROGRAMME FOR RADIOGRAPHY AND MAMMOGRAPHY EQUIPMENT

Urban Zdešar[1], Manca Podvratnik[1]

[1]*Institute of Occupational Safety, Ljubljana Slovenia*

Purpose/Introduction

In 2021 IAEA published a Human Health Report No. 39 entitled Implementation of a Remote and Automated Quality Control Programme for Radiography and Mammography Equipment. At the same time a Coordinated Research Project was launched (E 242025 CRP) with the aim to test the proposed methodology worldwide. 11 countries are participating in the project, among them Hungary and Slovenia.

Materials/Methods

The methodology proposed in the publication is based on simple, inexpensive test objects (one phantom for radiography and one for mammography - Image 1). The phantoms are built using simple, low cost materials that are widely available (PMMA, Cu and Al). Phantom images are analysed by a software tool (ATIA) also developed by the Agency and distributed to the project participants. Analysis can be done either on a local basis (ATIA is a stand-alone software) or centrally if there is a way of collecting DICOM images. Results derived by the software are presented within the software itself (Image 2) or can be exported as csv file. Institute of occupational safety have developed an application for collecting and analysing DICOM images, which is at the moment used in Slovenian mammography screening programme. Currently we are analysing flat field mammography images, produced daily in each screening center. We plan to extend the software with the capabilities offered by ATIA software, which would allow to automatcally analyse IAEA phantom images and track the imaging performance of radiography and mammography X-ray machines.

Results

The project is in its initial phase so there is not much results available. In the presentation we plan to present methodology and some of the issues that appear during the construction and first use of phantoms.

Conclusions

The aim of the presented CRP is to investigate the correlation of the image quality (IQ) metrics with equipment performance, including the establishment of typical reference values and acceptable ranges of variation. Project will create an international network of medical physicists that can interact and support each other in clinical practice through implementation of the remote automated QC program.

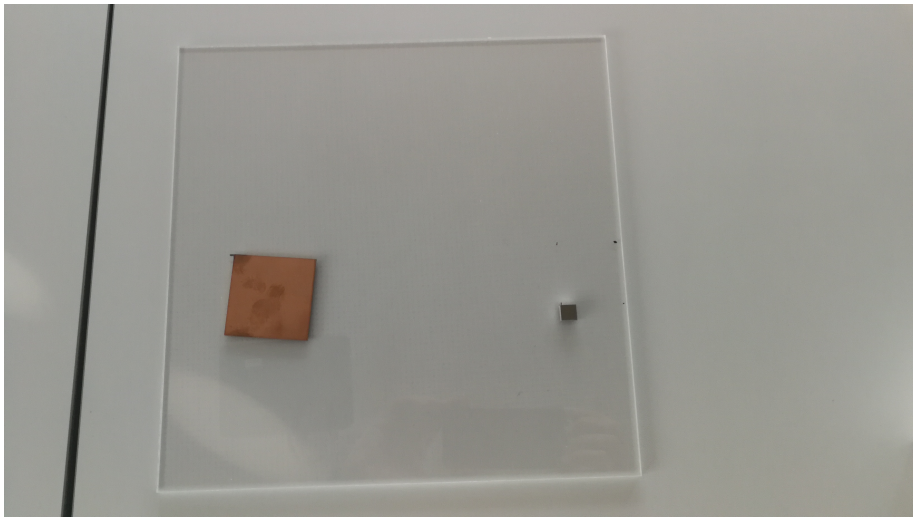

Photography of radiography test phantom, proposed by IAEA for automated QC. Phantom consist of 5 mm PMMA plate to which 2 mm Cu (5 cm x 5 cm) and 4 mm Al (1 cm x 1 cm) are attached. Phantom is used together with 2 mm Cu attenuator attached to the collimator of the X-ray machine.

References

1. IAEA. Human Health Report No. 39. Implementation of a Remote and Automated Quality Control Programme for Radiography and Mammography Equipment. International Atomic Energy Agency, 2021.

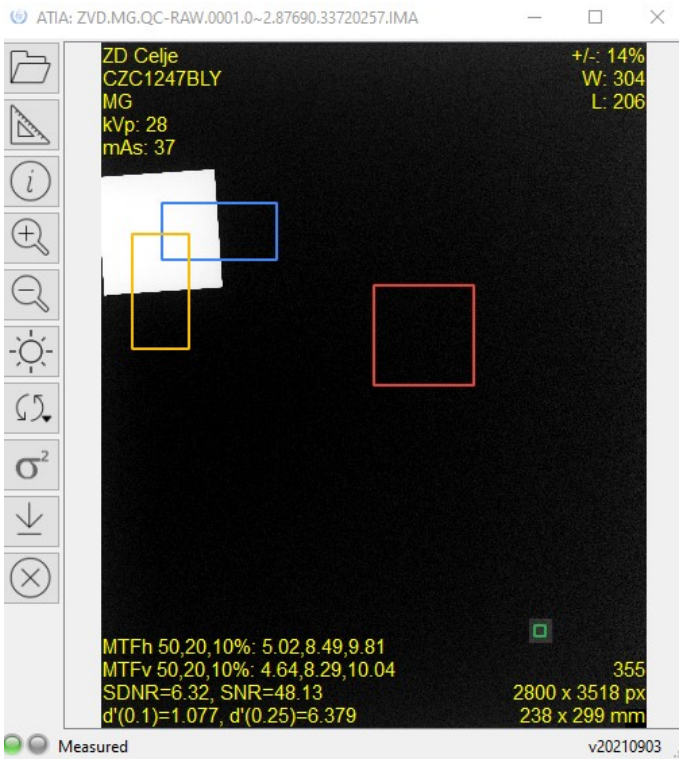

An example of ATIA software window with the results of mammographic QC phantom image. Coloured rectanles are ROIs analysed by the software, and data on the lower corner left of the image are summarised results from the analysis.

THE ITALIAN HOSPITAL NETWORK FOR THE CLINICAL TRAINING OF THE INTERNATIONAL MASTER IN MEDICAL PHYSICS

Paola Bregant[1], Renata Longo[2], Renato Padovani[3], Mara Severgnini[1]

[1]Medical Physics Department, ASUGI, Trieste, ITALY
[2]Department of Physics &INFN, Trieste University, Trieste, ITALY
[3]Abdus Salam International Centre for Theoretical Physics (ICTP), Trieste, ITALY

Purpose/Introduction

The Abdus Salam International Centre for Theoretical Physics (ICTP) and the University of Trieste have been organizing the Master of Advanced Studies in Medical Physics, opened to graduate students from low and medium income countries. The Master, accredited by IOMP and financially supported by IAEA, provides a two-year programme. During the first year, the students attend courses and practical sessions in Trieste (Italy); the second year is devoted to a supervised clinical training in a hospital facility. The Medical Physics Departments of various Italian Hospitals guarantee a network for hosting the student during the training.

Materials/Methods

The clinical training The Portfolio for the clinical training is derived from IAEA (TSC 37, 47 and 50) and AFRA recommendations. This document describes the content and the duration of the activities during the training for three different areas of interest: radiotherapy, nuclear medicine and diagnostic and interventional radiology. As an example, the modules for radiotherapy are reported in Image 1

An experienced medical physicist is identified as the Clinical Supervisor and guides the students in the training. He can adapt the portfolio by taking into account the existing competencies, needs and skills of resident. For specific modules or sub-modules, other medical physicists of the Department can be involved, sharing the tasks inside the Department. Periodically, the competencies have to be self-assessed by the Resident and assessed by the tutor/tutors; regular meetings with the Clinical Supervisor are mandatory for evaluating the improvement and, if necessary, for reframing the training programme. A thesis has to be prepared in the period of the clinical training and discussed at the end of the Master.

Results

The Network of hospitals for the clinical training Up to now, 9 cycles of the Master have been organized, involving 177 students (115 male and 62 female) from 70 countries (see Image 2) .

The Italian Medical Physicists community collaborates to the Master programme by hosting the students for the clinical training. The network of hospitals includes 25 different Medical Physics Departments and a higher number of clinical supervisors supported the residents.

Conclusions

Different opinions can be reported on the clinical training because of the not homogeneous preparation level and background of the residents. The presence of a student in the Department can range from a

valid support in the daily work to a heavy commitment for guarantee an useful teaching process. The collaboration offered from the clinical supervisor to the student is often not completed at the conclusion of the Master, but it can continue for years through remote support in the activities in the country of origin. Anyway, the human relationships among people coming from different areas of the world are always an enriching experience.

References

1. G. Loreti, H. Aslian, A. Brito, H. Delis, R. Longo, R. Padovani, Evaluation of the Impact of an International Master of Advanced Studies in Medical Physics, World Congress on Medical Physics and Biomedical Engineering 2018, IFMBE Proceedings 68/1, https://doi.org/10.1007/978-981-10-9035-6_162

DEVELOPMENT OF A PREGNANT FEMALE PHANTOM AND CALCULATION OF FETAL DOSE DURING A PHOTON BREAST RADIOTHERAPY

Hrvoje Brkić[1], Vjekoslav Kopačin[2], Dario Faj[1], Mladen Kasabašić[2], Stipe Galic[3], Ana Ivkovic[2]

[1]Faculty of dental medicine and health, J. J. Strossmayer University of Osijek Faculty of medicine, J. J. Strossmayer University of Osijek
[2]Faculty of medicine, J. J. Strossmayer University of Osijek Clinical hospital Osijek
[3]Clinical hospital Mostar

Purpose/Introduction

The incidence of carcinoma during pregnancy is reported to be 1:1000 – 1:1500 pregnancies, and it has increased over the last 30 years. Breast carcinoma is the most common malignant tumor diagnosed during pregnancy. Within this study a model of the pregnant female, in her second trimester of pregnancy, is developed. It that can be used for radiotherapy treatment planning (as DICOM data), Monte Carlo simulations (as voxelized geometry) and for experimental dosimetry using 3D printing of the molds (as STL files). As a proof of concept, the phantom was used for fetal dose estimation during a photon breast radiotherapy plan.

Materials/Methods

The developed phantom is based on an MRI and CT images of a female patient in her 18th week of pregnancy. For the treatment of a left breast carcinoma 3D conformational radiotherapy was used. Beam energy was 6 MeV and the prescribed dose was 50 Gy in 25 fractions. The voxelized geometry of the phantom was used for Monte Carlo (MC) simulations using MCNP code in which all radiotherapy fields were simulated independently to determine both the breast target dose and fetal dose.

Results

Phantom was developed in such a manner that pregnant female and her fetus were scanned “in vivo” using MRI during pregnancy and CT after childbirth. The modelled photon breast radiotherapy plan, applied to the phantom, indicated that the fetus dose is 59 mGy for 50 Gy prescribed to the breast. The results clearly indicate that only 9.5 % of the photons reaching the fetus are generated in accelerator head through scatter and leakage, but the dominant component is scattered radiation from the patient’s body.

Discussion

The study offers the possibility to perform treatment planning, Monte Carlo simulations and physical measurements on a pregnant female phantom which is important for the improvement of current dosimetry practices in clinics. Our feasibility study demonstrated that the dose received by the fetus, during photon breast radiotherapy was just above the recommendation level which demonstrates the need to have good dosimetry tools in place for dose assessment and optimization.

ASSESSMENT OF THE CT SCAN AND CBCT DOSES FOR DIFFERENT IMAGING PROTOCOLS USED IN RADIOTHERAPY

Anja Lazović[1], Snežana Vostinić[1], Borko Nidžović[1], Ivana Mišković[1]

[1]*Institute for oncology and radiology of Serbia, Belgrade, Serbia*

Purpose/Introduction

Modulated dose delivery techniques provide high degree of conformity of treatment dose delivered to the tumor, while also significantly decreasing the dose to the surrounding tissue. Verification of patient setup before treatment is an indispensable proceeding in ensuring high degree of accuracy in the delivery of treatment plan. Changes in patients anatomy, positional errors, as well as movement during the treatment, if not corrected, can all lead to discrepancies in dose that is being delivered to the target, as well as the dose being delivered to organs at risk in the tumor's surroundings. Dose received from CT scanner and from imaging procedures is often being overlooked in radiotherapy treatment, since it's a couple of orders of magnitude smaller than the prescribed dose. Furthermore, it is important to consider that daily imaging during radiotherapy treatment consisting of 30+ sessions can result in a notable cone-beam computed tomography (CBCT) imaging dose and lead to an increased risk of developing secondary malignancy. Two methods for quantifying the imaging dose were incorporated to evaluate CT scan dose and kilovoltage CBCT dose: Volume computed tomography dose index (CTDIvol) and dose length product (DLP) values; and the Cone-Beam Dose Index (CBDI). The aim of this study was to evaluate our clinics protocols for CT simulator and CBCT imaging by calculating CTDI and DLP for 2 CT scanners (General Electric healthcare CT 590 RT and Siemens Somatom definition edge); as well as CTDI, DLP and CBDI for 5 radiotherapy accelerators (2 Truebeam, 2 Halcyon and Clinac IX - Varian Medical Systems) using corresponding radiotherapy protocols for pelvis, head, thorax and pediatric, in order to estimate CT and CBCT doses that patients receive from imaging various localizations. Normalized effective dose per DLP was estimated for standard patients (adults and pediatric patients of diverse age) over different body regions.

Materials/Methods

The measurements on CT scanners were carried out with Magic Max solution (IBA Dosimetry, Germany) that consist of: 3 part PMMA CT phantom (body, head/pediatric body and pediatric head), ionization chamber with active length of 100 mm and Magic max universal basic unit. The length of the PMMA phantom is 15 cm, while the diameters for body, head/pediatric body and pediatric head were 32 cm, 16 cm and 8 cm, respectively. The same equipment was used on the three commercial Varian CBCT imaging systems: the Clinac IX On-Board Imager (OBI), the TrueBeam X-ray Imaging System (XI) and fast kV CBCT on Halcyon.

Results

Clinac IX gave the highest overall values for CTDI, CBDI and effective dose values across all the applied protocols, while the lowest recorded doses were for the two Halcyon machines. CTDI, CBDI, nCTDIw and nCBDIw differences were most notable for head and pediatric head protocol, where Clinac delivered approximately 2-3 times higher doses than the other machines. The difference in

effective CBCT doses between Clinac IX and Halcyon is most remarkable for pelvis protocol, with Clinac delivering approximately 2 times larger doses for given region. Effective doses for head and pediatric regions were comparable, for both TrueBeams and Halcyons, with Clinac giving insignificantly higher doses than the two.

Conclusions

Computed Tomography Dose Index underestimates CBCT doses as a consequence of an insufficient ionization chamber length needed for capturing the full dose profile, as well as insufficient phantom length for achieving scatter equilibrium in the center of the ionization chamber. One of the methods introduced to assess the dose with greater precision is The Cone-Beam Dose Index. Our measurements were in accordance with the statement above, as the end CBDI values gave a more realistic and expected dose assessment, than the CTDI values. It is important to indicate that since no additional scatter material was used, as required by the CBDI methodology, the measured dose is reduced. Estimated effective CT dose values for certain localizations were higher than expected, while effective CBCT doses were in accordance with the Varian standardized protocols. This led to detailed revision of currently employed CT protocols for given regions, with emphasis on using lower current settings in the future, without losing focus on preserving the image quality. Current was the parameter chosen for adjusting the received dose, since all utilized protocols have the same value of kVp and pitch. The next steps should be to include patient size correction to refine dose estimate. In first aproximation, CTDI calculations are likely enough for quality assurance (QA) and optimization of imaging dose.

COMMUNICATION PROCESS FOR QA ENFORCEMENT IN A LARGE CENTRAL EUROPEAN HOSPITAL

Angelika Osanna-Elliott[1], Natasa Brasik[1], Angelica de Leon[1], Alexander Gruber[1]

[1] *Universitätsklinikum AKH Wien, Austria*

Purpose/Introduction

Our hospital is associated with a medical university and has 120 x-ray devices for diagnostic and interventional radiology. During the COVID crisis of 2020 and 2021, it became clear that in order to insure uninterrupted QA processes for patient safety, a clear process for communication between hierarchical levels is necessary. We describe the newly implemented process and its implications.

Materials/Methods

QA of radiological equipment in our hospital is usually done according to Austrian standards (ÖNORM) or equivalent German or international norms. The necessary measurements are performed by "local" radiology technologists who are the experts in operating the equipment. The task of the medical physicists is to supervise the process and assist in case of problems. Due to personnel shortages during the COVID crisis, we noticed that QA tasks were postponed more frequently. In high frequency departments such as sugery, the technologists were not able to find time for QA. If QA is not performed according to legal requirements (as described in the legal documents which grant the individual operational permit for each x-ray device), eventually the permit holder (in our case, the Technical Director) will be held liable in case a patient suffers damage due to the neglect of QA procedures. Therefore, the medical physics team has defined a reporting process (escalation process) in order to inform all involved levels of management of a potential risk.

Results

The process has been defined. It is currently being presented to all involved hierarchical levels of our hospital. A first result of introducing the process is the new awareness at all levels on the importance of performing QA tasks on time.

Discussion

Since our hospital has a large hierarchical structure with strict lines of communication, this new process has caused some people to worry about being able to fulfil all QA requirements on time. The medical physics team has taken great care to ensure people that this process is meant to support their needs and increase patient safety.

Conclusions

Since implementation of the process, it has not yet been necessary to trigger higher levels of the process.

USE OF PROTON THERAPY IN PEDIATRIC PATIENTS: BREAST-LEUKEMIA CASE

Carlo Algranati[1], Lidia Strigari[2], Silvia Strolin[2], Michele Avanzo[3], Francesco Fracchiolla[1], Stefano Lorentini[1], Marco Cianchetti[1], Sabina Vennarini[4]

[1]U.O. Protonterapia, APSS-Trento
[2]Department of Medical Physics, IRCCS Azienda Ospedaliero-Universitaria di Bologna, 40138 Bologna, Italy
[3]Department of Medical Physics, Centro di Riferimento Oncologico di Aviano (CRO), Aviano, Italy
[4]Pediatric Radiotherapy Unit, Fondazione IRCCS Istituto Nazionale dei Tumori, Milan, Italy.

Purpose/Introduction

Acute lymphoblastic leukemia (LAL) is undoubtedly the most common pediatric patient disease and has peripheral recurrence characteristics, including solid lymphatic organs. We study an 11- year-old girl with LAL recurrence in the right mammary parenchyma that underwent proton therapy using active breath control.

Materials/Methods

3 CT imaging studies in treatment position were acquired in deep inspiration breath-hold (DIBH) with Active Breathing Coordinator ABC system (Elekta Instrument AB, Stockholm). The treatment plan was done on the Raystation Treatment Planning System (RaySearch Laboratories AB,Sweden). The physician contoured the target volumes in all studies. Based on that ITV, PTV was generated, and all principal organs at risk were contoured for CTs. A pencil beam scanning proton therapy plan was defined with two fields (see figure). Both fields were optimized with Single Field Optimization (SFO) technique and range robust optimized with the TPS tools. The prescribed dose was 1,8 GyRBE for 20 fractions (total dose 36GyRBE).The patient alignment was performed with Align-RT (Vision RT Ltd., UK) and orthogonal kilovolt X-rays before each treatment fraction. The beam delivery was performed synchronizing the DIBH of the patient with the machine using the ABC system together with an optical tracking system (Gate-RT, Vision-RT Ltd., UK) as safety control during the treatment. To evaluate the radioprotection and local control of the patient, two comparative plans with electrons and high conformal partial breast photons were created (see Fig.1). The Excess Absolute Risk (EAR) of radiation-induced solid cancer were calculated for all plans.

Conclusions

This treatment technique in an atypical localization due to a LAL recurrence proved to be feasible and safe in a collaborative pediatric patient. A comparison shows the superiority of the proton plan over the photon and electron plan.

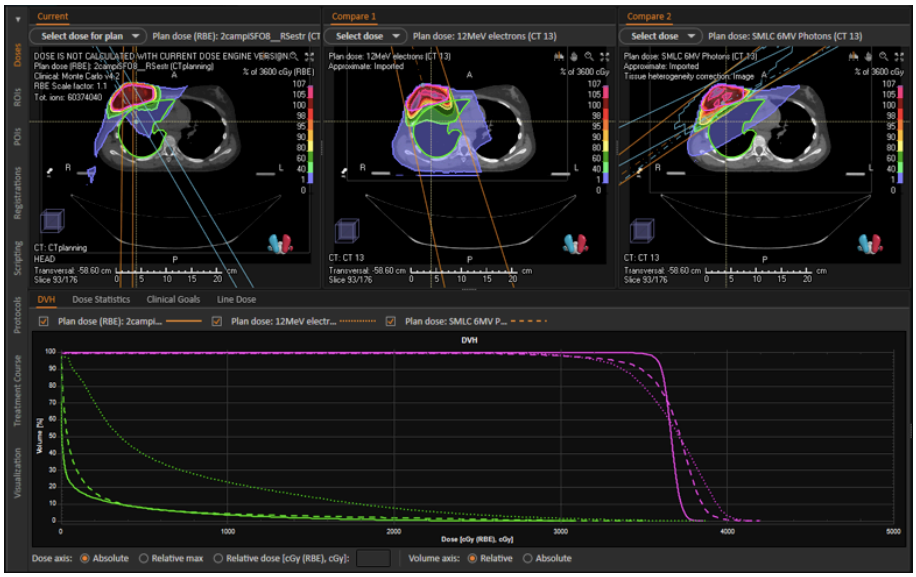

Fig.1: plan comparison among proton plan, 12MeV electron and 6MV photon plan.

USE OF 3D PRINTED BOLUS IN BRACHYTHERAPY

Ozren Čudić[1], Nemanja Golubovac[1], Laza Rutonjski[1]

[1]*Oncology Institute of Vojvodina*

Purpose/Introduction

3d printing is relatively new technique in radiotherapy.It has found its purpose in EBRT (for boluses and electron compensators), dosimetry (multiple dosimetry and QA phantoms) and brachytherapy. In brachytherapy 3d printed applicators are commonly used for skin cancer treatment, especially for highy irregular surfaces. 3d printed aplicators can reduce the total treatment time and achieve better dose distribution.

Materials/Methods

Here is presented a single case of brachytherapy skin cancer. 3d applicator is printed with Axiom 20 3d printer (Airwolf 3d), using the "3d bolus" software developed by Adaptiiv Medical Technologies to generate STL file ready for printing. The patient is irradiated with Varian GammaMed Plus afterloader using the 192-I brachytherapy source. Prescribed dose for this case was 40 Gy in 10 fractions. Four aplicators are used in this case with interapplicator distance of 1 cm. Distance from source to skin was 0.5 cm.

Discussion

The main goal of this plan is to deliver the presribed dose to CTV below the surface of 3d printed applicator. The dose distribution is shown on image_2. The dose distribition was optimized with TG-42 optimization algorithm. It can be noticed that the 100% isodose line follow the conture of CTV. Analyzing the DVH curve for this case, it can be seen that the CTV coverage is 95% with prescribed dose. DVH is shown on image_1.

Conclusions

3d printed bolus for brachytherapy applicators provides better conformity, reduce air gaps and surface dose uncertainty. It can be use for highly irrelgular surface. Also it is a more convenient approach for the patient because 3d printed bolus can replace the traditional hand made masks.

References

1. Scott Alan Clarke. 3D Printed Surface Applicators for High Dose Rate,Dalhousie University Halifax, Nova Scotia,August 2016
2. Xiran Wang, Xuetao Wang, The Clinical Application of 3D-Printed Boluses in Superficial Tumor Radiotherapy,Frontiers in Oncology, 19 August 2021.

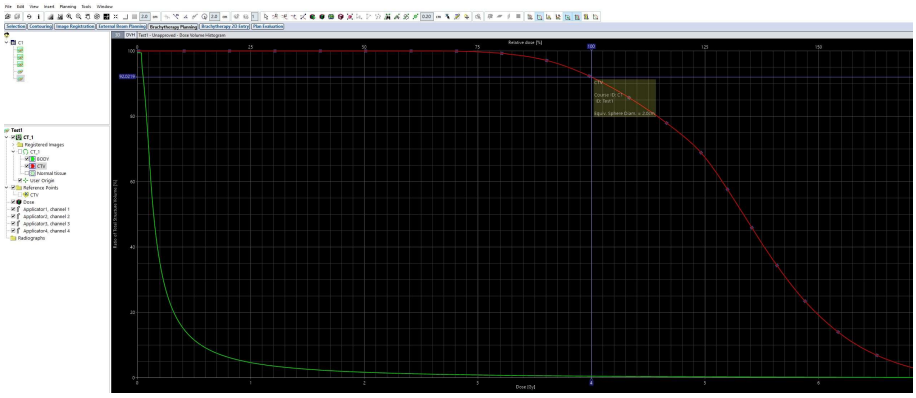

dose distribution

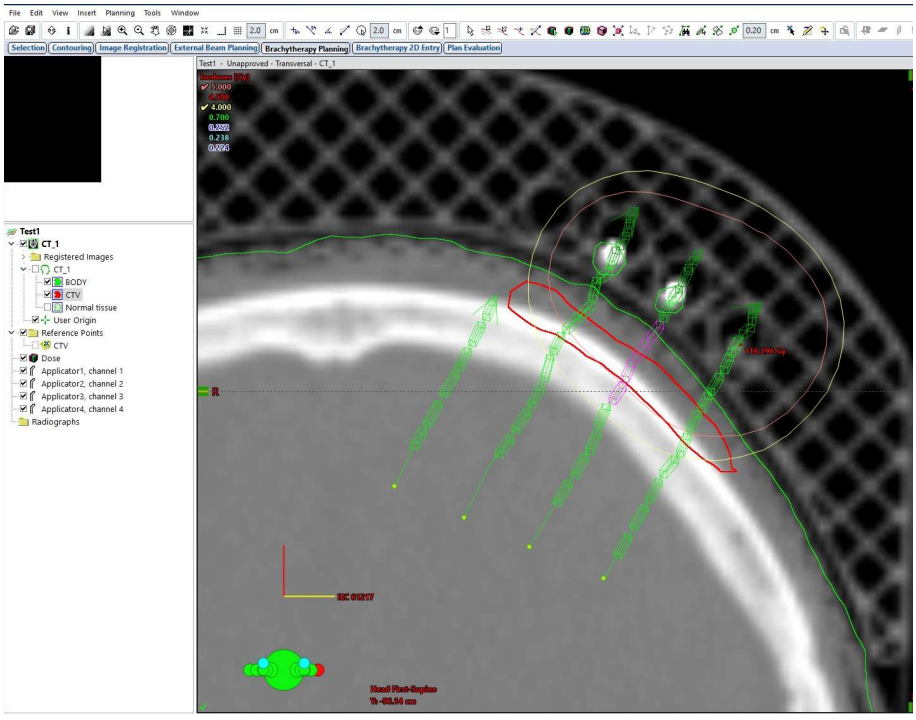

dose volume histogram

THE EFFECT OF LONGITUDINAL SETUP ERRORS IN CRANIOSPINAL IRRADIATION ON THE DOSE DISTRIBUTION AT THE FIELD JUNCTION AREAS

Tadeja Forjanič[1], Rihard Hudej[1], Matevž Mlekuž[1], Jernej Zlatič[1]

[1]*Institute of Oncology, Ljubljana, Slovenia*

Purpose/Introduction

Craniospinal irradiation (CSI) is used to treat various central nervous system malignancies that tend to spread through cerebrospinal fluid. The length of the irradiated volume, consisting of the whole brain and spinal canal, requires the use of multiple isocenters and field junctions, thus making the treatment planning process complex and time consuming. At our institute, CSI is delivered with the Elekta Synergy linear accelerator, with the maximum field size of 40 cm x 40 cm. Therefore, three isocenters are usually required to ensure an adequate coverage of the whole planning target volume (PTV) for adult patients. In recent years, VMAT delivery technique has gradually replaced the traditional 3D CRT treatment approach in our clinical practice. Despite the superior dose conformality of VMAT, it is still challenging to achieve homogeneous and robust dose distributions across field junctions [1-3]. Here we propose a treatment planning method for CSI using Monaco TPS (treatment planning system). This method has been developed to provide highly conformal treatment plans that are robust to small longitudinal setup errors. In order to evaluate the robustness of the proposed treatment planning approach, we simulated the effect of small shifts of the superior spinal isocenter to the delivered dose distribution in two recent clinical plans.

Materials/Methods

For the sake of simplicity, only patients with a uniform dose prescription were considered in the analysis. We have randomly selected two patients that have been treated with CSI at our clinic in the last two years. The prescribed dose (PD) to the PTV was 23.4 Gy (13 daily fractions of 1.8 Gy) for patient A and 30.6 Gy (17 daily fractions of 1.8 Gy) for patient B. Patients were treated in supine position and were immobilized with a long thermoplastic mask extending to the shoulder region. VMAT plans for each patient were generated in Monaco TPS and treatment was delivered using Elekta Synergy linear accelerator. Dose calculations were performed using the Monte Carlo algorithm with a calculation grid resolution of 0.3 cm.

VMAT plans were made with three isocenters which differed only in the longitudinal coordinate. Lateral and vertical coordinates of the isocenters were selected to lie approximately at the lateral and vertical center of the PTV volume, respectively. The exact placement of isocenters and beam geometry configuration selection were based on the following requirements: complete target volume coverage, sparing of normal tissues, sufficiently large overlapping areas of the fields with adjacent isocenters and high dose conformity. Additional care was taken to avoid irradiating the patient through the high density area where the H&N extension board attaches to the treatment table. Therefore, for the cranial irradiation we avoided using beam arcs that would enter the patient passing through the table. For the spinal irradiation, on the other hand, we used partial arcs from the posterior direction, which seemed the most suitable in terms of normal tissue sparing.

Once the isocenters were fixed, we divided the PTV into three target volumes, according to the position of field junctions, thus enabling a separate dose optimization for each of the target volumes.

Further, a set of 10 structures was created at each field junction. Each structure represents an intersection of the PTV with 2 adjacent CT slices (3 mm thickness) or more for longer junctions. Treatment plans for the cranial and inferior spinal part of the PTV were created first. The above mentioned structures were used to guide the dose optimization process to achieve gradual dose gradients across the junction regions. Finally, dose optimization was performed for the superior spinal part of the PTV, taking into account the dose contribution of the cranial and inferior spinal fields.

To evaluate the sensitivity of the two clinical plans to longitudinal setup errors, we shifted the superior spine isocenter for 3 mm, 5 mm and 10 mm in the cranial direction and recalculated the dose. The position of the cranial and inferior spinal isocenters was not changed, thus we can observe the effect of longitudinal shifts on hot spots and cold spots simultaneously.

Results

Moving the superior spinal isocenter in the cranial direction results in overdosage in the superior junction and underdosage in the inferior junction. For the purpose of our analysis we created two additional structures, PTVsup and PTVinf. They represent the part of the PTV at the superior and inferior junction, respectively, significantly affected by simulated cranial shifts.

Fig. 1 shows the DVHs for PTVinf (blue) and PTVsup (red) for patient A and patient B resulting from the simulated isocenter shifts of 3 mm (dashed line), 5 mm (dash dotted line) and 10 mm (dotted line). The lengths of the inferior junctions were 9 cm (patient A) and 12 cm (patient B) and the lengths of the superior junctions were 8.4 cm (patient A) and 6.6 cm (patient B).

As expected, steeper dose gradient across the junction leads to higher sensitivity of the dose distribution to longitudinal shifts. Namely, patient B with a shorter superior junction shows larger differences between DVH curves as isocenters move closer together. Moreover, patient B reaches substantially higher maximum doses than patient A, with the difference being more pronounced at larger isocentric shifts. Similarly, the shorter inferior junction of patient A results in poorer PTVinf coverage. Again, the difference is most pronounced at the largest shift of 10 mm (patient B has about 20% better coverage of PTVinf with 95% PD than patient A).

The junction regions represent a relatively small portion of PTV. As it turns out, small longitudinal isocenter shifts (up to 5 mm) still yield a clinically acceptable DVH for the PTV as a whole, but create a very inhomogeneous local dose distribution. We have to keep in mind, however, that increasing the size of the junction volume also increases the volume of PTV, affected by isocenter shifts (PTVsup and PTVinf). Therefore, the optimal length of the junction depends primarily on the expected longitudinal setup errors and target dose tolerances for PTVsup and PTVinf, but also on the volume of PTV susceptible to dose uncertainties.

Conclusions

Two clinical treatment plans for CSI, generated according to the proposed method, were evaluated in terms of the robustness to longitudinal setup errors. More precisely, we simulated the effect of small changes in the distance between adjacent isocenters on the delivered dose distribution in the region of field junctions. Changes of up to 5 mm resulted in dose distribution that would be considered clinically acceptable for our treatment planning approach. According to the simulations conducted on the two clinical cases the plan robustness increases with the length of the junction.

References

1. Lee YK et al, Development and evaluation of multiple isocentric volumetric modulated arc therapy technique for craniospinal axis radiotherapy planning, Int J Radiat Oncol Biol Phys, Volume 82, Issue 2, 1006-1012 (2012)

2. Strojnik A et al, Reducing the dosimetric impact of positional errors in field junctions for craniospinal irradiation using VMAT, Rep Pract Oncol Radiother, Volume 21, Issue 3, 232-239 (2016)
3. Wang K et al, Plan quality and robustness in field junction region for craniospinal irradiation with VMAT, Physica Medica, Volume 48, 21-26 (2018)

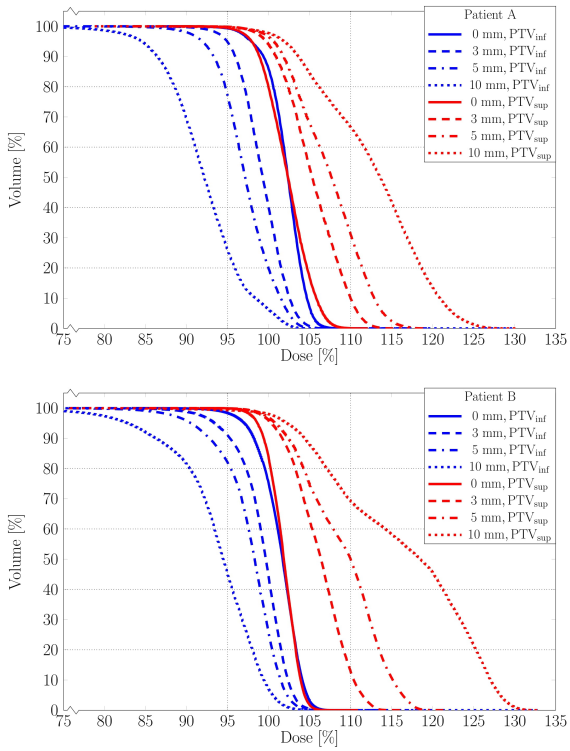

Fig.1: Dose Volume Histrograms for PTVinf (blue) and PTVsup (red) for patient A (above) and patient B (below) resulting from the simulated shifts of the upper spinal isocenter

CLINICAL INVOLVEMENT IN THE HYBRID PROCEDURE FOR DOSIMETRIC VERIFICATION OF VOLUMETRIC MODULATED ARC THERAPY USING COMPASS SYSTEM

Tamara Jovanović[1], Jelena Stanković[1], Jovana Zlatanović[1], Dragan Nikolić[1], Miloš Kopunović[1], Miloš Jonić[1]

[1]*University Clinical Centre Niš, Serbia*

Purpose/Introduction

Treatment plan verification (PSQA) is an important part of quality assurance of IMRT concerning patient safety in order to inspect:1)dose distribution and 2)safety of treatment delivery. PSQA is performed as:1)independent dose calculation and frequent machine QA, 2)measurement with detectors and 3)combination of both (2).The standard method for IMRT dose verification analyze is the gamma evaluation.Dose Volume Histogram (DVH) informations can be incorporated within PSQA procedure.Compass verification system (IBA dosimetry) allows comparison of the measured and TPS calculated dose by DVH using two independent calculation algorithms(1).The purpose of this work was to evaluate quantitatively the 3D Compass dosimetry for VMAT. The goal was twofold:1)to evaluate the efficiency of the Compass algorithm as a tool for the secondary dose calculation check and to compare with the standard planar gamma test and 2) to optimize DVH based PSQA clinical procedure.

Materials/Methods

Patients underwent VMAT treatment on Varian Clinac linear accelerator (Varian Medical Systems) in a beam quality of 6 MV. TPS Eclipse version 15.6 is used for the planning and the analytical anisotropic algorithm (AAA) algorithm for the dose computation. Epid dosimetry and the gamma analyze are performed (GPR more then 90 % points, 3 %, 2 mm global gamma, threshold maximum 10%) in order to meet AAPM TG 218 recommendations. Compass is the dosimetry system that consists of dose verification software version 4.1.3.0 and the Dolphin air-vented ionization chamber based array detector (3). Compass allows PSQA hybrid procedure based on the patient anatomy, as well as the DVH analyze due to independent dose calculation with collapsed cone convolution. The commissioning of the virtual linac model was done with an user-define option. With a file-based import into Compass plans are recomputed with collapse cone super position algorithm. The dose reconstruction according to real measurements is also done (CME). Comparison between the AAA based dose and CCA was done for the first thirty real VMAT patients with different treatment sites (brain, head and neck and pelvis). TPS vs. CCA dose distributions was quantitatively evaluated in terms of relative average dose difference (ADD%) and average gamma difference. 2D fluence verification from Epid dosimetry were compared in order to highlight the potential of Compass 3D dosimetry (3). For these patients measurements with Dolphin were performed. The differences between TPS vs. CME dose distributions were quantified in terms of 3D gamma analyze (4%, 3mm), ADD%, relative average dose difference more then 6% (ADD6%), average gamma for targets and OARs, as well as D95 and mean dose(%) for targets.

Results

Among thirty patients underwent VMAT treatment (ten brain, ten head and neck and ten pelvis) TPS, CCA and CME dose distributions were quantitatively evaluated and results are shown in terms of mean value and standard deviation (SD). The table in Fig.1 and the table in Fig.2 show statistical analyzies of differences TPS vs.CCA for target volumes and OARs respectively. For target volumes was observed relative average dose difference less then 1% and average 3D gamma value less then 0.5. The highest SD of ADD(%) was 1.5 for H&N patients. Results for target volumes are significant (one teil TTEST, paired) with p value less then 0.001 for prostate cases due to less complexity. Concerning OARs mean ADD was less then 6%, maximum SD for H&N of 9.5 (NS) and mean average gamma less then 0.5. According to the comparison TPS vs.CCA the evaluation TPS vs.CME was done for H&N and pelvis cases. Results are shown in the table in Fig.3 and the table in Fig.4.

Discussion

Complex plans need to be investigated whether or not are acceptable for treatment prior to the actual treatment (AAPM-TG report 82). Gamma analyze combines spatial information and dose differences for a 2D plane and has limited accuracy in areas with high dose gradients. This method is not also correlated with dose differences in target volumes and OARs (2,3). Because of the dose calculation complexity, verification of the treatment planning system (TPS) performance and the independent verification of the dose calculation algorithm is as much important as verification of the treatment delivery and the comparison of calculated and measured dose distibutions (1). The Compass workflow and algorithm is explained by Boggula et al.(4). Compass offers various statistical analysis tools. Many authors have concluded good agreement between TPS vs.CCA in validation of Compass as the secondary dose calculation check tool with action levels ADD 1% and mean gamma 0.5.(1,2,3). The other stated for OARs more realistic level of 6% for ADD (2,3). Our results of Compass validation have shown good agreement with literature action levels (0.5 average gama, 1% ADD for volumes of interest and 6% ADD for OARs). 2D local gamma evaluation with Portal dosimetry was NS for H&N and pelvis sites. TPS vs.CME dose comparison was also done and values for 3D GPR was more then 98%. This results consisting of 3D gamma criteria and DVH underline the sensitivity of Compass dosimetry.

Conclusions

Commercial hybrid dosimetry tool offers more complete PSQA methodology and workflow in addition to fundamental 3D dosimetry. Involvement of the radiation oncologist is required to determine the clinical relevance of observed evaluation. A consensus on DVH-based action levels is still lacking. Compass dose engine and Dolphin detector can be considered as a fast and reliable method of 3D dosimetry of IMRT/VMAT treatment plans.

References

1. Kunnanchath J, Majumdar SKD, Tharmarnadar G, Ramachandran M, Joshi RC, Devadason S. Validation of compass QA system and the independent verification of dose calculation algorithm for IMRT patient specific plans. Transworld Medical Journal. 2014;2(3):170-175.
2. Gueorguiev G, Cotter Ch, Turcotte JC, Crawford B, Sharp G, Mah,D M. Clinical implementation and error sensitivity of a 3D quality assurance protocol for prostate and thoracic IMRT. Journal of Applied Clinical Medical Physics. Vol.16, No. 5; 2015.
3. Vikraman S, Manigandan D, Karrthick KP, Sambasivaselli R, Senniandavar V, Ramu M, Rajesh T, Mueller L, Muthukumaran M, Karthikeyan N, Tejinder K. Quantitative evaluation of 3D dosimetry for stereotactic

volumetric-modulated arc delivery using Compass. Journal of Applied Clinical Medical Physics. Vol.16, No. 1; 2015.

4. Boggula R, Lorenz F, Mueller L, et. al. Experimental validation of a commercial 3D dose verification system for intensity-modulated arc therapies. Phys Med Biol. 2010; 55(19):5619-33.

TPS vs. CCA Target volume	ADD(%)	Average gamma	P value	2D GPR local gamma 3% 2mm, Th max.10%
Brain				CW
PTV	0.23±0.116	0.107±0.010	0.004	94.33±2.156
CTV	0.24±0.097	0.096±0.010	0.001	CCW
				95.96±2.470
				P value 0.04
Head&Neck				
PTV1	1.1±0.738	0.261±0.186	0.002	CW
PTV2	1.992±1.512	0.246±0.081	0.001	93.98±1.829
CTV1	0.449±0.464	0.158±0.070	0,05	CCW
CTV2	0.815±0.493	0.199±0.083	< 0.001	93.89±1.721
				P value NS
Pelvis				
PTV1	1.379±0.873	0.232±0.096	< 0.001	CW
PTV2	0.977±0.656	0.256±0.150	< 0.001	95.44±1.521
CTV1	1.25±0.7	0.231±0.102	< 0.001	CCW
CTV2	1.065±0.615	0.262±0.155	< 0.001	94.81±3.054
				P value NS

Figure 1 Quantitative evaluation of dose distributions TPS vs. CCA for target structure

TPS vs. CCA OAR	ADD(%)	Average gamma	P value
Brain			
Brain steam	3.86±5.527	0.162±0.05	0.03
Hiasm	1.63±2.161	0.148±0.088	0.03
Opt.nerveL	2.29±2.676	0.134±0.055	0.02
Opt.nerveR	2.38±2.206	0.156±0.069	0.005
EyeL	2.9±1.792	0.131±0.036	< 0.001
EyeR	3.27±2.215	0.138±0.035	0.001
Head&Neck			
Spinal cord	5.485±5.685	0.114±0.062	0.003
Oral cavity	3.5±6.148	0.146±0.071	NS
Pharynx const.	2.039±2.860	0.194±0.180	0.03
Larynx	5.18±9.509	0.175±0.071	NS
Mandible	1.915±2.386	0.150±0.070	0.01
Parot.L	3.062±2.314	0.155±0.082	< 0.001
Parot.R	2.154±1.783	0.146±0.058	0.001
Pelvis			
Bladder	2.529±1.275	0.268±0.071	< 0.001
Rectum	2.923±1.256	0.299±0.092	< 0.001
Fem.headL	4.106±2.479	0.289±0.080	< 0.001
Fem.headR	3.7±2.358	0.278±0.072	< 0.001

Figure 2 Quantitative evaluation of dose distributions TPS vs. CCA for OARs

TPS vs. CME Target volume	ADD(%) ADD6(%)	Average Γ	3D GPS	D95(%)	Dmean(%)
Head&Neck					
PTV1	1.1±0.84	0.25±0.07	99.29±0.82	97.66±1.13	102.02±0.74
PTV2	1.78±1.15	0.34±0.09	98.96±0.86	97.96±2	101.63±1.05
CTV1	0.52±0.63	0.48±0.57	99.64±0.34	99.61±1.13	102.93±0.39
CTV2	1.19±0.69	0.33±0.09	99.52±0.56	99.06±1.8	101.78±1.3
Pelvis					
PTV1	0.55±0.347	0.231±0.051	99.89±0.16	95.53±1.59	100.37±0.62
PTV2	0.846±0.739	0.305±0.111	99.66±0.56	96.65±1.56	100.05±1.41
CTV1	0.63±0.365	0.452±0.747	99.74±0.41	98.17±0.48	101.13±0.43
CTV2	0.779±0.607	0.279±0.113	99.86±0.18	97.39±1.33	100.12±1.66

Figure 3 Quantitative evaluation of dose distributions TPS vs. CME for target structure

TPS vs. CME OAR	ADD(%) ADD6(%)	Average Γ	3D GPR
Head&Neck			
Spinal cord	7.84±7.21	0.16±0.11	100
Oral cavity	8.22±8.48	0.3±0.12	99.93±0.1
Pharynx const.	3.44±3.8	0.33±0.1	99.72±0.7
Larynx	2.42±1.8	0.25±0.1	98.86±1.3
Mandible	3.71±3.3	0.24±0.09	99.91±0.2
Parot.L	5.92±4.9	0.23±0.14	100
Parot.R	4.29±2.8	0.24±0.14	99.99±0.2
Pelvis			
Bladder	5.485±5.685	0.114±0.062	99.58±0.8
Fem.headL	3.5±6.148	0.146±0.071	99.97±0.1
Fem.headR	2.039±2.860	0.194±0.180	99.78±0.5

Figure 4 Quantitative evaluation of dose distributions TPS vs. CME for OARs

AAA AND ACUROS XB DOSE CALCULATION ALGORITHMS COMPARISON IN TREATEMENT PLANNING FOR LUNG CANCER RADIATION THERAPY

Miloš Kopunović[1], Jelena Stanković[1], Miloš Jonić[1]

[1]*University Clinical Center Nis, Serbia*

Purpose/Introduction

Radiation therapy of lung cancer implies dose calculation within very inhomogenious media. These tishue inhomogenities are very challenging for every dose calculation algorithm and can lead to serious errors in dose distribution representation. There are three main goals of this study: to introduce Acuros XB dose calculating algorithm to clinical practice, to improve lung cancer treatement planning and also to provide better understanding of AAA and Acuros XB algorithms in order of correct aplication.

Materials/Methods

This study includes 25 patients treated on Electa Synergy linac with 60Gy in 30 fractions (2Gy daily). Treatement plans for each of them were created on Eclipse v.15.6 TPS. All plans were first calculated with AAA, and then recalculated with Acuros XB. Next, plans were compared in therms of PTV coverage with 95% dose(V95) and organs at risk dose load (spinal cord, heart and lungs). After that, both algorithms were validated comparing with meassured data obtained during TPS comissioning procedure, that was performed with CIRS Thorax Phantom, model 002LFC.

Results

Results obtained in real patients dose recalculation in terms of relative difference are given in table 1. Results obtained by comparison of measured data with dose calculated using AAA and Acuros XB are given in table 2.

Conclusions

When looking the overall picture (real-patient recalculation with two algorithms and measured-calculated data comparisson), we conclude that both algorithms are valid to use in clinical practice. However, AAA should be used with precaution in lung cancer treatement planning, since it can lead to underdossage of tumor and wrong estimation of organs at risk damage.

PTV	Spinal Cord	Lung - bilateral	Lung - ipsilateral	Heart
$\delta(V_{95}) = 1,5\%$ $\delta(D_{min}) = 3,7\%$ $\delta(D_{max}) = -1,9\%$ $\delta(D_{mean}) = -0,3\%$	$\delta(D_{max}) = 2,4\%$	$\delta(V_{20}) = -0,7\%$	$\delta(D_{mean}) = 0,4\%$	$\delta(D_{mean}) = 2,7\%$

Table 1: Results obtained by dose recalculation from AAA to Acuros XB, in terms of relative diferences.

Energy	Algorithm	Average deviation (%)	Maximal deviation (%)
6X	AAA	2,1	5,9*
	AXB	0,6	1,9
10X	AAA	1,7	5,0*
	AXB	0,8	1,4

Table 2: Results obtained in comparison of measured data with dose calculated using AAA and Acuros XB (values marked with * exceed agreement criteria). These results are given for measuring positions in phantom that recive 2Gy dose in calculated plans.

References

1. Yan Ch et al, Clinical implementation and evaluation of the Acuros dose calculation algorithm, Journal of applied clinical medical physics, Volume 18, Issue 5, 2017
2. IAEA-TECDOC-1583, Commissioning of Radiotherapy Treatement Planning Systems: Testing for Typical External Beam Treatment Techniques, IAEA, Vienna 2008

EFFECTS OF CHANGES IN SURFACE-TO-VOLUME RATIO OF PLANNING TARGET VOLUMES ON DOSE DISTRIBUTIONS FOR STEREOTACTIC RADIATION THERAPY PLANS: A COMPARISON BETWEEN VARIAN EDGE AND ACCURAY CYBERKNIFE

Vanda Leipold[1], Ivana Alerić[2], Hrvoje Kaučić[2], Domagoj Kosmina[2], Adlan Čehobašić[1], Mihaela Mlinarić[3], Sofija Antić[2], Mladen Kasabašić[1], Fran Stanic[4], Dragan Schwarz[2]

[1]*Medicinski fakultet Sveučilišta J.J. Strossmayera, Osijek, Croatia*
[2]*Radiochirurgia Zagreb, Croatia*
[3]
[4]*Bitwise Solutions, Zagreb, Croatia*

Purpose/Introduction

As planning target volumes deviate from spherical toward elliptical or more complex geometries, their surface-to-volume ratios increase, and so does the challenge to create a conformal dose distribution.

Our goal was to compare how differences in surface-to-volume ratios of planning target volumes (PTVs) affect dose distributions for two different stereotactic radiosurgery systems: MLC based Varian EDGE and fixed conus based Accuray CyberKnife.

Materials/Methods

A CT was acquired for stereotactic end-to-end phantom Stereophan (SunNuclear, USA).

The structures that represent planning target volumes of different surface to volume ratios, namely ellipsoids of varying eccentricities with and without cavities, were generated.

Plans for each PTV were generated using Varian Eclipse and Accuray Precision treatment planning systems.

A homogeneous dose of 12 Gy (11,4 Gy to 99% of the volume) was prescribed to each of the PTVs. Plans were optimized to achieve a better new conformity index (nCI), dose gradient index (DGI) and dose homogeneity index (HI).

Described plan metrics: HI, DGI(1) and nCI(2), were compared between Varian EDGE and Accuray CyberKnife for each plan.

Results

There were no significant differences in HIs between plans for different surface-to-volume ratios of PTVs for both systems.

However, for each PTV, CyberKnife achieved a more homogeneous dose distribution.

As expected, an increase of surface-to-volume ratio had an adverse effect on nCI and DGI for both systems.

EDGE achieved higher conformity and steeper dose gradient for all of the cases.

Discussion

Differences observed in dose distribution were likely caused by differences in collimator apertures and beam profiles, and can be an indicator for determining the choice of treatment machine to achieve the optimal plan quality.

In our study, surface to volume ratio was used to describe the eccentricity of the PTVs and complexity of their surfaces. It is a simple and easy to use tool, however, it does not convey the finer detail regarding PTV geometry; thus a more elaborate tool should be used for further analysis.

Since this experiment was conducted on a phantom, it has not taken into account a variety of factors that influence plan feasibility for different systems, such as CTV-PTV margin, patient immobilization, treatment time etc.

It should also be taken into account that only plans with homogenous prescriptions were analyzed in this study. A heterogeneous dose distribution might give different results.

Conclusions

According to our findings, both systems allowed generation of conformal plans due to multiple non-coplanar beam entries. CyberKnife system offered an advantage over EDGE in the cases of lesions prescribed with homogeneous doses. EDGE system generated more conformal plans with a steeper dose gradient, regardless of surface-area-to volume ratio.

References

1. Lomax NJ, Scheib SG. Quantifying the degree of conformity in radiosurgery treatment planning. Int J Radiat Oncol Biol Phys. 2003 Apr 1;55(5):1409-19. doi: 10.1016/s0360-3016(02)04599-6. PMID: 12654454.
2. Paddick, I., and Lippitz, B. (2006). A simple dose gradient measurement tool to complement the conformity index. Journal of Neurosurgery JNS 105, Supplement, 194-201
3. Kataria T, Sharma K, Subramani V, Karrthick KP, Bisht SS. Homogeneity Index: An objective tool for assessment of conformal radiation treatments. J Med Phys. 2012 Oct;37(4):207-13. doi: 10.4103/0971-6203.103606. PMID: 23293452; PMCID: PMC3532749.

RADIOTHERAPY CT IMAGING OF THREE ANTROPOMORPHIC PHANTOMS- DOSE TO ORGANS AT RISK IN PEDIATRIC AND ADULT IMAGING PROTOCOL

Mirjana Papić[1], Milana Marjanović[2], Jelena Moravčević[1], Ivan Gencel[1], Borislava Petrović[2]

[1]*Oncology Institute Vojvodina, Sremska Kamenica, Serbia*
[2]*Oncology Institute Vojvodina, Sremska Kamenica, Serbia; Faculty of Sciences, University Novi Sad, Novi Sad*

Purpose/Introduction

Imaging before and during radiotherapy treatment increases the doses to healthy tissues, including double exposures and repeated imaging for the purpose of adaptation of treatment plan to shrinkage of tumor.This is important in treatment of any patient, and becomes pronounced in case of pediatric patients.

Materials/Methods

Three different antropomorphic phantoms are used for the purpose of evaluation of dose during CT imaging. All were manufactured by CIRS- thorax IMRT phantom, head and neck SHANE phantom and pelvic IMRT phantom. Phantoms were scanned on a CT simulator by the adult protocols used clinically for CT scanning, and then by predefined child protocols of lower tube voltage. The measurements were performed by Farmer type chamber, during the scanning. The adult protocol included 140kV tube voltage, while child protocol was done with 120 kV. Both scans were performed with 2mm slice distance, as in clinical situation, and for child additionally on 4mm slice distance. The farmer chamber was calibrated in terms of air kerma in kV beam quality. The dose was measured in clinically relevant points inside phantom and in position of isocentar of phantom.

Results

The doses received by all three phantoms, different organs/measurement points and protocols are given in Table 1. Significant reduction of dose in all cases was confirmed for child protocol in comparison to adult protocol. The doses in child protocol registered on 4mm and 2 mm did not differ and are not shown here, for avoidance of duplicate results. The head and neck protocol shows significant doses and calls for optimisation.The values of CTDIvol are compared to different national results [1-4].

Discussion

Children should be CT scanned with lower voltage due to significant overall dose reduction in all cases. The radiotherapy CT scanning protocols should be optimized for frequent use, as patients are sometimes CT imaged sequentially in free-breathing and breath hold/gated treatment, are re-planned increasingly and afterwards regularly kV imaged during treatment. Re-planning increases the quality and outcome of treatment, but also increases significantly the workload and dose to healthy tissues. Great attention should be paid to volumes outside treatment area, especially in younger population.

Conclusions

Optimisation of all protocols is needed. Overall imaging dose should be added to absorbed dose to tumor and surrounding tissues. Younger patients have longer life-expectancy and this could be of great importance in their future life.

phantom type	measurement point inside phantom	Dose (cGy)		CTDIvol (mGy)		
		adult	child	adult	child	regional recommendation [1]
Head & Neck	right parotid gland	7.348(17)	4.85(5)	83.1	68.3	35
	isocenter/target	6.969(7)	4.787(3)			
	left parotid gland	7.164(7)	4.60(5)			
	brainstem	6.958(3)	4.469(7)			
	spinal cord	7.110(3)	4.883(5)			
Thorax	heart	0.959(6)	0.647(2)	16.4	16.2	17
	isocenter/target	0.906(5)	0.615(2)			
	right lung	0.866(3)	0.552(2)			
	left lung	0.860(2)	0.543(2)			
	spinal cord	0.603(3)	0.392(2)			
Pelvis	bladder	1.405(2)	1.182(2)	24.5	16.2	20
	isocenter/target	1.310(5)	1.086(2)			
	rectum	1.3008(3)	1.075(2)			
	right femoral head	3.345(9)	2.564(4)			
	left femoral head	3.280(14)	2.517(9)			

Table 1.

Table 1. Doses to organs at risk in both protocols/all phantoms and accompanying CTDIvol.

References

1. National reference levels of CT procedures dedicated for treatment planning in radiation oncology, A.Bozanic, D. Segota, D Dundara Debeljuh, M Svabic Kolacio, Đ Smilovic Radojcic, K Ruzic, M Budanec, M Kasabasic, D Hrepic, P Valkovic Zujic, M Brambilla, M K. Kalra, S Jurkovic, Physica Medica 96 (2022) 123–129.
2. Clerkin C, Brennan S, Mullaney LM. Establishment of national diagnostic reference levels (DRLs) for radiotherapy localisation computer tomography of the head and neck. Rep Practical Oncol Radiother 2018;23(5):407–12.
3. Zalokar N, Zager Marciu V, Meki N. Establishment of national diagnostic reference levels for radiotherapy computed tomography simulation procedures in Slovenia. Eur J Radiol 2020;127:108979. https://doi.org/10.1016/j.ejrad.20
4. Sanderud A, England A, Hogg P, Fosså K, Svensson SF, Johansen S. Radiation dose differences between thoracic radiotherapy planning CT and thoracic diagnostic CT scans. Radiography 2016;22(2):107–11.

IRRADIATION OF INOPERABLE BILATERAL BREAST AND REGIONAL LYMPHATIC CANCER WITH FIF TECHNIQUE

Nina Pavlović[1], Tatjana B. Miladinović[2], Ivana Rosić[1], Aleksandar Miladinović[1], Milena Živković[3], Marija Z. Jeremić[1]

[1]*University Clinical Center Kragujevac, Serbia*
[2]*Institute for Information Technologies, University of Kragujevac, Serbia*
[3]*Faculty of Science, University of Kragujevac, Serbia*

Purpose/Introduction

A major challenge in radiotherapy planning is bilateral radiation of the breasts and regional lymphatics. When making a plan of irradiation, the size and the irregularities of the structures located at different depths of a target can be a problem. Also, to achieve homogeneous irradiation of the target, it is necessary to avoid tangential overlaps of the field and protect the organs at risk (heart, lungs) at the same time

Materials/Methods

In this study, the case of a patient (female, 58 years old) with unoperated bilateral breast and regional lymphatics cancer was presented. Delineation of target volumes (PTV) and organs at risk was performed by a radiation oncologist. One-isocentric FiF (field in field) planning technique with two tangential fields for both breasts was used to obtain the plan. Isocentar is placed on the surface of the body structure, between the breasts and regional lymphatics. Radiotherapy was performed with a dose of 50 Gy in 25 fractions for breasts. Regional lymphatics were irradiated with the same dose. After the first part of the treatment, the boost target volumes were irradiated with a dose of 15 Gy in 5 fractions.

Results

Irradiation of all target volumes was 98% with a dose of 95%. The mean heart dose was 2.59 Gy, V10 = 1.74% and V5 = 6.04%, which corresponds to the set criteria. The mean lungs dose was 13.8 Gy, and the V20 for both lungs was 26.2%. The radiotherapy treatment was performed without complications and interruptions.

Conclusions

The isocentric FiF technique is clinically implemented for irradiation of bilateral breast, regional lymphatics and boost volumes. This technique has proven to be a quick and good choice of radiotherapy treatment for this type of cancer.

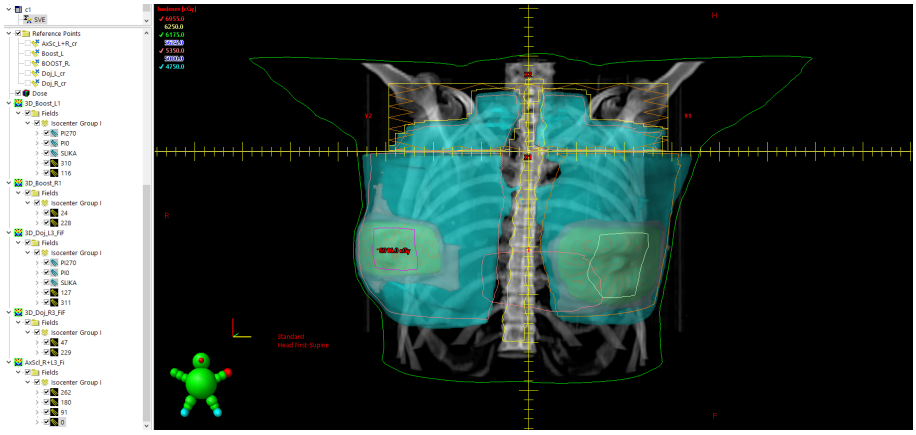

Image 1: Dose

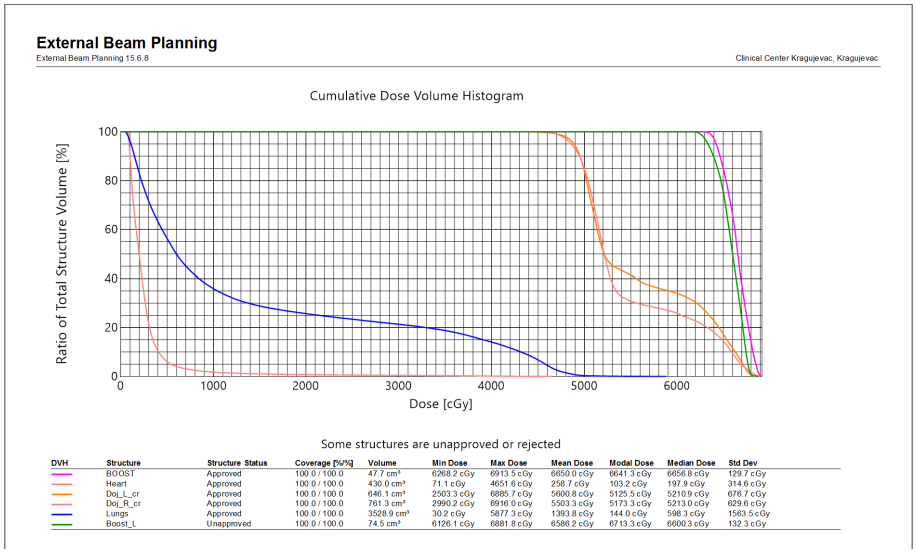

Image 2: DVH

HARNESSING THE WISDOM OF THE CROWD: RISK ESTIMATE BASED ON OPINIONS OF A TEAM OF DISSENTING EXPERTS

Primož Peterlin[1], Ivana Koceva[1], Valerija Žager Marciuš[1], Tanja Marinko[1]

[1]*Institute of Oncology Ljubljana, Zaloška 2, 1000 Ljubljana, Slovenia*

Purpose/Introduction

Failure Modes and Effects Analysis (FMEA) is an already established technique for risk management in radiotherapy (Huq et al, 2016). The basic premise of FMEA is simple: in a brainstorming, a group of experts decomposes the process into individual steps, creating a process map. Next, they identify failure modes associated with every step, then assess the probability of each failure mode (P), its severity (S), and the (in)detectability, i.e., probability that the failure mode is not detected in time (D). The failure modes which need to be adressed first are those which are both likely to occur, have grave consequences, and are hard to detect; FMEA methodology condenses these into risk priority number RPN = P·S·D. RPN thus serves as a quantitative measure for prioritization of risks and their subsequent reduction to an acceptable level. Even though FMEA methodology has been successfuly used in practice for decades, it continues to be challenged. One such challenges is the assumption of a consensus achieved among the team of experts, which is often impossible to achieve in practice. When a consensus cannot be reached, the authors usually use the mean or the median value instead, thus discarding the information on the dispersion of estimates. In this work, we examine an extension of FMEA which produces a priority list of failure modes incorporaing the information on the distribution of estimates.

Materials/Methods

The distribution of estimates for the probability, severity and detectability of a failure mode given by the team of experts is approximated by triangular fuzzy numbers, characterized by the first (Q1) and the third quartile (Q3) and the median value (Q2). Then, a multi-criteria decision-making method TOPSIS (Technique for Order of Preference by Similarity to Ideal Solution; Liu, 2016), extended to account for fuzzy values of estimates (Chen, 2000), is applied to arrive at the priority list of failure modes.

Results

The method was tested on a set of data on palliative virtual simulation-based treatment, collected in a survey. Four teams involved in different stages of the treatment compiled the list of failure modes for that stage and assessed the probability, severity and detectability of them. 7 radiation oncologists assessed 10 failure modes, 6 radiation therapists operating the CT simulator assessed 13 failure modes, 6 dosimetrists and medical physicists also assessed 13 failure modes, and 7 radiation therapists operating the medical linear accelerator assessed 12 failure modes. As an example, Figure 1 shows the results of the failure mode assessment done by the physicist and dosimetrists group. We performed two different rankings of the failure modes. In the first (Table 1), the probability, severity and detectability given equal weight as in the conventional FMEA. In the second (Table 2), severity given twice the weight of the other two. As expected, putting emphasis on severity gave priority to

more severe failure modes (e.g. »Incorrect patient scheduled«) over more common, but less severe failure modes (e.g. »Diagnostic documentation missing«).

Discussion

This ranking scheme presented in this paper is more flexible than the simple RPN product, in particular with respect to assigning different weights to probability, severity and detectability. More studies will however be needed to assess which weighting scheme yields best results in practice. Another area of further research we envision lies within the realm of fuzzy numbers. The triangular fuzzy numbers used in this study are just one of many shapes of fuzzy numbers, and while definitely superior at preserving the distribution of estimates to a single parameter like the mean or the median, other shapes seem worth investigating.

Conclusions

Expecting a consensus is often unrealistic. An assessment of a probability and detectability of a failure mode is inherently affected by uncertainty. We believe that this uncertainty ought to be propagated and taken into account when assembling the priority list of failure modes, and we believe that the methodology presented in this paper is a step forward from taking the mean or the median value.

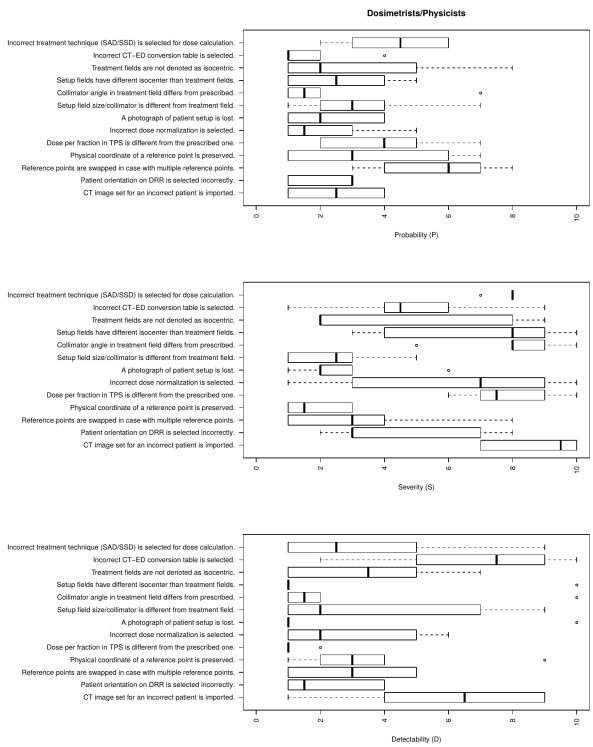

Figure 1: Boxplots of the estimates of probability, severity and detectability of the failure modes considered possible during the step of virtual simulation involving medical physicists and dosimetrists.

Radiation oncologists		
Failure mode	c_i	rank
The treatment field prescribed is either too large or too small	0.530	1
Diagnostical documentation is missing at the onset of procedure	0.458	2
Incorrect patient is scheduled for treatment with virtual simulation	0.387	3
Radiation therapists/CT simulator		
Failure mode	c_i	rank
Incorrect patient imaged	0.496	1
Incorrect patient scheduled for virtual simulation	0.402	2
Incorrect CT slices selected for virtual simulation	0.333	3
Dosimetrists, medical physicists		
Failure mode	c_i	rank
CT image set for an incorrect patient is imported	0.548	1
Incorrect treatment technique (SAD/SSD) is selected for dose calculation	0.462	2
Incorrect CT-ED conversion table is selected	0.383	3
Radiation therapists/medical linear accelerator		
Failure mode	c_i	rank
Incorrect patient answers the call (frequent last names)	0.434	1
Disagreement in monitor units is overlooked	0.428	2
At patient setup, alignment lines are used as isocentric lines	0.412	3

Table 1: Ranking of the most threatening failure modes for all four groups in the case in which the probability, severity and detectability are given equal weight.

References

1. Chen CT (2000). Extensions of the TOPSIS for group decision-making under fuzzy environment. Fuzzy Set Syst 114:1-9.
2. Huq MS, Fraass BA, Dunscombe PB, Gibbons JP, Ibbott GS, Mundt AJ et al (2016). The report of Task Group 100 of the AAPM: Application of risk analysis methods to radiation therapy quality management. Med Phys 43:4209-4262.
3. Liu HC (2016). FMEA using uncertainty theories and MCDM methods. Singapore: Springer.

Radiation oncologists		
Failure mode	c_i	rank
The treatment field prescribed is either too large or too small	0.559	1
Incorrect patient is scheduled for treatment with virtual simulation	0.517	2
During emergency procedure, the site to be treated is not known	0.472	3
Radiation therapists/CT simulator		
Failure mode	c_i	rank
Incorrect patient imaged	0.618	1
Incorrect CT slices selected for virtual simulation	0.500	2
Incorrect patient scheduled for virtual simulation	0.476	3
Dosimetrists, medical physicists		
Failure mode	c_i	rank
CT image set for an incorrect patient is imported	0.662	1
Incorrect treatment technique (SAD/SSD) is selected for dose calculation	0.539	2
Dose per fraction in TPS is different from the prescribed one	0.451	3
Radiation therapists/medical linear accelerator		
Failure mode	c_i	rank
Incorrect patient answers the call (frequent last names)	0.575	1
Disagreement in monitor units is overlooked	0.549	2
Site mix-up in case of multiple sites treated	0.538	3

Table 2: Ranking of the most threatening failure modes for all four groups in the case in which the probability, severity and detectability are weighted 1:2:1.

AUTOMATIC IMPORT AND POSITIONING OF LINAC'S COUCH TOP.

Sašo Pulko[1]

[1]*University Medical Centre Maribor, Slovenia*

Purpose/Introduction

The aim of this project was how to automatically import Elekta's couch top structure to CT image set in correct position according to patient's position on a CT simulator. If relative position of the couch to the patient is correct, we can predict which part of the couch the beam will cross, so we can also predict possible couch collisions and limitations of couch movement.

Materials/Methods

The first linac's couch top (Elekta Connection) was scanned on CT simulator and imported in treatment planning system (TPS). The linac's couch was positioned on CT scanner's table in such a way that index holes were aligned as shown in Figure 1. For all parts of the couch top, contours for different materials ware created (1), Fig. 2. Attenuation for carbon fibers and foam was determined following procedures outlined by TG 176(2).

If patient is set up on a linac's couch top according to protocol (linac's lateral table position is set to 0° before patient is positioned on the table, fixation equipment is placed into the same index hole as it was on the CT scan) vertical and lateral relation is constant for all patient's image sets. On the other hand, relation between patient's CT image set and linac's couch top in longitudinal direction needs to be found for every patient image set.

Siemens CT couch tops have a pre-install wire, which is divided in three sectors and is angled for 45° in coronal plane as shown in Figure 3. This helped us to define the relations between patient's CT image set and linac's couch top template in longitudinal direction.

Script was created to import linac's couch top template and to align image centre of couch top template with patient's CT image centre. On the central slice of the patient image set, x – coordinate (x_CTpatient_wire) of the wire was found. If the wire was not found, script moved for delta (as shown in Fig. 4) step and repeat the process. Then for the same x-value (x_CTpatient_wire), y-coordinate in linac's couch top template was calculated (y_couch_top_calculated) according to equations in Figure 3. The right equation is chosen based on the body site. Because the image centres were aligned and x was found in the central slice, the translation of the linac's couch top template is defined as:

y_translation = (y_couch_top_image_center + delta) - y_couch_top_calculated.

Translation in vertical direction, is defined as difference in z-coordinate between table surface:

z_translation = z_CTpatient_table_top – z_ couch_top.

Translation in x direction is 0, because linac's couch top was centraly aligned before it was scanned. All three translations are at the end combined with orientational vector into transformation matrix as shown in Figure 5. Transformation matrix is applied to all relevant linac's couch top structures, all other are remove as shown in Fig. 6.

We measured difference between imported and real position of the patient. We compare distance between zero isocentre to nearest index point in TPS and on patient on the linac table.

Results

We run the script on over 300 patients. Because importing couch top takes less then 30 seconds and script is a part of the script to import the CT image set into TPS, we took couch top into account for every patient. Error between imported position and measured on the patient is on average 1.8 mm, which is in a range of measured accuracy.

Conclusions

At the moment we are able to import linac's couch top into all cases. We noticed some problems in cases when patients have CT simulators without fixation equipment which needs a fixation in an index hole, because patient is not always in same longitudinal position on the table. We also noticed some problems when we needed to change the orientation of the patient during planning, because of limitation of table movement.

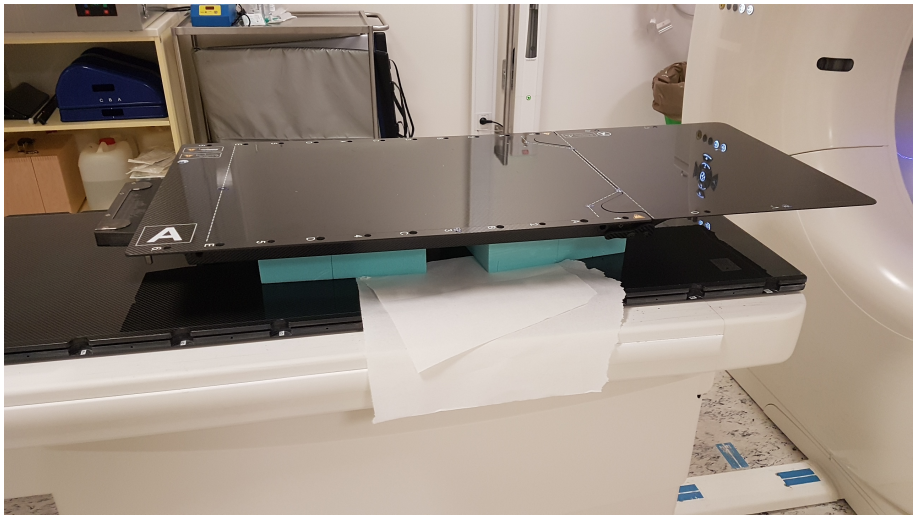

Fig. 1: Linac's couch top scanning setup position.

References

1. Zhang R, Gao Y, Bai W. Quantification and comparison the dosimetric impact of two treatment couch model in VMAT. J Appl Clin Med Phys. 2018;19(1):10-16. doi:10.1002/acm2.12206
2. Olch AJ, Gerig L, Li H, Mihaylov I, Morgan A. Dosimetric effects caused by couch tops and immobilization devices: report of AAPM Task Group 176. Med Phys. 2014;41:061501

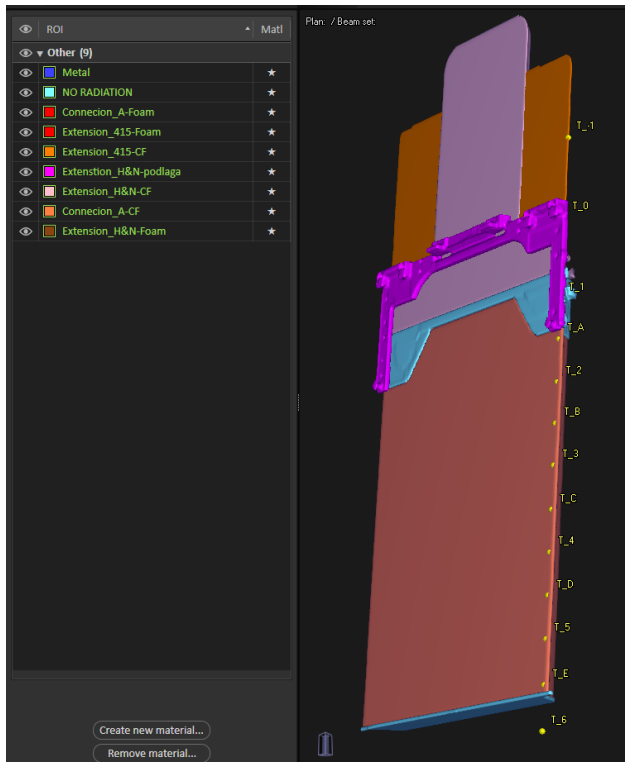

Fig. 2: 3D model of linac's base couch top with two additional extension (Head Step and Extension 415). No radiation zone is delineated with blue colour.

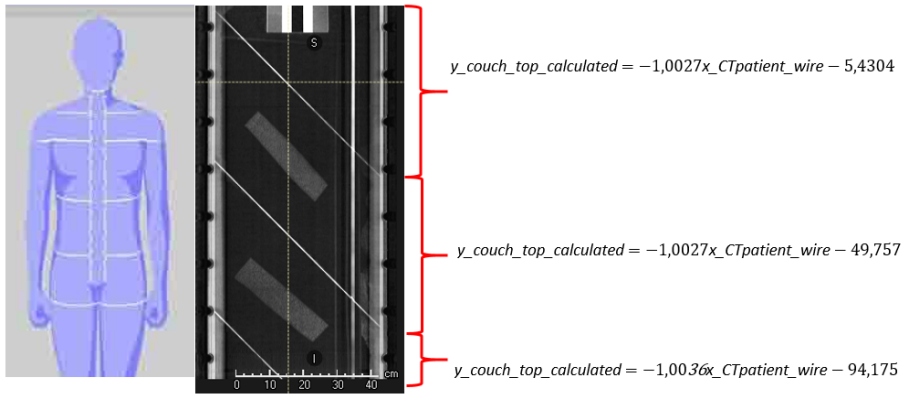

Fig. 3: Three different equations for three parts of the table.

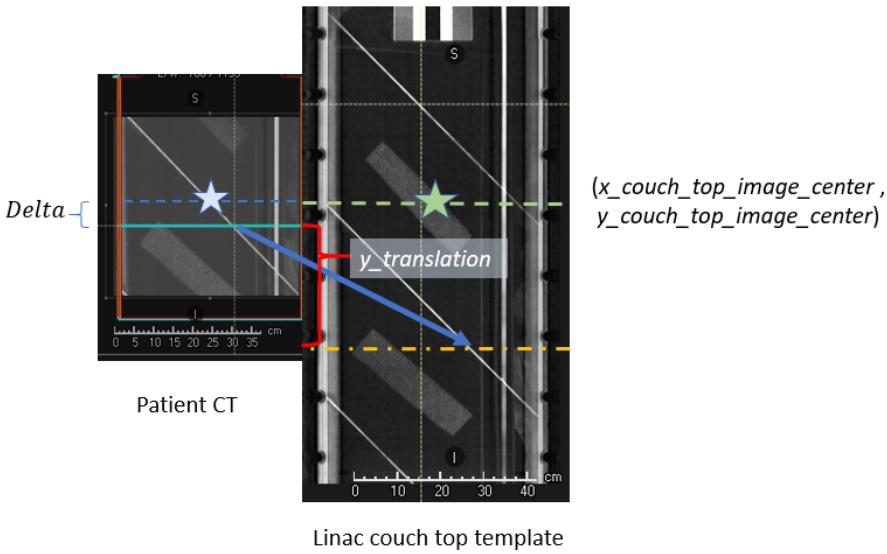

Fig. 4: Schematic presentation of transformation between patient CT image set and linac's couch top template.

Transformation matrix

$$\begin{bmatrix} M_{11} & M_{12} & M_{13} & M_{14} \\ M_{21} & M_{22} & M_{23} & M_{24} \\ M_{31} & M_{32} & M_{33} & M_{34} \\ M_{41} & M_{42} & M_{43} & M_{44} \end{bmatrix}$$

Translation:

$M_{14} = 0$

$M_{24} = y\_translation = (y\_couch\_top\_image\_center + delta) - y\_couch\_top\_calculated$

$M_{34} = z\_translation = z\_CTpatient\_table\_top - z\_\ couch\_top$

Rotation:

$$[M_{11} \quad M_{22} \quad M_{33}]$$

HFS - $[1 \quad 1 \quad 1]$

FFS - $[-1 \quad -1 \quad 1]$

HFP - $[-1 \quad 1 \quad -1]$

Fig. 5: Final transformation matrix whit all translation and rotation of linac's couch top template.

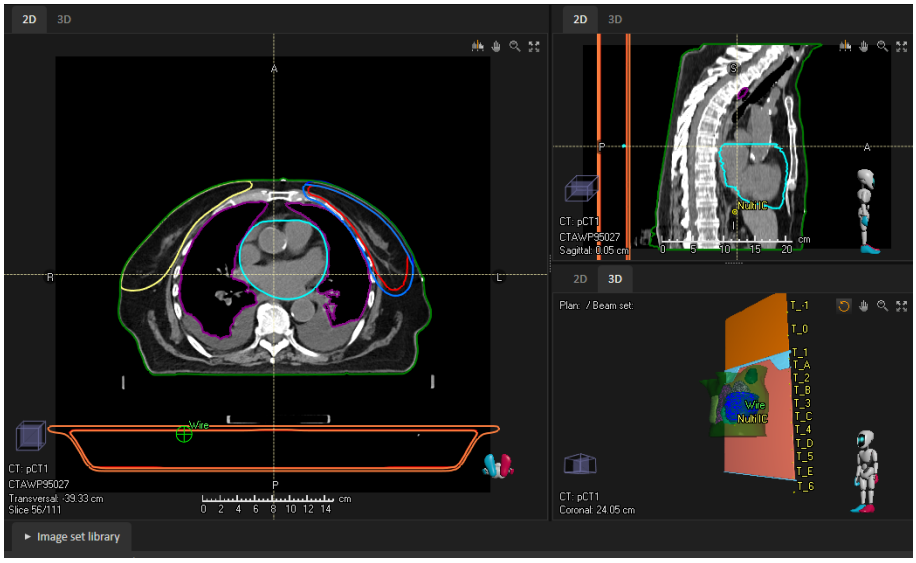

Fig. 6: Final result after couch top is imported to the patient.

CLINICAL IMPLEMENTATION OF CONSTANT DOSE-RATE VMAT IN THE ECLIPSE TREATMENT PLANNING SYSTEM

Andrej Strojnik[1], Denis Brojan[1], Primož Peterlin[1]

[1]*Institute of Oncology Ljubljana, Zaloška 2, Ljubljana, Slovenia*

Purpose/Introduction

Since its inception a decade ago (Otto, 2008), volumetric modulated arc therapy (VMAT) has proved to be the preferred technique of external photon therapy for many anatomical sites. Harnessing VMAT's full potential requires a linac capable of simultaneous variation of aperture shape, gantry rotation speed and dose rate. However even partial fulfillment of said requirements can prove itself beneficial (Yang, 2013; Hatanaka, 2014; Didona, 2018). One such implementation is the constant dose-rate (CDR) VMAT. Some treatment planning systems (Pinnacle SmartArc, RayStation, Elekta Monaco, Oncentra MasterPlan) indeed offer the option of creating CDR-VMAT plans along with the dynamic dose rate implementation. Varian Eclipse, as of version 15.6, does not offer this possibility in RapidArc (Varian trade name for their implementation of VMAT). Only fully dynamic RapidArc plans can be created, despite a wide base of installed low-energy medical linear accelerators which lack the capability of varying dose rate during beam-on time.

In this paper, we describe the modifications needed in the treatment machine description for the RapidArc optimization engine to produce a VMAT plan with near constant dose rate and gantry speed, and what further modifications are needed for the resulting VMAT treatment plan to be converted into a dynamic arc treatment plan which can be executed on an entry-level linear accelerator which doesn't support dose rate modulation. On a set of patient cases we also dosimetrically compare these CDR-VMAT treatment plans with regular RapidArc treatment plans.

Materials/Methods

Varian Unique Power Edition treatment machine has been used for this project. As a preparation, its machine description in the ARIA Oncology Information System (v15.6) was modified in a way which allows creating RapidArc treatment plans for a machine which doesn't support varying dose rate, allowing for a dynamic gantry operation yet prohibiting gantry acceleration (by setting its upper limit to 0), and configuring the Photon Optimizer (PO, v13.7) algorithm if necessary. With these modifications in place, RapidArc treatment plans can be created; because of the restricting gantry accelerator limit, PO will not attempt to modulate gantry speed, which will remain constant (apart from the initial acceleration from resting postion). As the dose rate is still allowed to vary, the target medical linear accelerator is not able to execute these plans.

Using Eclipse Scripting API (v15.6) each VMAT beam was substituted with a deliverable arc beam by using the AddConformalArcBeam method. This method creates a dynamic arc beam with a specified number of control points and allows the user to specify MLC and jaw positions for each control point. MLC and jaw positions were copied from the original VMAT beam, keeping other machine parameters, such as gantry start/stop angle, gantry direction, beam energy, collimator angle and nominal dose rate, the same.

The resulting plan is not identical to the RapidArc plan it was derived from, however the differences are usually small. After calculating the dose (AAA, v13.7), the planner has to review the treatment plan and check whether it still meets the objectives.

Per hospital regulations, patient-specific QA is required for all treatment plans employing non-conformal techniques. We use ScandiDos Delta4 phantom for this purpose at our clinic. Machine performance is tracked for each treatment fraction with Dynalog analysis.

As a clinical verification, we have selected a range of 23 brain cancer patients which were treated to 60 Gy in 30 fractions using the CDR-VMAT technique. Their treatment plans were replanned and re-optimized for a similar machine (Varian Unique Performance Edition) which supports RapidArc.

Results

Both treatment plans – CDR-VMAT and RapidArc – for each patient were compared using the parameters which are clinically relevant for this kind of treatment: the conformity number (CN) for the PTV, the homogeneity index (HI) for the PTV, the dose received by the 1% of the spinal cord, the dose received by the 1% of the brain stem (D1%), the dose received by the 1% of the optic chiasm, the dose received by the 1% of the optic nerve, and the dose received by the 1% of the left and right eye. The results are shown in Figure 1. The diagrams qualitatively show that neither method is convincingly better in any of the observed parameters. Comparing the results using paired t-test confirms this. In most parameters, t-test does not show a significant difference: CN ($p = 0.33$), HI ($p = 0.48$), spinal cord D1% ($p = 0.43$), brain stem D1% ($p = 0.83$), optic chiasm D1% ($p = 0.25$), optic nerve D1% ($p = 0.67$), and right eye D1% ($p = 0.21$). The only significant difference was observed in the left eye D1% ($p = 0.04$). This difference in favour of CDR-VMAT probably stems from the fact that since the values were in most cases substantially below the restriction (50 Gy), no particular constraint has been put to it during plan optimization.

Discussion

In their paper, Nicolini and coworkers (2011) have observed a correlation between the highest allowed dose rate in a RapidArc plan and the gantry speed. In this study, we have fixed both the gantry speed and the dose rate in the CDR-VMAT arm, while the RapidArc arm both can be modulated in principle, although in clinical plans, gantry speed usually stays constant. Since both techniques achieved comparable results, we expect CDR-VMAT plans to exhibit higher MLC modulation, which we intend to check in the future.

Conclusions

With no hardware modifications, minuscule modifications in the machine description, and with the help of a script which makes succesive cumulative meterset weights equidistant, we have demonstrated it is possible to create constant dose rate VMAT plans which are comparable to full RapidArc plans in clinically relevant parameters, and irradiate them on a treatment machine incapable of dynamic dose rate modulation.

References

1. Didona A, Lancellotta V, Zucchetti C, Panizza BM, Frettegiani A, Iacco M, et al (2018). Is volumetric modulated arc therapy with constant dose rate a valid option in radiation therapy for head and neck cancer patients? Rep Pract Oncol Radioth 23:175–182
2. Hatanaka S, Tamaki S, Endo H, Mizuno N, Nakamura N (2014). Utility of Smart Arc CDR for intensity-modulated radiation therapy for prostate cancer. J Radiat Res 55:774-779.
3. Nicolini G, Clivio A, Cozzi L, Fogliata A, Vanetti E (2011). On the impact of dose rate variation upon RapidArc ® implementation of volumetric modulated arc therapy. Med Phys 38:264-271.

4. Otto K (2008). Volumetric modulated arc therapy: IMRT in a single gantry arc. Med Phys 35:310-317.
5. Yang R, Wang J, Xu F, Li H, Zhang X (2013). Feasibility study of volumetric modulated arc therapy with constant dose rate for endometrial cancer. Med Dosim 38:351–355.

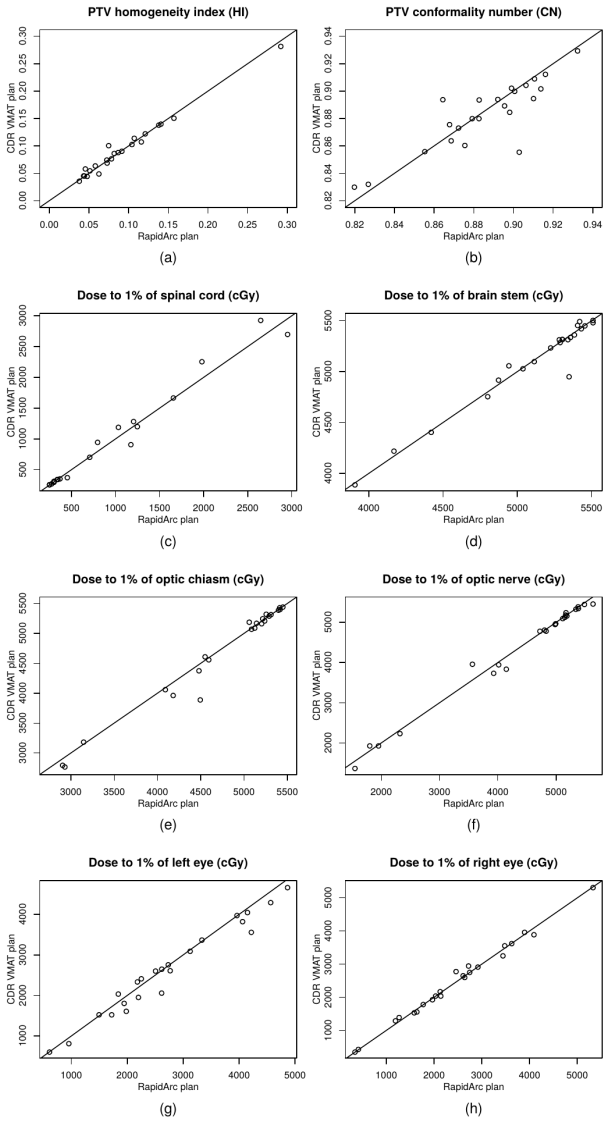

Figure 1: Comparision of clinical parameters in RapidArc and CDR VMAT treatment plans: PTV homogeneity index HI (a), PTV conformality number CN (b), dose to 1% of spinal cord (c), brain stem (d), optic chiasm (e), optic nerve (f), left eye (g) and right eye (h).

VALIDATION OF MONACO TPS MONTE CARLO BASED CALCULATION ALGORITHM THROUGH MONTE CARLO PARTICLE TRANSPORT SIMULATION

Manda Švabić Kolacio[1], Hrvoje Brkić[2], Dario Faj[2], Đeni Smilović Radojčić[3], David Rajlić[1], Nevena Obajdin[1], Slaven Jurković[3]

[1]*Medical Physics Department, University Hospital Rijeka, Croatia*
[2]*Faculty of Medicine Osijek, University of J.J. Strossmayer, Croatia*
[3]*Medical Physics Department, University Hospital Rijeka, Croatia Department of Medical Physics and Biophysics, Faculty of Medicine, University of Rijeka, Rijeka, Croatia*

Purpose/Introduction

The most accurate absorbed dose calculation in radiation oncology nowadays is provided by Monte Carlo based algorithms. Such algorithms inherently calculate absorbed dose to medium in medium Dm,m. They can also provide data as absorbed dose to water in medium Dw,m by conversion based on Spencer-Attix extension of Bragg-Gray small cavity theory. These two absorbed dose concepts do not necessarily provide similar results, which is particularly prominent in bone structures [1-2]. Monte Carlo based algorithms used in radiation oncology use several approximations and simplifications to speed up calculation time [3]. Furthermore, they do not use data of chemical composition of media which is the case with generalised Monte Carlo (MC) particle transport simulation algorithms (e.g., MCNP, EGS, GEANT…). Therefore, an investigation of the material chemical composition impact on calculation accuracy was performed comparing calculations obtained using Monte Carlo N-Particle code® (MCNP) and a clinical Monte Carlo based algorithm [4]. In this work the results of evaluation are presented [5].

Materials/Methods

The Monte Carlo based calculation algorithm built in Elekta Monaco treatment planning system (MCTPS) has three components dedicated to the absorbed dose calculation: a virtual source model (VSM), a transmission filter, and a patient model. VSM integrates three virtual sources to model the primary photon, secondary photon, and electron contamination sources at specified geometric locations. The primary collimator, jaws, and MLC are modelled using transmission filters. In fact, the Monte Carlo simulation is applied only in the patient model using the X-Ray Voxel Monte Carlo algorithm (XVMC). Absorbed dose data acquired by MCNP was used as reference data. Investigation of absorbed dose calculation accuracy was performed for 6MV X-ray beam (Siemens Oncor Expression linear accelerator) in various geometries of different complexities. The accuracy of MCNP absorbed dose calculations in virtual water phantom (MCNP model) was experimentally verified by ionization chamber (PTW30013 and IBA CC13) measurements in water phantom (IBA Blue2). Percentage depth dose curves and dose profiles at several depths for various field sizes were calculated and compared to measured data. For all MCNP calculations, cut-off energies of 1 keV for electrons (ECUT) and 1 keV for photons (PCUT) were applied. Statistical uncertainty for MCNP calculations was kept lower than 1%. The validation criterion was set on the central part of the beam where deviation between calculated and measured data lower than 0.5% was taken as acceptable. Comparison between two MCTPS dose calculation options and MCNP calculations in simple (homogeneous) and different heterogeneous geometries was performed using 13 different materials with mass densities ranging from 0.2 g/cm3 to 2.17 g/cm3. The MCNP calculations were performed by assigning material chemical

composition and mass density (MCNPMEDIUM). The absorbed dose was calculated as Dm,m. The Depth dose curves (DDs) calculated by MCNP were compared to Dm,m and Dw,m MCTPS calculated data using Root Mean Square (RMS) deviation. Additional validation of absorbed dose calculation accuracy was performed in heterogeneous phantoms. Namely, heterogeneous geometries were simulated by placing inserts of mass densities which mimic lung and bone tissue (ρ=0,205 g/cm3 and ρ=1,6 g/cm3) at different depths in the virtual water phantom (soft tissue). Furthermore, the influence of chemical composition on the calculation accuracy of absorbed dose in a semi-anthropomorphic phantom was also examined.

Results

Deviations in DDs, between Dm,m and Dw,m calculated by the MCTPS in different materials are the largest for the material of mass density 2.17 g/cm3, up to 13% (Fig. 1.). Dm,m calculation is in very good agreement with the MCNPMEDIUM , with the deviation less than 3% for the majority of examined materials except for the lowest mass density in this research (ρ=0.2 g/cm3), where the deviation was 4.8% (Fig.2.). On the other hand, the Dw,m calculation results are acceptable only in the mass density range from 0.5 g/cm3 to 1.06 g/cm3 with deviations lower than 2.5%. For the rest of the examined materials, the deviation increases, with a maximal value of 12.4% for mass density 2.17 g/cm3 [5]. Hence, the assumption of small cavity conditions applied through stopping power ratios of water and different materials for the Dw,m calculation was validated. The most probable energy of the secondary electrons for a 6MV X-ray beam is below 300 keV and such electrons have a range 0.0957 g/cm2 [6]. Therefore, the small cavity conditions when the MCTPS calculation voxel size of 3×3×3 mm3 is used, mainly cannot be fulfilled due to the secondary electron range for almost all materials used [5].

Discussion

The absorbed dose calculation accuracy is related to the capability of the algorithm to calculate absorbed dose at any point of interest within the patient and correlate it to the beam calibration point dose considered as the reference absorbed dose. In the MCTPS dose calculation engine, material chemical composition is not taken into account, thus introducing additional calculation uncertainty. Validation of absorbed dose calculation in more complex geometry was performed by comparison with MCNPMEDIUM calculations, when the conditions for charged particle equilibrium are not met due to heterogeneity. Here, deviations lower than 5% are considered acceptable. The analysis revealed the same trend as the validation of the absorbed dose calculation in a homogeneous phantom. Namely, the deviation in MCTPS Dw,m calculation in heterogeneities was outside the acceptability criterion. Also, the deviations for Dm,m follow the trend observed in the homogeneous phantom calculation with the tendency of deviation increase for more complex geometries. However, for high-density medium inserts this deviation is still acceptable. For low-density inserts, the deviation is significantly larger compared to the calculation in a homogeneous phantom, depending on the level of complexity of the examined geometries. Such a trend of deviations suggests that the empirical function used in XVMC calculation for assigning of cross sections and stopping power of materials in low-density range is not correctly defined and improvements are required. Additionally, Bragg-Gray cavity theory was applied under the assumption that there is no flux perturbation. However, the conditions for this assumption are not met, which is one of the reasons for the observed deviations in materials of different chemical compositions.

Conclusions

The results of the validation method of the Monte Carlo based algorithm calculation accuracy complementary to existing experimental verification methodology are presented. The Dm,m calculation shows very good agreement with standard MCNP calculations except for low-density medium. Therefore, the improvement of the accuracy of MCTPS Dm,m calculation option in low-density medium may be the further step of the research. Nevertheless, the results obtained in this work indicate that Dm,m could be regarded as the preferable dose calculation option.

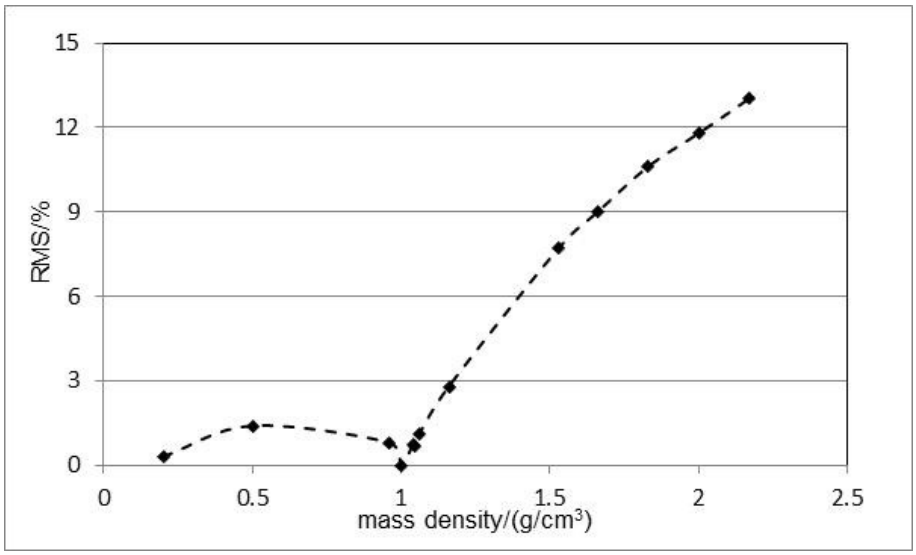

Fig.1. RMS deviation between DDs for dose calculation options Dm,m and Dw,m built in MCTPS for different materials.

References

1. Andreo P (2015). Dose to “water-like” media or dose to tissue in MV photons radiotherapy treatment planning: Still a matter of debate. Phys. Med. Biol. 60, 309–337.
2. Smilovic Radojcic D, Svabic Kolacio M, Radojcic M, Rajlic D, Casar B, Faj D, Jurkovic S (2018). Comparison of calculated dose distributions reported as dose-to-water and dose-to-medium for intensity-modulated radiotherapy of nasopharyngeal cancer patients. Med. Dosim. 43, 363–369.
3. Fippel M, Kawrakow I (2000). Investigation of variance reduction techniques for Monte Carlo photon dose calculation using XVMC. Phys. Med. Biol. 45, 2163–2183.
4. Cox LJ, Casswell L (2014). MCNP(TM) Release 6.1.1 beta: Creating and Testing the Code Distribution. Los Alamos, NM (United States).
5. Svabic Kolacio M, Brkic H, Faj D, Smilovic Radojcic D, Rajlic D, Obajdin N, Jurkovic S (2021). Validation of two calculation options built in Elekta Monaco Monte Carlo based algorithm using MCNP code. Radiation physics and chemistry, Volume 179.
6. Siebers JV, Keall PJ, Nahum AE, Mohan R (2000). Converting absorbed dose to medium to absorbed dose to water for Monte Carlo based photon beam dose calculations. Phys. Med. Biol. 45, 983–995.

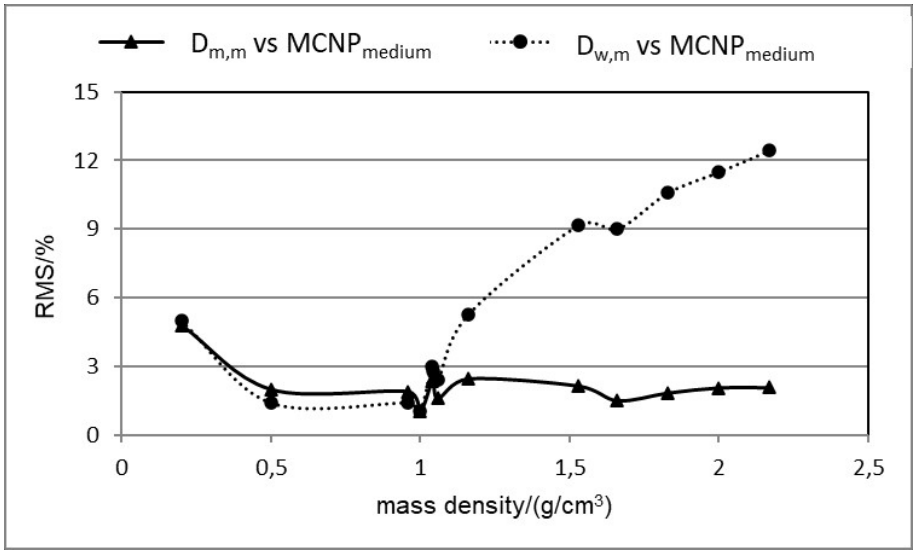

Fig. 2. RMS deviation between both MCTPS calculation options and MCNPmedium.

URINARY EXCRETION RATE OF I-131 DURING TREATMENT OF BENIGN THYROID DISEASES-A PILOT STUDY

Urša Beguš[1], Adrijana Oblak[2], Luka Jensterle[2], Katica Bajuk Studen[2], Petra Tomše[2], Urban Simončič[1], Simona Gaberščček[2], Katja Zaletel[2]

[1]*Faculty of Mathematics and Physics, University of Ljubljana, Slovenia*
[2]*Department of Nuclear Medicine, University Medical Centre Ljubljana, Slovenia*

Purpose/Introduction

Benign thyroid conditions causing hyperthyroidism (an overactive thyroid) are successfully treated with radioactive iodine I-131. The aim of therapy is to destroy hyperfunctioning thyroid tissue with beta rays emitted by I-131. However, I-131 also emits gamma rays and therefore patients treated with I-131 present a radiation hazard and can cause external radiation exposure to nearby individuals. Furthermore, considerable amount of administered I-131 is not taken up by the thyroid and is rapidly excreted, primarily via urine. As a result, the risk of contamination may also arise from I-131 excretion. Therefore, radiation safety is an integral part of I-131 therapy. We are presenting a pilot study performed at the Department of nuclear medicine at the University medical centre Ljubljana aimed to investigate the urinary excretion of I-131 as a function of time during patients' isolation period in hospital.

Materials/Methods

In the first part of our study we determined a calibration factor for measuring activity of I-131 with gamma counter (Hidex, Finland). To find the relationship between counts (cps) detected by the gamma counter and activity of I-131 in the sample (MBq), six samples of I-131 solution with known activity were measured. We prepared a solution of I-131 with activity 1 MBq, measured in the activity meter (Comecer, the Netherlands), and further prepared samples with stepwise decreasing activities of I-131 in 1 ml eprouvettes with an Eppendorf pipette (20 – 200 µl, 100 – 1000 µl). The samples were measured 1 minute with gamma counter and counts in two energy windows were recorded for the total count measurement (250 keV–435 keV and 585 keV–695 keV). Dependency between activity and counts in the gamma counter was plotted and calibration factor was obtained using a linear fit. Using the calibration factor activity was calculated from gamma counter measurements in the second part of the study.

In the second part we performed pilot measurements of patients' urine sample. Two female patients aged 54 and 65 years with hyperthyroidism (caused by autonomous thyroid tissue) and normal kidney function, being treated with I-131 were included. First patient's, urine samples were collected at 2, 4 and 24 h and second patient's at 2, 4.5 and 66 h after oral administration of I-131 in the form of Sodium Iodide 131 (NaI-131) capsule (activity: 935 MBq and 1095 MBq, respectively). The last time point was at the time patient was discharged from the hospital. The volume of each urine collection and the exact time of collection was recorded, then a sample of approximately 1 ml was taken from each collection to perform activity measurements. The mass of each urine sample was measured with Mettler Toledo AX105 scale, then the samples were diluted by taking 0.05 ml from urine sample and adding 0.95 ml of saline. Activity of diluted urine samples were measured with gamma counter using the same protocol as in the gamma counter calibration process. Dose rate at 1 m distance from patients was also measured with CoMo 170 contamination monitor before discharge as part of routine

patient treatment protocol. Previous study at the department determined relation between dose rate at 1 m and total I-131 activity in the patient [1], which allowed us to estimate remaining activity in our patients.

Results

Gamma counter count versus activity measurement plot shows a strong linear relationship (Figure 1). The fit over measurements yielded a linear relation counts = 2.7 * activity, representing gamma counter efficiency 37%.

Figure 2 shows activities of the patients' total urine samples at the time points of collection. In both patients, the excretion of I-131 was considerable at 2 and 4 hours after the activity administration (patient 1: 67 MBq/7%, 67 MBq/7%; patient 2: 96 MBq/9%, 154 MBq/14%) and decreased at late time points (patient 1: 14 MBq/1%; patient 2: 0.9 MBq/0.1%).

At the time of discharge from the hospital, dose rate at 1 m was 22.1 μSv/h for patient 1 and 15.2 μSv/h for patient 2, which implies retained I-131 activity 354 MBq (38%) and 290 MBq (26%) respectively.

Discussion

Excretion rate of I-131 through urinary tract from patients receiving I-131 therapy for thyroid cancer, was investigated in many studies [2]. However, we found only one previous study exploring the excretion rate of I-131 from patients receiving I-131 for treatment of hyperthyroidism [3]. Unlike thyroid cancer patients, patients with hyperthyroidism receive considerably lower activities of I-131, the treated volume is larger and I-131 thyroid uptake is significantly higher. Consequently, the excretion of I-131 in urine is lower and possible with different dynamics. Similar studies report that I-131 is excreted with urine rapidly within the first three days [2]. This pilot study confirms that great percentage of activity (three urine samples contained 16% and 9% of administered activity; retained body activity at discharge was 38% and 26%) is excreted in urine within three days, the early samples being much more active than the samples at the discharge. Therefore, considering radiation protection after discharge from hospital, a 3-day hospital stay is reasonable, as afterwards the risk for urine contamination is smaller.

Conclusions

Future prospects include a study with a higher number of patients (measurements of 30 patients are planned), including additional thyroid volume and standardized uptake value measurements along with clinical and laboratory data, including serum level of thyroid hormones. Subsequently we aim to establish the relationships between these factors and urinary excretion rate of iodine. The activity present in urine of these patients emphasizes the need for raising awareness of the contamination hazard for all individuals coming in contact with these patients. Consequently, the primary aim of the future study is to obtain information about I-131 excretion, and therefore give the patients more detailed information in terms of radiation protection after discharge from hospital.

References

1. Poljanšek N, Ocena prejete doze pri zdravljenju ščitničnih bolezni z I-131: master's thesis, 2016. Faculty of Mathematics and Physics, University of Ljubljana, Slovenia.
2. Demir M, Parlak Y, Cavdar I, Yeyin N, Tanyildizi H, Gümüser G, Sayit E, Erees S, Sayman H. The evaluation of urine activity and external dose rate from patients receiving radioiodine therapy for thyroid cancer. Radiat Prot Dosimetry, 2013;156(1):25-9.

3. Liu YL, Zhao ZX, Huo MH, Yin C, Tan J, Zhang WY, Jiao L. Study of the External Dose Rate and Retained Body Activity of Patients with Hyperthyroidism Who Are Receiving I-131 Therapy. Biomed Environ Sci, 2018; 31(12): 913-916.

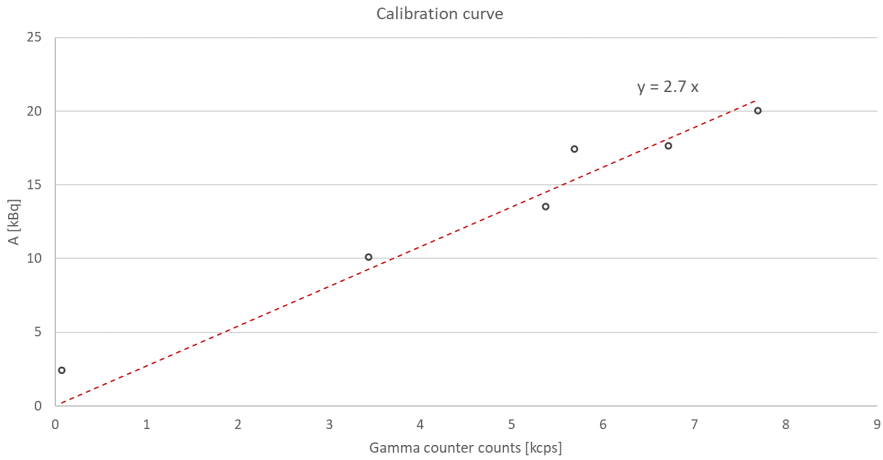

Measurements of I-131 samples with gamma counter and activity meter and fitted calibration curve.

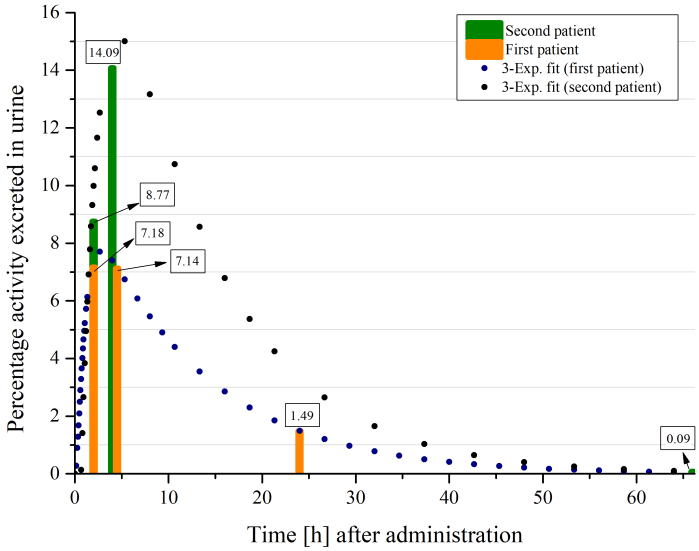

Percentage activity excreted in urine at different times after the administration of I-131 for two patients, wherein the first received activity of 935 MBq and second 1095 MBq.

INDIVIDUAL DOSIMETRY OF TARGETED RADIONUCLIDE THERAPY FOR TREATMENT OF SOMATOSTATIN RECEPTOR-POSITIVE GEP NET

Gašper Strnad[1], Petra Tomše[1], Luka Jensterle[1], Daša Sfiligoj Planjšek[1], Anja Androjna[1], Luka Ležaič[1]

[1]*Department of Nuclear Medicine, University Medical Centre Ljubljana, Slovenia*

Purpose/Introduction

Lu-177 DOTATATE targeted radionuclide therapy is used for treatment of patients with somatostatine receptor-positive gastroenteropancreatic neuroendocrine tumors. Lu-177 DOTATATE is a somatostatine analog, with Lu-177 having a half life of 6.73 days and emitting beta radiation with a maximum energy of 0.498 MeV and gamma radiation of 0.208 MeV and 0.113 MeV. Individual dosimetry calculations are necessary because of the high injected activities with potential for radiation doses approaching critical values for organs such as the kidneys. The aim of this report is to present doses on relevant organs in the abdominal cavity in a transparent way for a group of patients who have had at least one radionuclide therapy.[1]

Materials/Methods

In the years 2013 – 2021 28 patients (M/F: 18/10) were treated with Lu-177 DOTATATE radionuclide therapy (A = 6603±1434 MBq) at the Department of nuclear medicine at the University medical centre Ljubljana. For dosimetry purposes planar whole body images were acquired with Siemens Symbia SPECT/CT at selected time points. In the optimal case imaging was performed immediately after the radionuclide application and 1, 2, 4, 24, 48 and 168 hours after the application. Note that many patients had only 4 or 5 time points, as the image acquiring process can be time consuming and puts strain on the patient. We used ImageJ software[2] to outline ROIs in each image of each patient. ROIs were the following: liver, kidneys, spleen, bladder, region of whole body and background region, additionally in 4 cases we also defined ROIs for tumor tissue. Total activity within the ROIs was determined. For each ROI we collected the measurements from all images and plotted the points representing activity relative to the total body activity captured in the first image versus time past from the injection of the radionuclide. For each ROI the points were then fitted to align with an exponential curve model of the form $\sum(i=1,2,3)k\_i*\exp(-\lambda\_i*t)$, where k_i and λ_i are parameters used to fit the curve. We used Microsoft's Excel's Solver function to determine the model, which is based on the nonlinear Generalized Reduced Gradient (GRG) method. Using the model parameters we calculated the residence times for each ROI. The residence time is equivalent to the area under the curve in the activity/time plot and represents the total number of Lu-177 decays within the ROI. For determining the absorbed radiation dose to the specific organs we used OLINDA/EXMR software, applying the Medical Internal Radiation Dose (MIRD) methodology. The input parameters were the radionuclide used, the patient model (sex and weight) and residence times. We compared the residence times and radiation doses for all treated patients and separately for patients who had undergone multiple radionuclide treatments.

Results

Figure 1 shows the scattering of calculated residence time values for all patients. In this figure, each stack of vertically positioned dots corresponds to one of the source organs. The data presented in Figure 1 is summarized in Table 1, which is showing the average values of residence times and absorbed doses for source and target organs. Kidneys, being the most critical organ, have residence time 3 ± 1.2 h and absorbed dose 5.6 ± 2.2 Gy. Table 2 presents the range of residence times for source organs and total kidney dose for six patient undergoing multiple therapies. For multiple therapies of the same patient the range of residence times is wide, for kidneys we can see the value can differ for factor 2. Total absorbed dose to the kidneys for all therapies of one patient was up to 21.6 Gy.

Discussion

This report is an overview of the individual dosimetry of radionuclide treatments with Lu-177 DOTATATE at the University medical centre Ljubljana for 28 patients.

We can observe that the kidneys and spleen received the highest radiation dose. Bladder dose is mostly dependent on the time and frequency with which the patient urinates after the application. The kidneys received an average dose of 5.6 ± 2.2 Gy, while the maximum tolerable absorbed dose fort he kidneys is 27 Gy. Patients with multiple therapies received a total absorbed kidney dose of 15.9 ± 4 Gy.

Due to various sources of uncertainty, the method is estimated to have an error up to 30%[3]. The sources of the deviations are use of 2 D images lacking the 3 D information about organ size and activity distribution, the subjectivity of organ ROIs delineation and approximations in the MIRD method used for calculating the dose. MIRD method presumes that the intraorgan dose distribution is homogenous, which in reality may not always be the case. OLINDA/EXM software requires for users to choose a human model, either male or female with a standard weight (60 kg for females and 72 kg for males), correlating with patient organ weight. This is not always linear. OLINDA has an option for bodyweight corrections, but we used this only in cases where the patient's body weight was significantly different than the models.

Conclusions

We presented results of dosimetry calculations for patients undergoing Lu-177 DOTATATE targeted radionuclide therapy. The dosimetry is crucial for planning further treatments for the patient. Current protocol in University medical centre includes analysis of 2 D whole body images, whereas more accurate dose estimations may be obtained with 3 D SPECT images. Therefore a protocol upgrade in 3 D analysis is planned in the near future.

References

1. Schneider, C. A., Rasband, W. S., & Eliceiri, K. W. (2012). NIH Image to ImageJ: 25 years of image analysis. Nature Methods, 9(7), 671–675. doi:10.1038/nmeth.2089
2. Sandström M, Garske U, Granberg D, Sundin A, Lundqvist H. Individualized dosimetry in patients undergoing therapy with (177)Lu-DOTA-D-Phe (1)-Tyr (3)-octreotate. Eur J Nucl Med Mol Imaging. 2010 Feb;37(2):212-25. doi: 10.1007/s00259-009-1216-8
3. Stabin MG, Sparks RB, Crowe E. OLINDA/EXM: the second-generation personal computer software for internal dose assessment in nuclear medicine. J Nucl Med. 2005 Jun;46(6):1023-7. PMID: 15937315.

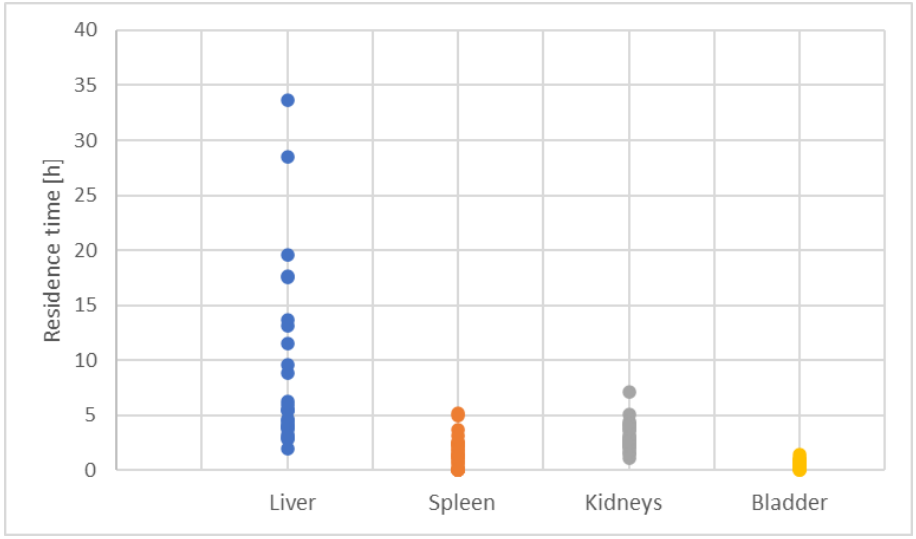

Fig 1: Residence times for source organs for all patients. Each point represents the residence time of one patient with prescribed [177Lu]Lu-DOTATATE radionuclide therapy.

Organ	Residence time [h]	Dose [Gy]
Liver	8 ± 7.9	3.1 ±2.1
Spleen	2.1 ± 1.3	6.4 ±5.8
Kidneys	3 ± 1.2	5.6 ±2.2
Bladder	0.5 ± 0.3	0.9 ±0.6
Red marrow	-	0.2±0.1
Whole body	31.5 ± 13.3	-

Table 1:. Residence time and radiation dose per organ from 28 individual [177Lu]Lu-DOTATATE therapies, delivering activity $\bar{A}$=6603±1434 MBq of Lu-177. Red marrow does not have a residence time value because we do not include it as a source organ in the calculation, whereas whole body is used as a source but is not a relevant target organ.

Patient	No. of therapies	Residence time range per organ [h]				Total kidney dose [Gy]
		Liver	Spleen	Kidneys	Bladder	
M #1	4	9.6 - 17.6	-	1.8 - 3.1	0.3 - 0.9	18.6
M #2	3	4 - 4.3	1.9 - 2.6	1.1 - 2.2	0.3 - 1	15.7
M #3	4	3.8 - 6.2	0.7 - 2.4	1.1 - 2.2	0.2	16.9
M #4	2	11.5 - 19.6	1.1 - 1.5	4.1 - 5.1	0.6 - 0.8	21.6
F #1	2	28.5 - 33.6	-	3.6 - 4.1	-	8.9
F #2	2	4 - 5.5	2.3 - 3.7	4.4 - 7.1	0.4 - 0.8	13.8

Table 3: Residence time of source organs range determined for patients with multiple therapies.

DAILY QUALITY CONTROL IN DIGITAL MAMMOGRAPHY USING QUANTITATIVE IMAGE ANALYSIS

Urška Poje[1], Urban Zdešar[2], Andrej Studen[3]

[1]*Medical Physics Student University of Ljubljana*
[2]*Institute of Occupational Safety, Ljubljana, Slovenia*
[3]*University of Ljubljana, Faculty of Mathematics and Physics and Jožef Stefan Institute, Ljubljana, Slovenia*

Purpose/Introduction

As part of the quality assurance system in the Slovenian Breast Cancer Screening Programme (DORA), regular or preferably daily scans of homogeneous PMMA-plate phantoms are performed on every mammography unit in the programme. Visual inspection of images can be time consuming and due to large image resolution, some irregularities can easily be overlooked. This study focused on finding new methods, sensitive enough to automatically detect such irregularities.

Materials/Methods

The Slovenian breast cancer screening programme is organized centrally with mammography units located in different parts of Slovenia and a centralized picture archiving system PACS that collets images from all units. Eighteen mammography units were included in the study, half of which are Siemens units and the other half Hologic. Altogether approximately 4000 test phantom images in the period from October 2019 to March 2021 were evaluated within the study.

The images were analyzed by first dividing the image into areas of 50x50 pixels, so that the areas overlapped by 25 pixels. In each area, the mean, variance, skewness and kurtosis were calculated. The results were stored in matrix form and displayed as grayscale images, thus obtaining statistical images for each test phantom image. The pixel values are a good indicator of how the detector elements work, because when they are not working properly, the values start to deviate from one another. Of all the statistical measures calculated, skewness (g1) seems to be the best one for detecting malfunctions of the detector elements. Skewness describes the shape of the distribution of pixel values in the 50x50 pixel areas. In case the distribution has one of the tails longer than the other, this may be an indication that some pixel values in the image are much larger or much smaller than the surrounding pixel values. In addition, skewness is independent of absolute values, so the parameters of the images captured are comparable between different mammography units.

Results

Using this method, a total of 13 point artefacts and 4 line artefacts have been identified in the set of test phantom images from October 2019 to March 2021. Some artefacts disappeared after detector recalibration or replacement, but some persisted. An example of line artefact as seen on statistical image is shown on Fig. 1. For a few mammography units charts of the time dependence of the 98th percentile of the absolute value of skewness are presented.

Conclusions

Daily monitoring of test phantom images is very important to ensure the constant quality of mammographic images. With the help of computer image analysis, the search for artefacts affecting image quality is faster and independent from human factors. Skewness has proven to be a reliable and robust estimator of point and line artefacts and is a potential metric for automated quality control.

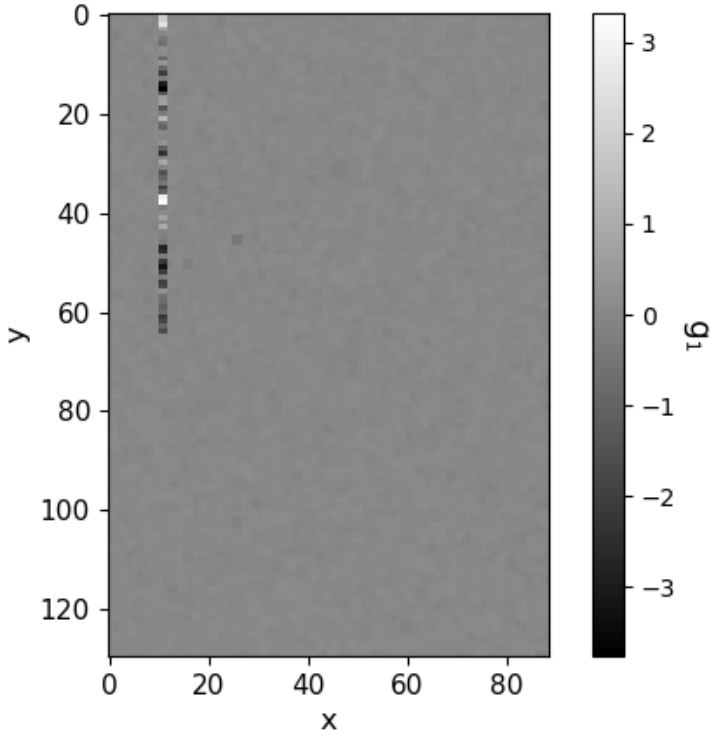

Line artefact as seen on statistical image.

References

1. M. J. Yaffe. Developing a quality control program for digital mammography: achievements so far and challenges to come. Imaging Med. 3(1) (2011). 123–133.
2. R.E. van Engen, et al. Using a Homogeneity Test as Weekly Quality Control on Digital Mammography Units. IWDM 2006. 259 (2006). 259–265.
3. M. J. Yaffe, Digital Mammography. Berlin: Springer. (2010).
4. J. Binst, et al. 15 years of remotely controlled daily quality control in digital mammography. Proc. SPIE. 11513. (2020).

COMPARING SIMULTANEOUS INTEGRATED BOOST AND SEQUENTIAL BOOST IN LARYNGEAL AND PAROTID GLAND HEAD AND NECK CANCER PATIENTS

Elena Hristovska[1], Lenche Kostadinova[2], Dushko Lukarski[3]

[1]City General Hospital 8th September, Skopje, N. Macedonia
[2]University Clinic for Radiotherapy and Oncology, Skopje, N. Macedonia
[3]University Clinic for Radiotherapy and Oncology, Skopje, N. Macedonia; Faculty of Medicine, Ss Cyril and Methodius University, Skopje, N. Macedonia

Purpose/Introduction

Radiation therapy has a key role in treating patients with head and neck cancer. The most often employed radiation therapy technique for head and neck patients, due to the high concentration of vital organs near the tumour, is intensity-modulated radiation therapy (IMRT) either at several fixed gantry angles or as an arc therapy. There are two types of delivery: sequential (SEQ-IMRT) and simultaneous integrated boost (SIB-IMRT) [1]. SEQ-IMRT consists of two sequential plans. In the first plan the target structure is the low risk planning target volume (PTV-LR) and then, with a second plan, a boost dose is applied only to the high risk planning target volume (PTV-HR). The SIB-IMRT technique consists of a single plan with different radiation doses applied appropriately to the PTV-HR and PTV-LR [2]. Both techniques are wieldy used in practice. The aim of this study is to make a treatment planning comparison of both techniques by comparing the doses received by the organs at risk (OARs), keeping the target coverage radiobiologically equal [3]. For that purpose, two groups of patients were evaluated, for a total of thirty patients. The first group comprises of 15 patients with inoperable advanced stage laryngeal cancer, while the second group includes 15 parotid gland cancer post-op patients. In the laryngeal group, definitive radiotherapy was the main treatment, while in the parotid group radiotherapy was added as adjuvant postoperative treatment. The main side effect during the course of radiotherapy is mucositis, which is also a limiting factor for the completion of the radiotherapy treatment. A second side effect after the end of treatment is xerostomia, which affects the long term oral health of patients.

Materials/Methods

Patient selection Thirty patients that were treated at the University Clinic of Radiotherapy and Oncology in Skopje, Macedonia were selected for this study. They were divided in two groups of 15 patients depending on the location of the primary tumour.

Treatment planning technique Static gantry IMRT plans with 6 MV photon beams were optimized and calculated using Eclipse 16.1 treatment planning system (Varian Medical) for Varian Clinac iX linear accelerator, 120 leaves MLC. The arrangement of the beams for the first plan of the SEQ-IMRT (target PTV-LR) and for the corresponding SIB-IMRT plan was the same and it consisted of 6-7 coplanar beams. The second plan of the SEQ-IMRT consisted of 5-6 beams arranged according to the position of PTV-HR and OARs.

Radiation dose and fractionation The goal was to achieve the same radiobiological effect for the PTVs with both techniques. Therefore, we calculated the Biological Effective Dose for the SEQ-IMRT treatment according to [4] and then considering the rate of proliferation of the tumour and its type, we calculated the dose/fractions that should be used in SIB-IMRT technique. In the table in Fig. 1 we

present the doses and fractions prescribed to the different targets using both techniques for the two localizations.

Plan evaluation and comparison The plans were optimized to provide proper coverage of the target volumes with normalization of 100% at dose mean. Evaluation of the plans was made using DVH as follows:

• First criteria was 98 % coverage of the volumes of PTVs with 95 % of the prescribed dose.

• For evaluation of the OARs, recommendations from QUANTEC [5] were followed. For oral cavity, recommendation found in literature [6] was followed. We evaluated the spinal cord, oral cavity, parotid glands and larynx. Since the fractionation in the plans was different, EQ2 doses were used to compare the OARs. In the table in Fig.2 we provide the used EQ2 dose limits.

The coverage of the OARs was compared with the nonparametric two-tailed Wilcoxon signed-rank test for paired values. Statistical significance was assumed at $p \leq 0.05$.

Results

In the table in Fig.3 we present the results for percentage of the volume receiving 95% of the prescribed dose for all the target structures, for both techniques and localizations. All results fulfilled the 98% coverage criterion with 95% dose.

In the table in Fig.4 we present the evaluated OAR doses and volumes for both techniques, for patients with parotid gland cancer. The OAR doses were within the limits for both techniques, with oral cavity and larynx receiving smaller doses with the SEQ-IMRT technique than with the SIB-IMRT technique.

For laryngeal cancer, as presented in the table in Fig.5, the doses received by the OARs were also in limits with the exception of the parotids. Again, the results show that the SEQ-IMRT technique gives smaller doses to the oral cavity and to the parotids.

Discussion

The dose to PTV-LR and PTV-HR in both techniques was prescribed in a way that the radiobiological effect in both cases is equivalent, taking in consideration the proliferation of the tumours. The optimization was performed in such a way that more than 98% of the volumes of PTVs were covered with 95% of the prescribed dose. In laryngeal cancer, the dose to the parotids was out of limit because part of the PTV-LR extended in the parotids. However, the position of parotid glands in this case was not overlapping with PTV-HR, thus allowing the SEQ-IMRT to better spare the parotids in comparison to SIB-IMRT. Oral cavity was also spared more in this case. In parotid gland cancer the PTV-HR is concentrated to only one parotid and therefore there is substantial sparing of the OARs and they are all within limits. Again SEQ-IMRT spares the larynx and the oral cavity better, which is not seen in the contralateral parotid.

Conclusions

From this research we can conclude that SEQ-IMRT is better at sparing the OARs when treating these two types of cancer. However, in all cases when one of the techniques conformed to the OAR limits, so did the other. Therefore, when deciding on the optimal technique, additional factors should be taken into account as well, such as the position and delineation of the PTVs, the volume and position of the OARs relative to the PTVs etc. One strong point for SIB-IMRT technique for a department with a heavy patient load is that the overall treatment time for SIB-IMRT technique is 3-5 days shorter. Therefore, the clinical choice of the technique should include all the patient specific, but also department specific factors.

Type of cancer	Techniques	SEQ-IMRT	SIB-IMRT
Parotid gland cancer	Total dose to PTV-LR (Gy)	50	54
	Total dose to PTV-HR (Gy)	66	63
	Dose per fraction of PTV-LR (Gy/fraction)	2	1.8
	Dose per fraction of PTV-HR (Gy/fraction)	2	2.1
	Number of fractions	33	30
Laryngeal cancer	Dose to PTV-LR (Gy)	50	54
	Dose to PTV-HR (Gy)	70	66
	Dose per fraction of PTV-LR (Gy/fraction)	2	1.8
	Dose per fraction of PTV-HR (Gy/fraction)	2	2.2
	Number of fractions	35	30

Table 1: The prescription dose of SEQ-IMRT and SIB-IMRT techniques

References

1. Dogan N, King S, Emami B et al (2003). Assessment of different IMRT boost delivery methods on target coverage and normal-tissue sparing. Int J Radiat Oncol Biol Phys 57:1480-1491.
2. Rastogi M, Sapru S, Gupta P et al (2017). Prospective evaluation of Intensity Modulated Radiation Therapy with Simultaneous Integrated Boost (IMRT-SIB) in head and neck squamous. Oral Oncol 67:10-16.
3. Mohan R, Wu Q, Manning M, Schmidt-Ulrich R (2000). Radiobiological considerations in the design of fractionation strategies for Intensity-Modulated Radiation. Int J Radiat Oncol Biol Phys 46:619-630.
4. Joiner M, Van der Kogel A (2009). Basic Clinical Radiobiology. London: Hodder Arnold, pp. 114-116; 125-126.
5. Bentzen SM, Constine LS, Deasy JO et al. (2010) Quantitative analyses of normal tissue effects in the clinic (QUANTEC): An introduction to the scientific issues. Int J Radiat Oncol Biol Phys 76:S3-S9.
6. Hansen EK, Roach M (2018). Handbook of evidence based radiation oncology, 3rd Ed. New York: Springer.

OAR		Dose criteria
Spinal cord		$D_{max} < 50$ Gy
Parotid glands	Unilateral	$D_{mean} < 20$ Gy
	Bilateral	$D_{mean} < 25$ Gy
Oral cavity		D_{mean} (excluding PTV) < 40 Gy
Larynx		$D_{mean} < 44$ Gy
		V50 < 27 %

Table 2: The dose criteria for OARs

		SEQ-IMRT		SIB-IMRT	
Organ	Target	Mean ± SD	Median	Mean ± SD	Median
Parotid glands cancer	PTV-LR	99.7 ± 0.2	99.8	99.9 ± 0.2	100
	PTV-HR	99.4 ± 0.3	99.5	99.6 ± 0.3	99.7
Laryngeal cancer	PTV-LR	99.8 ± 0.2	99.9	99.9 ± 0.2	99.9
	PTV-HR	99.8 ± 0.2	99.8	99.8 ± 0.3	100

Table 3: Coverage of the target volumes for both techniques

		SEQ-IMRT		SIB-IMRT		
Organ	Dose criteria	Mean ± SD, Gy	Median, Gy	Mean ± SD, Gy	Median, Gy	p-value
Spinal cord	$D_{max} < 50$ Gy	34.9 ± 2.5	35	36.4 ± 2	36.4	-
Oral cavity-PTV	$D_{mean} < 40$ Gy	21.8 ± 3.2	21.7	23.4 ± 3.7	22.7	.003
Larynx	$D_{mean} < 44$ Gy	23.5 ± 2.5	24	27.2 ± 3.4	27.1	< .001
Larynx	V50 < 27 %	3 ± 1.6	3.1	13.4 ± 4.4	11.6	< .001
Parotid gland	$D_{mean} < 20$ Gy	5.5 ± 1	5.4	5.2 ± 1.2	5.1	.20

Table 4: The dose to OARs for SEQ-IMRT and SIB-IMRT in parotid glands cancer patients

		SEQ-IMRT		SIB-IMRT		
Organ	Dose criteria	Mean ± SD, Gy	Median, Gy	Mean ± SD, Gy	Median, Gy	p-value
Spinal cord	$D_{max} < 50$ Gy	44.1 ± 0.9	44.4	46.4 ± 1.8	47	-
Oral cavity-PTV	$D_{mean} < 40$ Gy	30.0 ± 3.1	30.6	30.9 ± 2.7	31.6	.047
Parotid gland – L	$D_{mean} < 20$ Gy	29.7 ± 5.9	28.7	33.1 ± 5.5	33.6	< .001
Parotid gland – R	$D_{mean} < 20$ Gy	31.3 ± 5.9	33.3	34.1 ± 5.6	34.8	< .001
Bilateral Parotid	$D_{mean} < 25$ Gy	30.6 ± 5.6	29.8	33.7 ± 5.3	33.9	< .001

Table 5: The dose to OARs for SEQ-IMRT and SIB-IMRT in laryngeal cancer

Index of Authors

Adlan Čehobašić, 108
Adriano Contillo, 82
Adrijana Oblak, 130
Aleksandar Miladinović, 112
Alessio Boschini, 55
Alexander Gruber, 47, 93
Ana Božanić, 68
Ana Ivkovic, 90
Ana Marija Kožuljević, 71
Andraž Koritnik, 44
Andrej Strojnik, 123
Andrej Studen, 137
Angelica de Leon, 47, 93
Angelika Osanna-Elliott, 47, 93
Anja Androjna, 134
Anja Lazović, 91
Attila Šarvari, 57

Benedetta Santoro, 48
Borislava Petrović, 110
Borko Nidžović, 91
Božidar Casar, 14, 24, 63

Carlo Algranati, 41, 94
Chiara Reverberi, 61

Damijan Škrk, 44
Damir Bosnar, 71
Daniela Marfisi, 61
Dario Faj, 90, 126
David Rajlić, 25, 126
Davide Canonico, 55
Davide Maestri, 55
Daša Sfiligoj Planjšek, 134
Dea Dundara Debeljuh, 36
Denis Brojan, 57, 123
Dietmar Georg, 15
Domagoj Kosmina, 108
Doris Šegota, 68
Dragan Nikolić, 101
Dragan Schwarz, 108
Dushko Lukarski, 139

Ehsan Abadi, 82
Ehsan Samei, 82

Elena Hristovska, 139
Emese Csiki, 18
Emina Grgurević Dujmić, 68
Eugenia Moretti, 61

Fran Stanic, 108
Francesco Fracchiolla, 94
Fulvia Arfelli, 48

Gašper Strnad, 134
Giorgia Condarelli, 61
Giuseppe Rinaldin, 55

Hrvoje Brkić, 90, 126
Hrvoje Kaučić, 108

Ignasi Méndez, 63
Ilenia Giovannini, 41
Ivan Gencel, 110
Ivan Pribanić, 36
Ivana Alerić, 108
Ivana Koceva, 114
Ivana Mišković, 91
Ivana Rosić, 112

Jelena Moravčević, 110
Jelena Stanković, 101, 106
Jernej Zlatič, 98
Josh Naylor, 20
Jovana Zlatanović, 101
Juan José Rovira, 63
Judit Papp, 18

Katica Bajuk Studen, 130
Katja Zaletel, 130
Kristian Stojšić, 78

Laza Rutonjski, 96
Lenche Kostadinova, 139
Lidia Strigari, 94
Luca Bindoni, 55
Luka Jensterle, 130, 134
Luka Ležaič, 134
Luka Pavelić, 71

Maja Karić, 68
Manca Podvratnik, 76, 85
Manda Švabić Kolacio, 25, 126
Mara Severgnini, 48, 88
Marco Cianchetti, 94
Marco Trovo', 61
Maria Rosa Fornasier, 48
Marija Z. Jeremić, 112
Marika Guernieri, 61
Markus Stock, 23
Matevž Mlekuž, 98
Michele Avanzo, 16, 94
Michele Signoriello, 48
Mihael Makek, 71
Mihaela Mlinarić, 108
Mihály Simon, 18
Milana Marjanović, 110
Milena Živković, 112
Miloš Jonić, 101, 106
Miloš Kopunović, 101, 106
Mirjana Papić, 110
Mladen Kasabašić, 90, 108

Natasa Brasik, 47, 93
Nemanja Golubovac, 96
Nevena Obajdin, 25, 126
Nina Pavlović, 112

Ozren Čudić, 96

Paola Bregant, 88
Paolo Scalchi, 61
Paul Segars, 82
Petar Žugec, 71
Petra Tomše, 130, 134
Petra Valković Zujić, 68
Primož Peterlin, 114, 123

Renata Longo, 82, 88
Renato Padovani, 88
Rihard Hudej, 98

Sabina Vennarini, 94
Sara Barbiero, 55
Sašo Pulko, 65, 118
Siddharth Parashari, 71
Silvia Strolin, 94
Simona Gaberšček, 130
Slaven Jurković, 25, 36, 68, 78, 126
Snežana Vostinić, 91
Sofija Antić, 108
Stefano Lorentini, 41, 94
Stevan Vrbaski, 82
Stipe Galic, 90

Tadeja Forjanič, 98
Tamara Jovanović, 101
Tanja Marinko, 114
Tatjana B. Miladinović, 112
Tomislav Bokulić, 71
Trianni Annalisa, 41

Urban Simončič, 130
Urban Zdešar, 76, 85, 137
Urša Beguš, 130
Urška Poje, 137

Valerija Žager Marciuš, 114
Vanda Leipold, 108
Vito Gagliardi, 61
Vjekoslav Kopačin, 90

Werner F. O. Schmidt, 32

Árpád Kovács, 18

Đeni Smilović Radojčić, 25, 126

Acknowledgements

Special thanks to our sponsors:

Platinum:

Gold:

Silver:


BRAINLAB


Elekta


elimpex
Medizintechnik GesmbH


Emedis


KVARKdoo
KRAGUJEVAC


SIEMENS
Healthineers


STARGEN EU s.r.o.


RaySearch
Laboratories


ZVD

Bronze:

And to our partner:

ISBN 978-961909426-6